DISSERTATION

DEVELOPMENT OF STRATEGIES FOR THE DETECTION, EXTRACTION, AND RECOVERY OF AQUEOUS ANIONS USING HIGHLY SELECTIVE REDOX-RECYCLABLE MATERIALS

Submitted by

Matthew A. Odom

Department of Chemistry

In partial fulfillment of the requirements

for the Degree of Doctor of Philosophy

Colorado State University

Fort Collins, Colorado

Fall 2001

COLORADO STATE UNIVERSITY

October 18, 2001

WE HEREBY RECOMMEND THAT THE DISSERTATION PREPARED UNDER OUR SUPERVISION BY MATTHEW A. ODOM ENTITLED *DEVELOPMENT OF STRATAGIES FOR THE DETECTION, EXTRATION, AND RECOVERY OF AQUEOUS ANIONS USING HIGHLY SELECTIVE REDOX-RECYCLABLE MATERIALS* BE ACCEPTED AS FULFILLING IN PART REQUIREMENTS FOR THE DEGREE OF DOCTOR OF PHILOSOPHY.

Committee on Graduate Work

Adviser

Department Head

ABSTRACT OF DISSERTATION

DEVELOPMENT OF STRATEGIES FOR THE DETECTION, EXTRACTION, AND RECOVERY OF AQUEOUS ANIONS USING HIGHLY SELECTIVE REDOX-RECYCLABLE MATERIALS

Highly selective redox-recyclable extractant materials were prepared by physisorbing the redox active lipophilic extractant $HEP^{+}NO_3^{-}$ [HEP = 1,1',3,3'-tetrakis(2-methyl-2-hexyl)ferrocene] onto various polymeric supports. Simple adsorption of the tetraalkylated ferrocenium salts onto polymeric supports was preferred to the more difficult and more expensive alternative of covalently grafting redox active moieties onto a solid support. The new materials were evaluated for their effectiveness towards the extraction of ReO_4^{-} and $C_nF_{2n+1}SO_3^{-}$ (PFS) ions from a variety of aqueous solutions. The effects of coverage and size of the tetraalkylated ferrocenium cation (size of the tetraalkylated ferrocene was adjusted by varying the length of the alkyl substituents attached to the ferrocene from four to ten carbon atoms in length) were evaluated as well as the selectivity over several redox cycles. The materials were also evaluated for their effectiveness under a variety of conditions including contact time, pH, and concentration of a competing ion. The materials were found to be highly selective for NO_3^{-}/ReO_4^{-} ion exchange even in the presence of 1.0 M $NaNO_3$. The polarity, pore size, and surface area of the polymer used as a support had a dramatic effect on the effectiveness of the resulting anion-exchange materials. More polar polymers achieved faster anion-exchange kinetics compared to non-polar polymers. The polymer beads with larger pores and lower surface areas were found to give higher distribution ratios. It was also found that as the size of the cation increased, the material became more selective, indicating a size bias towards ReO_4^{-} for larger cations. The new materials were stable over several extraction-deactivation/recovery-reactivation cycles, with no loss in effectiveness over seven redox cycles, compared to previous studies in which silica gel supported materials lost 20% of their capacity over five cycles.

The new redox-recyclable material $HEP^{+}NO_3^{-}$/XAD-7 (XAD-7 = acrylic ester polymer) was found to efficiently remove PFS anions from aqueous solutions, but because of the low solubility of longer-chain PFS surfactants in water at room temperature, deactivation of the loaded extractant material resulted in immediate precipitation of longer-chain PFS salts. The precipitation of the PFS salts was initially perceived as a problem for the recovery of the pollutant in a small volume, however, this disadvantage was turned into an advantage. The solubility of PFS salts dramatically increased when the aqueous solution was heated above the Krafft point of the PFS salts. A hot-water/cold-water recovery process was developed in which extracted PFS salts were efficiently washed from a deactivated column by heating the recovery solution to temperatures above the Krafft point of the surfactant and recovering them as a solid in a cold trap. This technique allowed the recovery of the PFS pollutant as a crystalline solid, resulting in a volume reduction of 99.99%. Without the ability to easily activate and deactivate the extractant material, this type of recovery and subsequent volume reduction would not be possible.

Several methods for the detection, identification, and quantification of fluorinated surfactants have been investigated. A colorimetric assay method was developed that allowed a one-step detection scheme using spectrophotometry. The method involved exchanging the colorless surfactant in the aqueous solution quantitatively with a colored anion that had been immobilized onto a solid support, and subsequent spectrophotometric detection. The assay provided a general test for the presence of anionic surfactants, and was quantitative between 50 and 275 $\mu g\ L^{-1}$ for one formulation of aqueous film forming foam (AFFF) that contained a mixture of fluorinated and non-fluorinated surfactants.

A negative ion electrospray mass spectrometric method ((–)ES-MS) was developed for the detection and identification of fluorinated surfactants in aqueous solution. The method was able to achieve a much lower detection limit compared to the colorimetric method (below 6 $\mu g\ L^{-1}$), and had the added advantage of identification

through mass analysis. Reliable quantification information was achieved by using an internal standard with a similar sensitivity coefficient to the anions of interest.

To determine capacity and extraction performance of a column packed with $HEP^{+}NO_3^{-}$/XAD-7, an ATR-FTIR technique was developed to monitor the breakthrough of an IR-active analyte in real time. This technique, although limited by the strong absorbance of water in the infrared region, was able to detect 10 mM triflate within one minute of breakthrough.

Enhancing the sensitivity of an ATR-FTIR spectrometer for IR-active anions in aqueous solutions by physisorbing highly selective water insoluble organometallic extractants to the surface of the probe was investigated. A thin film of the organometallic extractant 1,3-bis(diphenylphosphino)propanedichloronickel(II) ($NiCl_2$(dppp)) applied to the tip of the ATR probe was used to detect CN^{-} in the low microgram per liter (ppb) concentration range. The detection limit for an unmodified probe was found to be 130,000 $\mu g\ L^{-1}$. By simply applying a thin film of $NiCl_2$(dppp), the detection limit for aqueous cyanide dropped to 5 $\mu g\ L^{-1}$, thereby increasing the sensitivity by a factor of 26,000. Applying a thin film of 1,1',3,3'-tetrakis(2-methyl-2-nonyl)ferrocenium nitrate ($DEC^{+}NO_3^{-}$) afforded a sensitivity increase of 96,000 for ClO_4^{-} and 4,000 for $C_8F_{17}SO_3^{-}$. The added advantage of using infrared spectroscopy was positive identification of the target analytes through the unique IR absorbances produced in the resulting spectra. The detection limits reported here are unprecedented for infrared detection of these ions in aqueous solutions.

Matthew A. Odom
Department of Chemistry
Colorado State University
Fort Collins, CO 80523
Fall 2001

ACKNOWLEDGMENTS

I would like to thank all the members of the Strauss research group who have been my friends and colleagues over the past several years. I would especially like to acknowledge Dr. C. Kevin Chambliss, Brady J. Clapsaddle, Gretchen N. Hebert and Dr. Kristina M. Rohal-Gansle for their support and assistance. I thank my advisor Professor Steven H. Strauss for his patience, wisdom and guidance. Thank you for believing in me and encouraging me over the years. I would also like to thank my parents for their constant support and encouragement. Most of all, I would like to thank my wife Jennifer for her support, encouragement, and understanding. You never stopped believing in me.

Table of Contents

List of Tables

List of Figures

List of Abbreviations and Definitions.

abbreviation	definition
ACN	acetonitrile
AFFF	aqueous film forming foam (3M product)
ATR-FTIR	attenuated total reflectance Fourier transform Infrared
BET	Brunauer, Emmet and Teller surface area determination
BV	bed volume, volume of solution contained in a column
DDS	sodium dodecylsulfate
DEC	1,1',3,3'-tetrakis(2-methyl-2-nonyl)ferrocene
DiComp®	18-bounce diamond ATR probe
FC-95	mixture of five fluorinated surfactants (3M product)
HEP	1,1',3,3'-tetrakis(2-methyl-2-hexyl)ferrocene
K_d	measure of selectivity, in unites of mL g^{-1}
K_d*	measure of selectivity, in units of mL $mmol^{-1}$
PFC	perfluoroalkylcarboxolate
PFS	perfluoroalkylsulfonate
PFOS	perfluorooctylsulfonate
R^2ER	redox-recyclable extraction and recovery
R^+	lipophilic cation
SiComp®	30-bounce silicon ATR probe
THA-FR	tetraheptylammonium Fast Red
XAD-7	acrylic ester polymer, 90 Å pores, 450 m^2 g^{-1} surface area
(–)ES-MS	negative ion electrospray mass spectroscopy

Chapter 1

Redox-Recyclable Materials. An Introduction

Introduction

The separation and recovery of inorganic ions (i.e., nuclear fission products, precious metals), organic ions (i.e., antibiotics), and ionic pollutants (i.e., ClO_4^-, CN^-, $C_nF_{2n+1}SO_3^-$) from aqueous media is an important area of research that addresses both environmental and industrial concerns. Traditionally, anion separation has been carried out using anion-exchange resins such as Dowex, Reillex-HPQ, Amberlite, Purolite, Aliquat-336, and Sybron Ionac, which contain quaternary ammonium or pyridinium sites with exchangeable anions.[1] More recently, efforts have been made to make extractants with varying sized exchange sites that combine both high selectivity and fast kinetics.[2–4] The majority of research has been focused on improving the selectivity and capacity of the ion-exchange materials for the specific ions of interest, as well as improving kinetics. However, when ion-exchange chromatography has been used for the remediation of toxic and/or radioactive aqueous waste streams, minimization of the volume of secondary waste (i.e., the strip solution) destined for permanent disposal has been a significant challenge. Waste minimization becomes even more problematic as the concentration of the target ion in primary hazardous waste streams becomes dilute. Generally, as the concentration of the target ion in the primary waste stream decreases, the volume of the secondary waste stream generated increases.[5] Furthermore, tougher environmental

regulations[6] and high initial cost of new, more effective, and more selective extractants have made the reuse of the extractant an increasingly important issue.

New Approach Towards Extraction and Recovery of Pollutant Ions. To address the need for new extractants, organometallic complexes have been developed that are (i) highly selective, (ii) have high capacities, (iii) undergo rapid ion-exchange, and (iv) are recyclable. These extractants are incorporated into a Redox-Recyclable Extraction and Recovery (R^2ER) scheme in which the target ion is selectively removed from the bulk waste and recovered in a minimal volume. A general R^2ER scheme is depicted in Figure 1.1. The R^2ER process begins with the redox-active organometallic material, confined to a water-immiscible organic phase or immobilized onto an inert solid support, in its neutral state, denoted EXTR. When the extractant becomes activated by oxidation (for the extraction of anions) or reduction (for the extraction of cations) in the presence of an abundant exchangeable ion, $X^{\pm}$, the species, EXTR, is converted to the organometallic salt, $EXTR^*X^{\mp}$, which exchanges its ion, $X^{\mp}$, for the target ion, $Y^{\mp}$, in the subsequent extraction step. After extraction, a final redox deactivation step regenerates the neutral form of the extractant and releases the target ion in a minimal volume of secondary waste.

The R^2ER strategy offers a novel stripping/regeneration method based on an extractant redox-process rather than a displacement principle. The ease with which the extractant can be switched "on" and "off" allows for a strategy in which pollutant ions are selectively removed from complex matrixes, efficiently recovered, and the extractant reused multiple times without loss of selectivity or capacity. Since the extractant is simply switched "off," the target ion may be quantitatively concentrated into a small volume without the use of a high concentration of a displacing ion (e.g., 8 M HNO_3) or complexing reagent.

Certain criteria are required for successful application of an organometallic

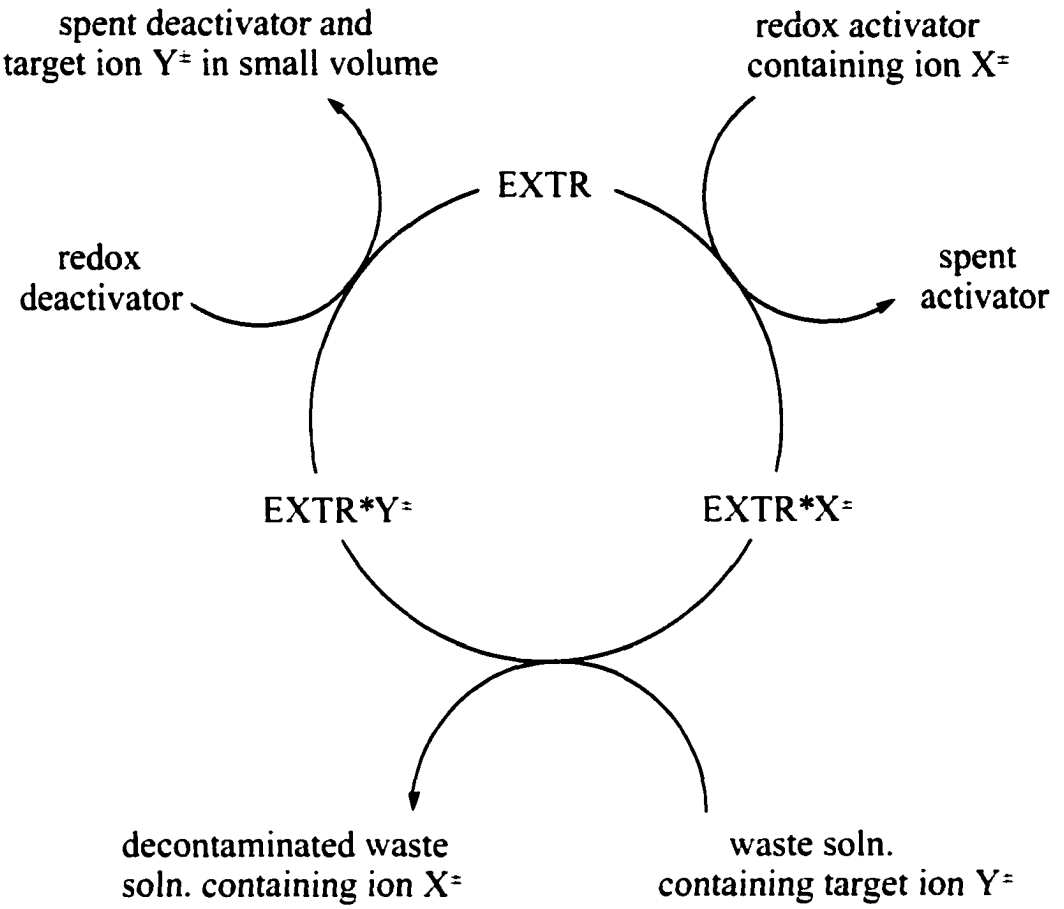

Figure 1.1. General representation of the complete Redox-Recyclable Extraction and Recovery process (R^2ER). The species, EXTR, is a neutral, redox-active, transition-metal complex. The species, EXTR*, is the oxidized, cationic transition metal species (for extraction of anions) or the reduced, anionic transition-metal species (for the extraction of cations). The species, EXTR, $EXTR^*X^{\pm}$, and $EXTR^*Y^{\pm}$, are confined to a water-immiscible organic phase or a stationary phase for solvent extraction or ion-exchange chromatography processes, respectively.

extractant to the R^2ER process. The organometallic complex must undergo facile one-electron oxidation and reduction, and remain stable with respect to ligand substitution, hydrolysis, and irreversible over-oxidation or over-reduction. Loss of the extractant to the aqueous phase must also be prevented, therefore, the extractant must be extremely lipophilic. When immobilization of the extractant onto a solid support is desired, the structure of the extractant must also provide for favorable interfacial forces or covalent bonding to the surface. Finally, the extractant must exhibit high selectivity for a target ion, which can be achieved by adding specific functionality or increasing the size of the organometallic complex.

Initially, the R^2ER strategy was applied towards the difficult separation of pertechnetate (TcO_4^-) from nuclear process waste.[7] The separation of pertechnetate from such a complex matrix requires high selectivity, high capacity, and minimal secondary waste. The need to clean contaminated areas and properly dispose of nuclear waste has been a problem that many communities continue to face across the country.[8,9] The bulk of the nuclear waste accumulated during the cold war era was in the form of aqueous acidic process waste, containing fission products, uranium, transuranic elements, and some heavy metals. The waste was made alkaline and stored in large underground tanks.[10,11] Recently, reports of leaking tanks and potentially explosive gas generation in some tanks have raised environmental as well as safety concerns at such storage sites as the Hanford Reservation site in Hanford, Washington.[8,12-15] Radioactive technecium (^{99}Tc) along with several other byproducts, including $^{137}Cs^+$ and $^{90}Sr^{2+}$, are produced in ~ 6% yield or higher from the thermal neutron fission of ^{235}U.[16] ^{99}Tc is a weak β^- emitter, however, $^{137}Cs^+$ and $^{90}Sr^{2+}$ are high-activity γ-and/or β-emitters with half-lives of ca. 30 years and account for 97% of the penetrating radiation and 98% of the thermal energy in high-level waste 30 years, after fuel irradiation.[17] ^{99}Tc does not contribute significantly to the heat and radiation load but it has a relatively long half life (2.13×10^5

years) and once in the form of the pertechnetate ion ($^{99}TcO_4^-$), it becomes a water soluble species that is mobile in the environment.[18–20] Greater than 1,800 kg of ^{99}Tc are believed to be present in the Hanford tank waste, and new estimates of [$^{99}TcO_4^-$]/[^{99}Tc] range from 40% to 80%.[21,22]

The current site for long-term storage of nuclear waste is the Yucca Mountain repository in Nevada. The site has a maximum capacity of 70,000 metric tons. The Hanford nuclear site alone contains an estimated 770,000 metric tons of process waste and contaminated soil.[8] Without an efficient, cost effective means to minimize hazardous waste, current repositories would only hold a fraction of the total nuclear waste in this country. Ion exchange processes are planned to remove $^{137}Cs^+$ and $^{90}Sr^{2+}$ from liquid fractions of contaminated waste. This will essentially separate the waste into high level waste (HLW) and low level waste (LLW). In the past, zeolites, as well as other ion-exchange materials, have been used to separate both cesium and strontium from solutions containing high levels of sodium, but they tend to have low distribution coefficients, and it has proven difficult to recover the radioactive ions from the ion-exchange matrix.[23] More recently, redox-active transition metal-containing extractants for the separation and recovery of $^{137}Cs^+$ and $^{90}Sr^{2+}$ have been developed by Strauss, Chamberlin, and co-workers at Los Alamos National Laboratory.[17] These extractants were found to be highly selective towards $^{137}Cs^+$ and $^{90}Sr^{2+}$, but more importantly, the radioactive cations were recovered in a minimal volume of secondary waste, and the extractants were reusable.

To date, both liquid-liquid and chromatographic techniques have been employed to extract $^{99}TcO_4^-$ from ground water and process nuclear waste. New anion-exchange resins have been developed for the efficient removal of $^{99}TcO_4^-$ from aqueous solutions.[24–28] Schroeder and co-workers at the Los Alamos National Laboratory have demonstrated that Reillex™–HPQ (a strong base anion-exchange resin containing both

methylpyridinium and pyridinium sites) can selectively remove $^{99}TcO_4^-$ from acidic, neutral, and alkaline waste simulants containing a complicated matrix of interfering ions.[26,27] The traditional method of recovery involves passing large volumes of an aqueous solution containing a high concentration of a displacing ion (8 M HNO_3) through the column. An alternative stripping solution used by Schroeder and co-workers contained 1.0 M NaOH, 1.0 M ethylenediamine, and 5 mM Sn^{2+}. When this solution was passed through the column, Tc was reduced to a lower valent species that was subsequently complexed by ethylenediamine and eluted from the column. Although the extractant can be reused, this was a fairly lengthy process, taking up to 11 hours to regenerate the extractant material.

Another approach for removing $^{99}TcO_4^-$ from aqueous solutions has been developed by Rogers at the University of Alabama and his collaborators at Argonne National Laboratory.[29–31] Their system involves high-molecular-weight polyethylene glycol (PEG) covalently bonded to a polystyrene support. The resin material behaves as an aqueous biphasic system when the mobile phase contains a high concentration of water structuring ions (e.g., SO_4^{2-}, CO_3^{2-}, OH^-). Weakly hydrated ions, present in the mobile phase, preferentially partition into the PEG phase. Selective partitioning of $^{99}TcO_4^-$ from Hanford waste simulants has been demonstrated using ABEC™-5000.[29] Stripping was accomplished by simply washing the resin with water. When the mobile phase was changed from high ionic strength to low ionic strength, an aqueous biphasic environment was no longer supported, and the weakly hydrated ions partitioned out of the PEG phase. A major limitation of this innovative approach was that a high-salt mobile phase was required for extraction. This type of process would not be applicable to removal of $^{99}TcO_4^-$ or other ionic contaminants from low-ionic-strength matrices such as groundwater.

Solvent extraction systems have been successfully used for the removal of >99% of the $^{99}TcO_4^-$ from simulated nuclear waste in a single contact. For example, Strauss and co-workers used organic solutions containing the commercially available anion-exchange reagent Aliquat™–336 nitrate ($[NMe(C_8H_{17})_3][NO_3]$) to establish benchmarks for the extraction of $^{99}TcO_4^-$ from a number of aqueous waste simulants.[7] Values of the technetium distribution coefficient, $D(^{99}TcO_4^-)$, exceeding 100 were obtained when organic solutions of the quaternary ammonium salt were contacted with various acidic, neutral, and alkaline waste simulants containing high concentrations of NO_3^-. Although the extractant performed quite well, the recovery of $^{99}TcO_4^-$ in a small volume still posed significant problems. Traditionally, recovery involved using a strip solution containing a high concentration of a displacing ion (i.e., NO_3^-). Many investigators have used 8 M HNO_3 to strip (i.e., back-extract) $^{99}TcO_4^-$ from the organic phase.[32-34] Usually, several aliquots of stripping solution were required to fully displace $^{99}TcO_4^-$ and regenerate the material. This is less than desirable for two reasons. First, $^{99}TcO_4^-$ would be contained in a high volume form. Second, the secondary waste remains quite hazardous because of the corrosive and oxidizing nature of 8 M HNO_3. The large volume of secondary waste and the corrosive nature of the waste have prevented the implementation of a convenient and efficient extraction cycle based on traditional anion-exchange strategies.

To address the recovery issues, Moyer, Sachleben, Bonnesen, and co-workers at Oak Ridge National Laboratory have developed a solvent extraction process in which the extracted $^{99}TcO_4^-$ can be recovered by stripping with water.[35] The mechanism involves the extraction of an alkali metal ion (i.e., Na^+ or K^+) by the crown ether bis-4,4'(5')[(*tert*-butyl)cyclohexano]-18-crown-6. An anion was necessary to maintain charge neutrality, and in this way the $^{99}TcO_4^-$ was also extracted:

$$Na^+ + TcO_4^- + \overline{CE} \rightleftharpoons \overline{(CE)NaTcO_4}$$

Here, CE is the crown ether and overbars indicate the organic-phase species. When the organic phase containing the crown ether complex was contacted with water, the equilibrium was reversed, which promoted dissociation of the complex to free alkali metal salt in the aqueous phase and free crown ether in the organic phase. A complete extraction-recovery cycle was demonstrated based on this principle, and a patent covering the process has been issued.[36] An inverse relationship between the degree of extraction and the stripping efficiency was identified. Thus, multiple contacts of the aqueous and organic phases were required for complete extraction and recovery to be achieved.

To address some of the concerns presented by difficult separations, Strauss and co-workers have applied the new R^2ER strategy towards the extraction and recovery of $^{99}TcO_4^-$.[7,30] In one study $^{99}TcO_4^-$ was extracted from an aqueous waste simulant containing 1 M NaOH, 1.5 M $NaNO_3$, and 10^{-5} M $^{99}TcO_4^-$ using the hydrophobic organometallic complex 1,1',3,3'-tetrakis(2-methyl-2-hexyl)ferrocenium nitrate ($HEP^+NO_3^-$) dissolved in organic solvents.[7] The active form of the redox-active, tetraalkyl substituted ferrocenium extractant is show below:

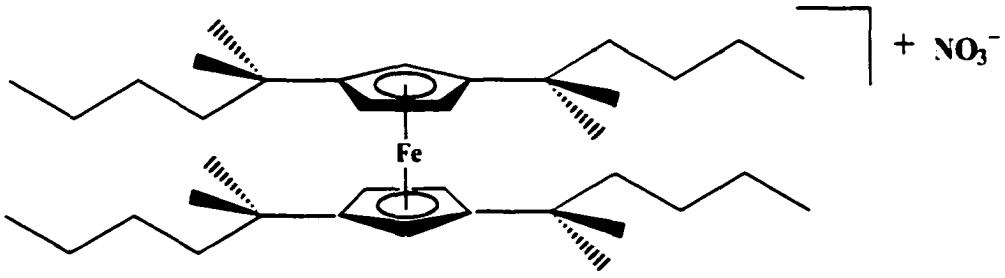

This organometallic complex in its active, oxidized form, ion paired with an exchangeable anion (NO_3^-) was able to selectively extract from aqueous media, anions with lower hydration energy then nitrate. In its reduced form (HEP), no extraction was

observed.[7] The extractant was found to be highly selective towards the removal of $^{99}TcO_4^-$ from the waste simulant, and upon deactivation of the extractant material with powdered iron, the secondary waste produced contained a mixture of solids containing >99% of the radioactivity originally in the primary waste and a total volume less than 1% of the primary waste volume. This new type of redox-recyclable extraction and recovery process (R^2ER) was found to accomplish three important things simultaneously: (i) high selectivity with large capacity for the target ion (TcO_4^-), (ii) efficient reuse of the extractant, and (iii) recovery of the target ion in a minimal volume. The primary advantage of this type of extraction/recovery process is not the selectivity of HEP^+ for pertechnetate but the *minimization* of the volume of the secondary waste containing the target ion. More recently, redox-recyclable materials have been developed by adsorbing highly selective redox-recyclable extractant salts, HEP^+X^-, onto high surface area silica gels. These materials were then evaluated for their selectivity towards $^{99}TcO_4^-$ and ReO_4^-, and their effectiveness over multiple R^2ER cycles. The results of these investigations indicated that: (i) salts of HEP^+ can be adsorbed onto silica gels using organic solvents and will not appreciably desorb into the aqueous phase when the dried materials are treated with 1 M HNO_3, (ii) NO_3^- co-adsorbed with HEP^+ will selectively exchange with both $^{99}TcO_4^-$ and ReO_4^- in aqueous solutions, and (iii) adsorbed HEP^+ can be rapidly activated and deactivated using water-soluble redox reagents. These materials have the added advantage that no organic solvents are used once the organometallic complex has been loaded onto the support, unlike the case with the solvent extraction systems.

The Scope of the Dissertation

The work described in this dissertation expands upon the development of organometallic extractant materials for the redox-recyclable extraction and recovery of

anionic pollutants. Also, detection techniques for monitoring the extraction of anions and evaluating the new ion-exchange materials are described. In Chapter 2, anion-exchange materials consisting of a variety of tetraalkylated ferrocenium salts physisorbed onto polymeric solid supports are evaluated for their selectivity towards aqueous ReO_4^-. Properties such as loading, contact time, matrix affects, recyclability, and size of the tetraalkylated ferrocenium were evaluated. This type of analysis was necessary to understand the mechanism(s) that govern the effectiveness of the material.

The focus of Chapter 3 is the application of these extractant materials and the R^2ER technique towards the extraction and recovery of perfluoroalkylsulfonates ($C_nF_{2n+1}SO_3^-$) from aqueous solutions. Detection schemes were also developed for analyzing solutions containing fluorinated surfactants including negative ion electrospray mass spectrometry ((–)ES-MS) and a colorimetric assay. A new hot water/cold water recovery scheme is presented. It utilizes the selectivity and ease of recyclability of the $HEP^+NO_3^-$/XAD-7 material for the recovery of perfluoroalkylsulfonate salts as a solid, which affords a volume reduction by a factor of 2,000. This method is currently undergoing patent approval.

Described in Chapter 4, is the development of an ATR-FTIR technique that allows for detection of aqueous anions at several orders of magnitude below that of a commercially available ATR-FTIR spectrometer. The technique involves applying a thin film of a selective water insoluble organometallic salt on the ATR crystal, which acts to concentrate the anions of concern within the sensing region of the probe. Sensitivity increases from 4,000–96,000 over that of an unmodified probe have been demonstrated for IR-active anions in aqueous solutions, even in the presence of competing anions. This work has been accepted for publication (J. Amer. Water Works Assoc.).

References

(1) All resins are commercially available.

(2) Marsh, S. F.; Jarvinen, G. D.; Bartsh, R. A.; Nam, J.; Barr, M. E. *J. Radioanal. Nucl. Chem.* **1998**, *235*, 37.

(3) Gu, B.; Brown G. M.; Bonnesen, P. V.; Liang, L.; Moyer, B. A.; Ober, R.; Alexandratos, S. D. *Eviron. Sci Technol.* **2000**, *34*, 1075.

(4) Bonnesen, P. V.; Brown G. M.; Alexandratos, S. D.; Bavoux, L. B.; Patel, V.; Ober, R.; Moyer, B. A. *Eviron. Sci Technol.* **2000**, *34*, 3761.

(5) Tedder, D. W. *Sep. Purif. Methods* **1992**, *21*, 23.

(6) Kirschner, E. M. *Chem. Eng. News* **1994**, (June 20), p 13.

(7) Clark, J. F.; Clark, D. L.; Whitner, G. D.; Schroeder, N. C.; Strauss, S. H. *Environ. Sci. Technol.* **1996**, *30*, 3124.

(8) Illman, D. L *Chem. Eng. News* **1993**, *June 21*, 9.

(9) Renner, R. *Eviron. Sci. Tech.* **1997**, *31*, 134A.

(10) Babad, H.; Fulton, J. C.; DeFigh-Price, B. C. *A Strategy for Resolving High-Priority Hanford Site Radioactive Waste Storage Tank Safety Issues*; report WHC-SA-1661-FP, Westinghouse Hanford Co.: Richland, WA, 1993.

(11) Barker, S. A.; Thornhill, C. K.; Holton, L. K. *Pretreatment Technology Plan*; report WHC-EP-0629, Westinghouse Hanford Co.: Richland, WA, 1993.

(12) Babad, H; Johnson, G. D.; Reynolds, D. A.; Pederson, L. R.; Strachan, D. M.; Meisel, D.; Jonah, C.; Ashby, E. C. *Evaluation of the Generation and Release of Flammable in Tank 241-SY-101*; report WHC-EP-0517, Westinghouse Hanford Co.: Richland, WA, 1991.

(13) Babad, H.; Turner, M. D.; Gerber, M. A. *Resolving Safety Issues for Radioactive Waste Tanks with Organic Content*; report WHC-SA-1671-FP, Westinghouse Hanford Co.: Richland, WA, 1993.

(14) Babad, H.; Camaioni, D. M.; Lilga, M. A.; Samuels, W. D.; Strachan, D. M. *Tank Waste Chemistry – A New Understanding of Waste Aging*; report WHC-SA-1661-FP, Westinghouse Hanford Co.: Richland, WA, 1993.

(15) Simpson, B. C.; Babad, H.; Cash, R. J. *Recent Results from Characterization of Ferrocyanide Wastes at the Hanford Site*; report WHC-AS-1701-FPM, Westinghouse Hanford Co.: Richland, WA, 1993.

(16) Katcoff, S. *Nucleonics* **1958**, *16*, 78.

(17) Clark, J. F.; Chamberlin, R. M.; Abney, K. D.; Strauss, S. H. Design and Use of Redox-Recyclable Organometallic Extractants for Cationic Radionuclides $^{137}Cs^{+}$ and $^{90}Sr^{+}$. *Environ. Sci. Technol.*, **1999**, *33*, 2489.

(18) Schroeder, N. C.; Morgan, D.; Rokop, D. J.; Fabryka-Martin, J. *Radiochim. Acta* **1993**, *60*, 203.

(19) Garten, Jr., C. T. *Environment International* **1987**, *13*, 311.

(20) Wildung, R. E.; McFadden, K. M.; Garland, T. R. *J. Environ. Qual.* **1979**, *8*, 156.

(21) Schroeder, N. C. Los Alamos National Laboratory, Los Alamos, NM. Personal communication, 1996.

(22) Blanchard, Jr., D. L.; Brown, G. N.; Conradson, S. D.; Fadeff, S. K.; Golcar, G. R.; Hess, N. J.; Klinger, G. S.; Kurath, D. E. "Technetium Removal and Characterization: A Progress Report," unpublished report prepared for Westinghouse Hanford Co. by PNL, dated May 30, 1996.

(23) Clearfield, A. In Inorganic Ion Exchange Materials for Nuclear Waste Effluent Treatment: Industrial Environmental Chemistry; Sawyer, D. T.; Martell, A. E. Plenum Press, New York, 1992.

(24) Kawasaki, M; Omori, T.; Hasegawa, K. *Radiochimica Acta* **1993**, *63*, 53.

(25) Ashley, K. R.; Ball, J. R.; Pinkerton, A. B.; Abney, K. D.; Schroeder, N. C. *Solv. Extr. Ion Exch.* **1994**, *12*, 239.

(26) Ashley, K. R.; Whitener, G. D.; Schroeder, N. C.; Ball, J. R.; Radzinski, S. *The Ion Exchange Behavior of Pertechnetate on Reillex™-HPQ Anion-Exchange Resin in Simulated Hanford Tank Waste*; submitted for publication.

(27) Liang, L.; Gu, B.; Yin, X. *Sep. Technol.* **1996**, *6*, 111.

(28) Bonnesen, P. V.; Alexandratos, S. D.; Brown, G. M. In *Recent Developments and Future Opportunities in Separations Technology*, Topical Conference Preprints of the American Institute of Chemical Engineers 1995 Annual Meeting, Miami, Fl, Nov. 12-17, 1995, Vol. 2; American Institute of Chemical Engineers: New York, 1995;pp 294-299.

(29) Rogers, R. D.; Griffin, S. T.; Horwitz, E. P.; Diamind, H. *Solv. Extr. Ion Exch.* **1997**, *15*, 547.

(30) Rogers, R. D.; Zhaung, J.; Griffin, S. T. *Sep. Sci. Technol.* **1997**, *32*, 699.

(31) Rogers, R. D.; Bond, A. H.; Griffin, S. T.; Horwitz, E. P. *Solv. Extr. Ion Exch.* **1996**, *14*, 919.

(32) Macásek, F.; Rajec, P.; Mikulaj, V.; Kopunec, R.; Cech, R. *Coll. Cxech. Chem. Commun.* **1978**, *43*, 200.

(33) Dyrkacz, G. R.; Vandegrift, G. F.; Thomsen M. W.; Horwitz, E. P. *J. Phys. Chem.* **1979**, *83*, 670.

(34) Tse, P. K.; Horwitz, E. P. *Solv. Extr. Ion Exch.* **1990**, *8*, 353.

(35) Bonnesen, P. V.; Moyer, B. A.; Presley, D. J.; Armstrong, V. S.; Haverlock, T. J.;Counce, R. M.; Sachleben, R. A. *Alkaline-Side Extraction of Technetium from Tank Waste Using Crown Ethers and Other Extractants*; report ORNL/TM-13241, Oak Ridge National Laboratory: Oak Ridge, TN, June 1996.

(36) Moyer, B. A.; Sachleben, R. A.; Bonnesen, P. V. *Process for Extracting Technetium from Alkaline Solutions*; U. S. Patent 5,443,731, August 22, 1995.

Chapter 2

Development of Redox-Recyclable Materials for the Extraction and Recovery of Weakly Hydrated Anions

Introduction

As part of an ongoing effort to develop new redox-recyclable materials for the removal and recovery of ionic contaminants from acidic, neutral and alkaline aqueous waste streams, a variety of organometallic extractants physisorbed onto polymeric supports have been developed. Researchers in the Strauss group have recently developed a liquid-liquid extraction-recovery process for radioactive pertechnetate, a nuclear fission product of environmental concern, from an aqueous waste simulant containing 1 M NaOH, 1.5 M $NaNO_3$, and 10^{-5} M $^{99}TcO_4^-$ using the redox-recyclable extractant $HEP^+NO_3^-$.[1] This new type of redox-recyclable extraction and recovery process accomplished three important goals simultaneously: (1) high selectivity with large capacity for the target ion, (2) efficient reuse of the extractant, and (3) recovery of the target ion in a minimal volume. Redox-recyclable materials have been developed by adsorbing highly selective redox-recyclable extractant salts, HEP^+X^-, onto high surface area silica gels.[2,3] These materials have the added advantage that no organic solvents are used once the organometallic complex has been loaded onto the support, unlike the solvent extraction systems. The $HEP^{+/0}$ redox couple was chosen for use in this study based on its success in the development of a liquid-liquid R^2ER process. It was found that the pore size and surface area of the silica gel used as the solid support have a

dramatic effect on the effectiveness of the resulting anion-exchange materials. A support with a high surface area and a large pore diameter (i.e., ≥100 Å) showed the highest capacity (i.e., loading) and selectivity, and also had the shortest cycle time required to completely activate and then deactivate the adsorbed extractant. An aqueous waste simulant consisting of 1 M HNO_3 was chosen so that a direct comparison of selectivity between the new redox-recyclable anion-exchange materials and the commercially available anion exchanger, Reillex™-HPQ (pyridinium and methylated pyridinium ion exchange sites), could be made. The material $HEP^{+}NO_3^{-}/SiO_2$ (1,1',3,3'-tetrakis(2-methyl-2-hexyl) ferrocenium nitrate physisorbed onto silica gel), with a capacity of 0.22 mmol g^{-1}, measured a $K_d^*(ReO_4^-)$ (which takes into account capacity) of 454 mL $mmol^{-1}$, whereas Reillex™-HPQ, with a capacity of 3.34 meq g^{-1}, measured a $K_d^*(ReO_4^-)$ of 87 mL $mmol^{-1}$. It was found, however, that a steady decrease in capacity occurred over multiple cycles, presumably, due to the slow agglomeration of $HEP^{+}NO_3^{-}$ on the SiO_2 surface. There was a 10% drop in capacity over five R^2ER cycles for the $HEP^{+}NO_3^{-}/SiO_2$ material. In comparison, there was a 30% drop in the capacity of Reillex™-HPQ resin over eleven cycles.[4,5]

An important property of any extractant material is its selectivity towards the target ion in complex matrixes. Although one of the primary advantages of redox-recyclable materials is the ability to easily reuse the material, the selectivity of the material is related to the volume of secondary waste upon deactivation of the material. The more selective the extractant material, the greater the fractional composition of the target ion in the secondary waste. In a recent paper by Moyer and Bonnesen,[6] the physical factors that describe the basis for anion separations (selectivity) were outlined. The two predominant factors controlling selectivity in anion separation are solvation environment and the concept of size bias. A simple model generalizing the exchange of anions in a liquid-liquid anion-exchange process is shown in Figure 2.1. Here the

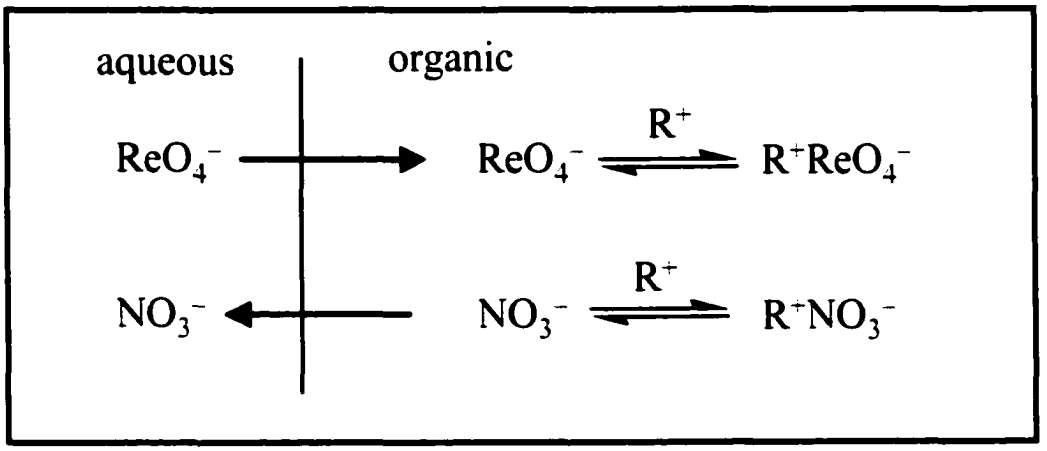

Figure 2.1. Model representing the liquid-liquid exchange of ReO_4^- for NO_3^-. R^+ represents a lipophilic cation soluble in organic solvents.

extractant (R^+) is ion-paired with NO_3^- and is dissolved in the organic solvent. Upon contact with an aqueous solution containing an extractible anion (ReO_4^-), NO_3^- partitions into the aqueous phase while simultaneously, ReO_4^- partitions into the organic phase. This exchange maintains electroneutrality of the system, but electroneutrality does not initiate this exchange. The net driving force for this transfer is the difference in standard Gibbs energy of transfer ($\Delta\Delta G°_{tr}$) for the two ions. This process refers to the removal of an ion from water into the gas phase as the bare ion, and resolvating it in a dry solvent. Therefore, $\Delta\Delta G°_{tr}$ reflects the solvation energy and hydration energy differences between the two ions and the ion-pair energy differences as shown below:

$$\Delta\Delta G°_{tr} \approx \Delta\Delta G°_{hyd} + \Delta\Delta G°_{solv} + \Delta\Delta G°_{ion\text{-}pair} \qquad (1)$$

Let us consider the case where the target ion is ReO_4^- (*aq*), and $R^+NO_3^-$ (*org*) will be used to exchange the anion. Using the example of liquid-liquid extraction, NO_3^- is ion-paired with a lipophilic cation (R^+) and dissolved in an organic solvent. Upon contact with an aqueous solution containing ReO_4^-, NO_3^- replaces ReO_4^- in the aqueous solution as indicated below:

$$ReO_4^-(aq) + R^+NO_3^-(org) \rightleftharpoons NO_3^-(aq) + R^+ReO_4^-(org) \qquad (2)$$

The over all ΔG for this process is:

$$R^+NO_3^-(org) \rightleftharpoons R^+(org) + NO_3^-(org) \qquad \Delta G_{ion\text{-}pair} \qquad (3)$$

$$NO_3^-(org) \rightleftharpoons NO_3^-(aq) \qquad \Delta G_{hyd} \qquad (4)$$

$$ReO_4^-(aq) \rightleftharpoons ReO_4^-(org) \qquad \Delta G_{solv} \qquad (5)$$

$$R^+(org) + ReO_4^-(org) \rightleftharpoons R^+ReO_4^-(org) \qquad \Delta G_{ion\text{-}pair} \qquad (6)$$

The solvation of ReO_4^- requires the unfavorable transfer from the aqueous solution into the organic solvent. The ion-pairing energy of $R^+NO_3^-$ must also be overcome before ReO_4^- can be ion-paired with R^+. These processes both work against the ion-exchange of ReO_4^-. Conversely the transfer of NO_3^- from the organic phase into the aqueous phase is favorable. The hydration energies for ReO_4^- and NO_3^- are –240 and –314 kcal mol^{-1} respectively.[6] Thus, the difference in hydration energy ($\Delta\Delta G°_{hyd}$) is –74 kcal mol^{-1}, which indicates an overall favorable exchange. So the question becomes, how does one minimize the $\Delta\Delta G°_{solv}$ and $\Delta\Delta G°_{ion\text{-}pair}$ in order to take advantage of the favorable $\Delta\Delta G°_{hyd}$? Minimizing $\Delta\Delta G°_{solv}$ can be accomplished by using a solvent with a low dielectric constant. In general, differences in solvation energies become less pronounced in solvents with dielectric constants below 10. Minimizing $\Delta\Delta G°_{ion\text{-}pair}$ can be accomplished by using an organic solvent with a high dielectric constant and using a large extractant. Tight ion-pairs occur in solvents with low-permittivity, therefore, solvents with high dielectic constants will produce ions with lower ion-pair energy. Ion-pairing energy is also inversely dependent on the radius of the ions. According to the modified Born model shown below, there is a 1/r dependence on the Gibbs free energy of transfer ($\Delta\Delta G°_{tr}$).

$$\Delta\Delta G°_{tr}(\text{kJ mol}^{-1}) = B\left(\frac{1}{rY} - \frac{1}{rX}\right)\left(\frac{1}{\varepsilon W} - \frac{1}{\varepsilon S}\right) \qquad (7)$$

Here, B is a temperature independent constant equal to -69.47 kJ nm mol^{-1}, rY and rX are the size of the respective ions, εW is the dielectric of water, and εS is the dielectric of the solvent. Because a low dielectric solvent both helps and hinders the ion-exchange process, the compromise to obtain the most negative $\Delta\Delta G°_{tr}$, is to use a low dielectric solvent but to make the cation (R^+) as large as possible. Work performed by Chambliss et al.[7] demonstrated a point of diminishing returns when increasing the size of R^+. This work compared the selectivity of $HEP^+NO_3^-$ to that of $(heptyl)_4N^+NO_3^-$ by measuring the liquid-liquid extraction of $^{99}TcO_4^-$ from a range of $NaNO_3$ containing solutions. The extraction data was examined by slope analysis and fit with the equilibrium modeling program SXLSQI.[8] The refined equilibrium constants as a result of these experiments suggested that the selectivities are nearly the same for both extractants ($\log K_{exch}$ was 3.86 ± 0.01 for $HEP^+NO_3^-$ and 3.70 ± 0.01 for $(heptyl)_4N^+NO_3^-$). Electrostatic principles predicted that these large cations (r(HEP^+) = 0.600nm and r($heptyl_4N^+$) = 0.548 nm) have reached the point of "diminishing returns", such that a further increase in cation size would yield only a small increase in selectivity. It was also found that the selectivity under these conditions was primarily governed by the difference in the Gibbs energies of solvation, $\Delta G°_{solv}$, and hydration, $\Delta G°_{hyd}$, for the two anions (NO_3^- and $^{99}TcO_4^-$).[7]

In this chapter new strategies to circumvent the problem of diminished selectivity and capacity over multiple cycles are investigated. $HEP^+NO_3^-$ was physisorbed onto a variety of polymeric supports and their extraction efficiencies evaluated. The polymers used in this study varied in both chemical nature and physical nature. The effect of polarity of the polymeric support (aromatic vs. acrylic ester) and physical characteristic (pore size and surface area) are evaluated. The performance of the new materials was evaluated by monitoring ReO_4^- extractions from a variety of matrixes. The effects of loading, pH dependence, recycling efficiency, and base stability were also evaluated.

Also, experiments were designed to measure the selectivity of varying sized ferrocenium cations (0.403 – 0.600 nm) were performed. This was achieved by adsorbing the NO_3^- salts of the tetraalkylated ferrocenium cations onto the acrylic ester polymer XAD-7 and measuring their selectivity towards ReO_4^- from a 1.0 M $NaNO_3$ matrix.

Experimental Section

Materials and Reagents. The compounds 1,1',3,3'-tetrakis(2-methyl-2-propyl)ferrocene (BUT), 1,1',3,3'-tetrakis(2-methyl-2-butyl)ferrocene (PENT), 1,1',3,3'-tetrakis(2-methyl-2-pentyl)ferrocene (HEX), 1,1',3,3'-tetrakis(2-methyl-2-hexyl)ferrocene (HEP), and 1,1',3,3'-tetrakis(2-methyl-2-nonyl)ferrocene (DEC) were prepared using literature procedures.[9] The compounds were oxidized by $AgNO_3$ to make the tetraalkylated ferrocenium nitrate compounds.[1] The following chemicals were Reagent Grade or better and were used as received: $Fe(NO_3)_3 9\ H_2O$ (Fisher), $K_4Fe(CN)_6$ (Fisher), HNO_3 (Mallinckrodt), $KReO_4$ (Aldrich), $Ce(NH_4)_2(NO_3)_6$ (Aldrich), $Na_2S_2O_4$ (Lancaster), toluene (Fisher), dichloromethane (Fisher), and chlorobenzene (Aldrich). The following polymers were purchased from Supelco: Amberlite XAD-2, Amberlite® XAD-4, Amberlite® XAD-7, Amberlite® XAD-16, Amberlite® XAD-2000, Amberlite® GS-1000s, Amberchrom® CG-71C, Diaion® HP2MG, Diaion® SP207, Diaion® S-587, Duolite® S-761, and Supelite® DAX-8. The resins were shipped from the manufacturer wetted in a mixture of methanol and water. Before use, each resin was dried under vacuum at 24 °C until a constant weight was obtained (typically 24 hours). The water used in each experiment was purified and deionized (to 18 MΩ) with a Barnstead NANOPure water purification system, and stored in a 20 L carboy. The pH of the water before use was typically 5–6.

Preparation of $R^+NO_3^-$/Polymer. A known amount of $R^+NO_3^-$ (R^+ = tetraalkylated ferrocenium) was first dissolved in dichloromethane (~30 mL) and then the

dried polymer was added (usually 5.0 g). The solvent was then slowly removed on a rotory evaporator (BÜCHI Rotovapor R-124) operated at 150 rpm with a bath temperature of 30 °C. The material was then dried under vacuum for several hours.

$$\underset{\text{dark green}}{R^{+}NO_3^{-}(org)} + \underset{\text{white}}{\text{polymer beads}(s)} \overset{\text{evaporation}}{\rightleftharpoons} \underset{\text{dark green}}{R^{+}NO_3^{-}/\text{polymer}\ (s)}$$

The amount of $R^{+}NO_3^{-}$ adsorbed onto the polymer beads was determined by washing a known amount of material several times with dichloromethane to remove the ferricenium salt from the polymer, then collecting the washings and diluting to a known volume. The polymer beads returned to their original white color after the $R^{+}NO_3^{-}$ was desorbed. The ratio mmol $R^{+}NO_3^{-}$ per gram of material, was determined by UV-Vis at 686 nm (ε = 455 L mol^{-1} cm^{-1}) from a calibration curve that was linear over the range of 1.0 mM – 0.05 mM $HEP^{+}NO_3^{-}$ in CH_2Cl_2. Note that the visible peak at 686 nm, used for quantifying the alkylated ferroceniums, was the maximum peak height for all compounds in CH_2Cl_2 with an extinction coefficient of 455±5 L mol^{-1} cm^{-1}.

The following polymers were loaded with $HEP^{+}NO_3^{-}$ and the coverage determined as outlined above. The calculated percent of theoretical monolayer, shown in parentheses, was based on surface area measurements provided by the manufacturer and assuming a "foot print" size for $HEP^{+}NO_3^{-}$ of 180 $Å^2$. XAD-2, 0.17 mmol g^{-1} (74%); XAD-4, 0.45 mmol g^{-1} (91%); XAD-16, 0.38 mmol g^{-1} (76%); XAD-1180, 0.35 mmol g^{-1} (87%); XAD-2000, 0.27 mmol g^{-1} (70%); SP207, 0.39 mmol g^{-1} (91%); XAD-7, 0.27 mmol g^{-1} (84%); DAX-8, 0.13 mmol g^{-1} (99%); S-761, 0.20 mmol g^{-1} (85%)

Batch K_d and K_d* Values. The distribution coefficient K_d is the figure of merit for expressing ion-exchange selectivity; in general, the larger the K_d value the more

selective the extractant is for the target ion. For this system the distribution coefficient is defined as:

$$K_d = \frac{\{[\mathrm{Re}]_i - [\mathrm{Re}]_f\}V}{\{\text{mass of } HEP^+NO_3^-/\text{polymer}\}[\mathrm{Re}]_f} \text{ in units of mL g}^{-1}. \quad (8)$$

Alternatively, the distribution coefficient can be expressed as:

$$K_d^* = K_d\left\{\frac{\text{mass of } HEP^+NO_3^-/\text{polymer}}{\text{mmol of adsorbed } HEP^+}\right\} \text{ in units of mL mmol}^{-1}. \quad (9)$$

The distribution coefficients K_d and K_d^* of ReO_4^- for all ion-exchange materials were determined by measuring total Re concentration before and after extractions using inductively coupled plasma atomic emission spectroscopy (ICP-AES) on a Perkin-Elmer P400 spectrometer equipped with a high-salt nebulizer. The emission intensity was monitored at the rhenium line of 221.426 nm. The difference in the initial and final amounts of rhenium, $[Re]_i$ and $[Re]_f$ respectively, follows this ion-exchange equilibrium:

$$HEP^+NO_3^-/\text{support } (s) + ReO_4^-\ (aq) \rightleftharpoons HEP^+ReO_4^-/\text{support } (s) + NO_3^-\ (aq)$$

Calibration curves, which were linear over the concentration range of 1.00–0.010 mM, were constructed using known concentrations of $KReO_4$ in each particular aqueous solution studied (i.e., matrix matching was done for all experiments). For each sample, five readings of the ICP-AES intensity were recorded and averaged. Triton-X-100 (Mallinckrodt), a non-ionic surfactant, was added (1% total) to solutions that contained high concentrations of sodium salts (i.e., 0.02 M and higher). The addition of a non-ionic

surfactant increases the wettability of the sample introduction system and has been shown to increase reproducibility.[10]

Breakthrough Experiments. A column measuring 1 cm i.d. × 9 cm in length with #7 Ace-Thread connectors was dry packed[11] with 1.8 g of 0.38 mmol g^{-1} $HEP^{+}NO_3^{-}$/XAD-7. Aqueous solutions were pumped through the column (3.5 ml min^{-1}) using a Fluid Metering Model QSY pump equipped with a low-flow isolation kit (1/16-in. i.d.). The column was conditioned by pumping distilled and deionized water at 3.5 mL min^{-1} for 15 min (no air pockets were observed in the column after conditioning).

Preparation of Ion-Exchange Columns and Column K_d* Values. The ion-exchange materials were dry-packed into 8 mm i.d. x 43 mm long glass columns with #7 Ace-Thread connectors. Each packed column contained ~ 1.0 g of material. Aqueous solutions were pumped through the columns under similar conditions as outlined above. In each K_d* experiment, the aqueous simulant solution was recirculated through the column until the concentration of all rhenium species were constant (usually 50 min). Initial and final concentrations of rhenium were determined by ICP-AES spectroscopy as described above.

Nitrogen Adsorption BET Surface Area Determination. Nitrogen adsorption experiments were performed on a high-vacuum line equipped with a Rodder Toepler pump, and a Baratron electronic manometer (MKS) was used to measure amounts of nitrogen added to the sample. In a typical experiment, ~1 g of material was dried under reduced pressure until a constant weight was obtained. The flask used in all experiments had a reservoir volume of 23.52 mL and was equipped with Teflon-glass valve and Urry-type glass O-ring joint. The flask was immersed in liquid nitrogen up to the neck of the valve and allowed to equilibrate under constant vacuum. Once the system equilibrated, the Baratron readout was set to zero and nitrogen gas (99.995 % pure) was added to the

sample in 10 Torr increments and allowed to re-equilibrate (usually 15 minutes). Nitrogen gas was added until the final pressure readout was 300 Torr.

Results and Discussion

K_d*(ReO_4^-) Batch Extraction Studies. Initial experiments were carried out to evaluate the effect of loading $HEP^+NO_3^-$ onto a representative polymer, XAD-7 (acrylic ester, 450 $m^2\ g^{-1}$, 90 Å pore diameter). Unlike the technique employed to coat silica gel with $HEP^+NO_3^-$, the organometallic extractants could not be adsorbed from organic solvents onto the polymeric supports. Instead, the extractants were physisorbed, through evaporation techniques,[11] onto the polymer beads (see Experimental Section). Although it is difficult to apply a uniform coverage using the evaporation method, the application of sub-monolayer as well as multi-layer coverages is possible. One of the benefits of controlling coverage is the ability to adjust the capacity of the material. To study the behavior of loading, four separate $HEP^+NO_3^-$/XAD-7 materials were made, differing in the number of millimoles of $HEP^+NO_3^-$ loaded per gram of polymer beads. The four loadings were 0.10, 0.19, 0.28, and 0.43 mmol g^{-1}. The loadings may be related to the area of surface covered; a loading of ~0.41 mmol g^{-1} corresponds to nominal monolayer coverage of the manufacturer-specified BET surface area of the polymer beads. Batch distribution ratio $K_d^*(ReO_4^-)$, which takes into account loading, was determined for each of the four extractant/support materials. In a typical experiment, a 0.200 g sample of $HEP^+NO_3^-$/XAD-7 was shaken with an aqueous solution containing 0.50 M $NaNO_3$ and 1.00 mM $KReO_4$. After a specified amount of time, the mixture was filtered and the final aqueous concentration of ReO_4^- was determined by ICP atomic emission spectrophotometry. Figure 2.2 is a family of plots showing $K_d^*(ReO_4^-)$ over time for the four materials. The curves are least-squares fits to the following exponential function with two adjustable parameters, K_d^* and k:

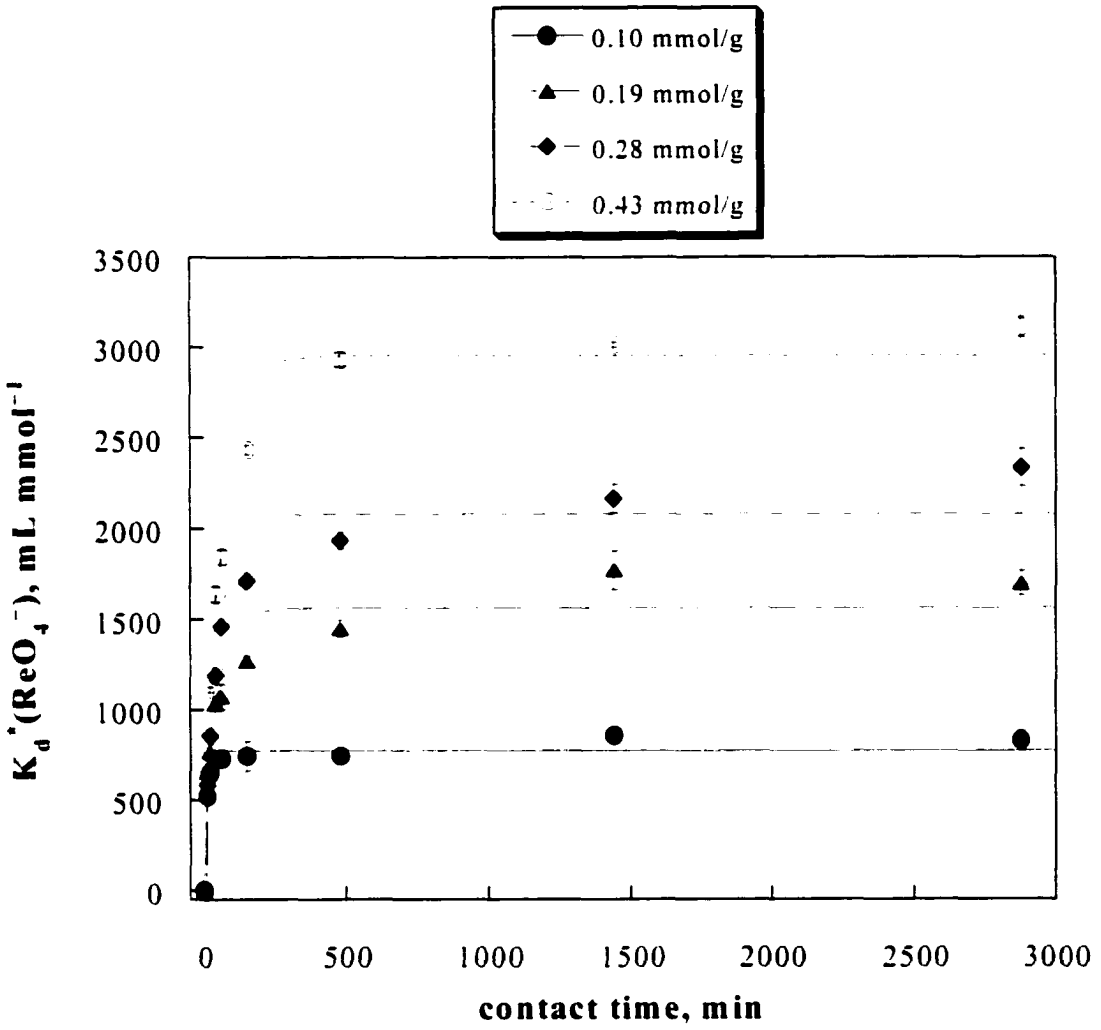

Figure 2.2. A family of plots showing the extraction of ReO_4^- from 0.5 M $NaNO_3$. The figure illustrates the approach to ion-exchange equilibrium for four $HEP^+NO_3^-$/XAD-7 materials, with 0.10, 0.19, 0.28, and 0.43 mmol of $HEP^+NO_3^-$ per gram XAD-7. The error bars are an average of three samples. The curves are least-squares fits to the general exponential function $K_d^*(t) = [K_d^*][1 - e^{-kt}]$.

$$K_d^*(t) = [K_d^*][1 - e^{-kt}] \quad (10)$$

where $K_d^*(t)$ is the kinetic, non-equilibrium distribution coefficient at time t, K_d^* is the maximum equilibrium value of the distribution coefficient, and k is the time constant, a measure of the rate of ion-exchange. As an example, the least-squares values of k and K_d^* for the 0.10 mmol g^{-1} material are 0.12(2) min^{-1} and 726(8) mL $mmol^{-1}$, respectively.

An important trend in Figure 2.2 is that K_d^*, the equilibrium ion-exchange selectivity of the material, increases as the coverage increases and approaches a maximum value as the loading approaches nominal monolayer coverage (~0.41 mmol g^{-1}). Figure 2.3 shows a plot of $K_d^*(ReO_4^-)$ vs. increased loading of $HEP^+NO_3^-$ onto the acrylic ester polymer, XAD-7. Recall that K_d^* takes into account loading; therefore, the K_d^* for each material should show the same selectivity regardless of concentration (if every extractant molecule is accessible). Let us assume a simple model for the loading of $HEP^+NO_3^-$ onto the polymer surface; one in which the surface density of HEP^+ cations is uniform at all coverages. The trend in the plots in Figure 2.2 and Figure 2.3 can be understood as follows. Below monolayer coverage, the extractant material becomes more selective as the HEP^+ cation coverage increases. This result demonstrates that the HEP^+ cations do not act independently of each other on the surface of the polymer. They act cooperatively, and the degree of cooperativity increases as the coverage increases, and hence, as the distance between neighboring HEP^+ cations decreases. This type of cooperation should reach a maximum effect once monolayer coverage is reached. Another possible explanation is that the surface dielectric changes as the loading of $HEP^+NO_3^-$ increases. As was reported in earlier work[10] the dielectric of the solvent used in liquid-liquid extraction effected the extent of the

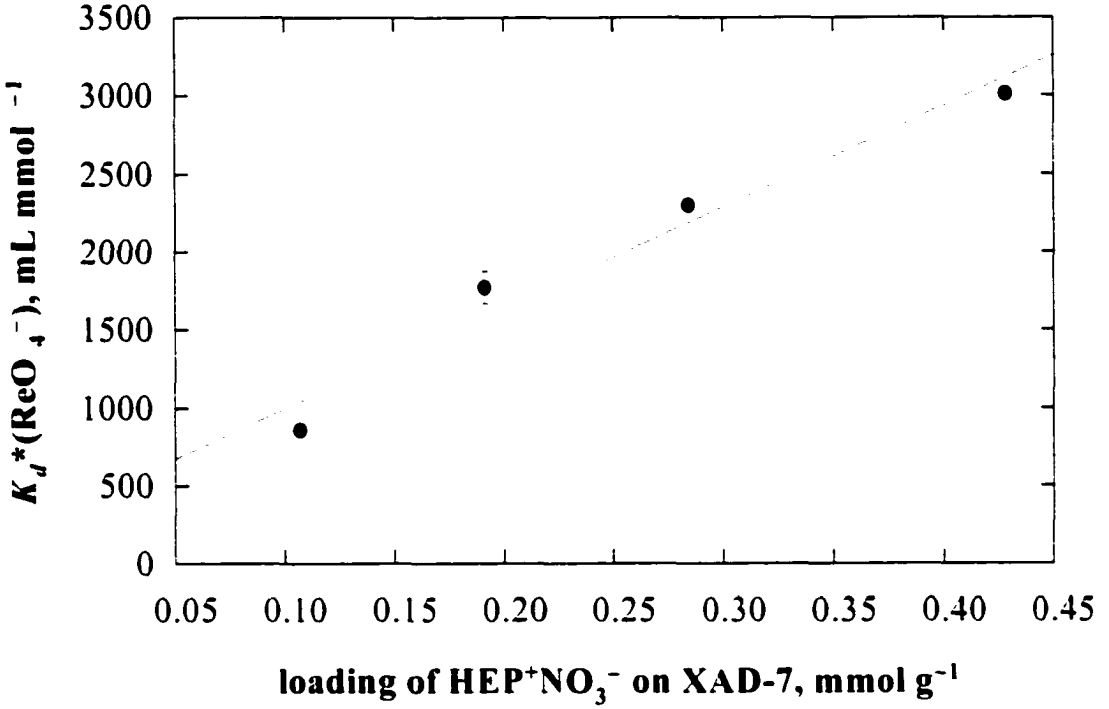

Figure 2.3. Plot of $K_d^*(ReO_4^-)$ vs. loading of $HEP^+NO_3^-$ onto the acrylic ester polymer, XAD-7. The error bars are an average of three samples. The line is the best linear fit to the data.

equilibrium of exchange (i.e., selectivity of the extractant). Generally, the lower the dielectric of the solvent, the greater the size bias towards larger anions.[6] The effects on selectivity caused by the dielectric in a liquid-liquid system could also play a role in the case of solid-liquid extraction. The more non-polar the surface of the material, the lower the dielectric of the surface. This should increase selectivity towards larger anions, but this is complicated because non-polar polymers tend to be less wettable then more polar polymers. A more easily wetted material should allow better access to all the ion-exchange sites within the material. Conversely, if the material was highly non-polar (polyaromatic) the aqueous solution would have a more difficult time reaching into the pores and accessing the ion exchange sites that may be buried within the matrix of the material. It is possible that loading $HEP^{+}NO_3^{-}$ onto the polymer surface changes either the dielectric of the material or the wettability, or perhaps, both. Therefore, the effect of increasing $K_d^*(ReO_4^-)$ with increasing coverage of $HEP^{+}NO_3^{-}$ could be the result of a decrease in dielectric of the material along with increase in wettability. However, dielectric analyzer (DEA) scans of uncoated XAD-7 and XAD-7 loaded with 0.01 and 0.42 mmol g^{-1} $HEP^{+}NO_3^{-}$ showed that increasing the loading of $HEP^{+}NO_3^{-}$ increased the permittivity of the material from 1.0 to 1.5. The actual numbers were 1.0, 1.3, and 1.5 for uncoated XAD-7, 0.01 mmol g^{-1}, $HEP^{+}NO_3^{-}$/XAD-7 and 0.42 mmol g^{-1} $HEP^{+}NO_3^{-}$/XAD-7, respectively. This suggests that the ionic extractant physisorbed onto the surface of a polymer increases the dielectric of the material. An increase in dielectric should cause a decrease in K_d^* (which takes into account loading) according to equation 7. This suggests that an increase in dielectric decreases bias (selectivity) towards larger anions. However, an increase in K_d^* as more $HEP^{+}NO_3^{-}$ was loaded onto XAD-7 was observed, suggesting that a change in dielectric may only be one factor in the effectiveness of the material. It may be that the increase in dielectric of the material changes the wettability, allowing better access to the ion-exchange sites.

Another effect observed with increased loading was an increase in the time required to reach equilibrium. In general, the more extractant loaded onto the surface of the polymer, the longer it took to reach equilibrium. As can be seen in Figure 2.4 the rate of anion-exchange, derived from equation 10, decreased as the loading of $HEP^+NO_3^-$ on XAD-7 increased. This suggests that accessibility to all anion-exchange sites becomes hindered as more extractant was loaded on to the polymer. It is not clear whether or not the pores of the polymer were filled. It is reasonable to assume that at low loadings the pores are simply coated along with the surface of the polymer. At higher loadings, however, the pores may become filled with extractant. Once the pores are filled, the HEP^+ molecules buried deep within the pores may no longer be accessible to the aqueous solution. To determine if the surface area was affected by the physisorption of extractant molecules onto the polymer surface, the surface area of the materials was measured using nitrogen adsorption methods.[12] The surface area of the material can be obtained from the adsorption isotherm of nitrogen gas. One of the best-known methods for determining surface area using gas adsorption isotherms is the BET method. Brunauer, Emmet, and Teller (BET)[12,13] developed a series of equations that use isotherms of inert gas adsorption on surfaces to calculate surface area. The BET equation is shown below:

$$\frac{p}{V(p_s - p)} = \frac{1}{cV_m} + \frac{(c-1)}{cV_m} \times \frac{p}{p_s} \qquad (11)$$

where p_s denotes the saturated vapor pressure above the liquid phase of the gas, V_m is the volume of the gas adsorbed when the surface is covered by a single layer, V is the volume adsorbed at dynamic equilibrium, p is the pressure at dynamic equilibrium, and c is a constant. Plotting values of $p/V(p_s - p)$ against p/p_s gives a straight line with intercept $a = 1/cV_m$ (cm^{-3}) and slope $b = (c - 1)/cV_m$ (cm^{-3}). The constant c and the

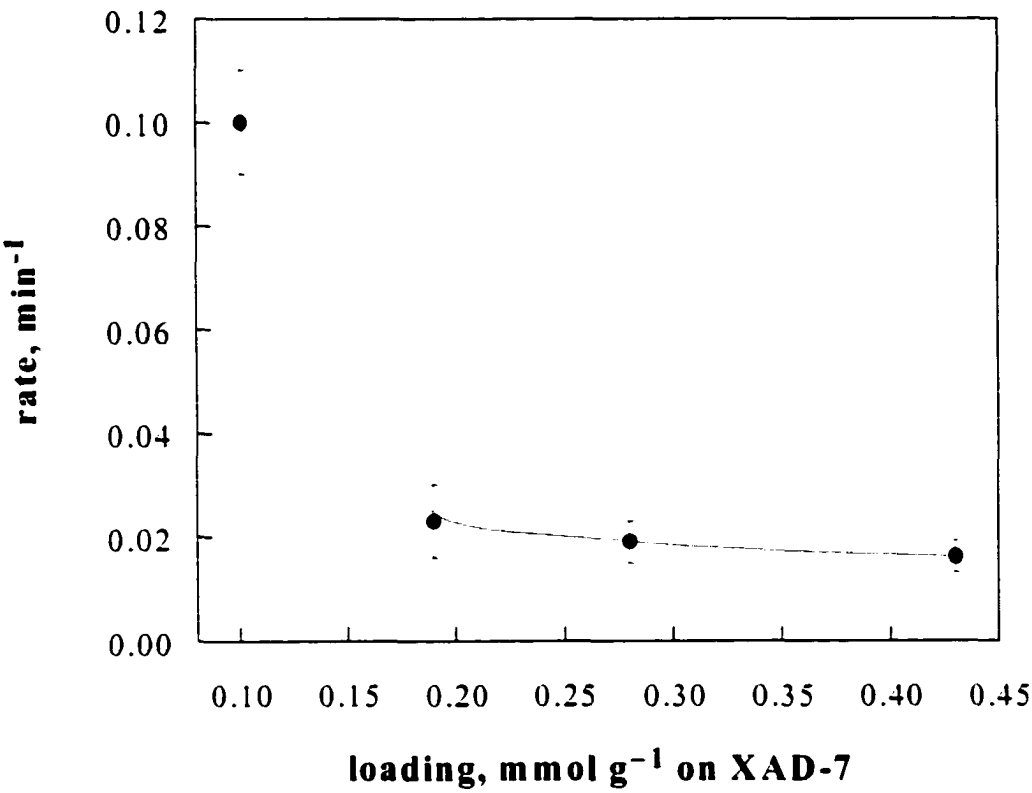

Figure 2.4. Rate of anion-exchange of ReO_4^- for NO_3^- verses loading of $HEP^-NO_3^-$ on XAD-7. The rate is derived by fitting $K_d^*(ReO_4^-)$ vs. time curves to the equation $K_d^*(t) = [K_d^*][1 - e^{-kt}]$. The error bars represent the average extraction rate of three separate samples.

volume V_m can be calculated from the two equations. The number of moles (z) taken up by the surface is given by $z = V_m/22.41$ (if nitrogen is the inert gas used) where V_m will occupy a total area, $S = 6.023 \times 10^{23} \times z \times s$ (m^2) ($s = 16.2 \times 10^{-20}$ m^2 for nitrogen). The specific surface will accordingly be $S_{sp} = S/g$ (m^2 g^{-1}) where g is the gram weight of the sample. In a typical experiment 1.0 g of the material was placed in a Shlenk flask and nitrogen gas introduced incrementally until the pressure above the sample (immersed in liquid nitrogen) reached 300 Torr (see Experimental Section for more detail). The data was then plotted as described above and the surface area calculated. As a control experiment, the surface area of the unmodified XAD-7 polymer was measured and compared to published measurements. The surface area measured for XAD-7 was 470(20) m^2 g^{-1} (average of 3 measurements), which is in agreement with reported measurements of 450 m^2 g^{-1} for XAD-7. The surface areas of 0, 26, 103, 206, and 300 percent loading of $HEP^+NO_3^-$ on XAD-7 were measured, and a plot of BET surface area vs. loading is shown in Figure 2.5. There was a steady decrease in surface area as the loading of $HEP^+NO_3^-$ increased. The material lost more then 90% of its surface area at 300% loading. This indicated that the surface, including the pores, were coated and filled with the extractant during the physisorption process. As was described previously, the rate of extraction decreases as loading increases. This could be a result of multilayer loading on the polymer surface and within the pores, blocking immediate access to extractant molecules buried underneath the outer extractant molecules. To minimize the effects of multilayer loading, the majority of the studies were carried out using materials with monolayer or submonolayer loading except where noted.

Stability of $HEP^+NO_3^-$ Anion-Exchange Materials. As reported in previous work[2], there was a decrease observed in the value of $K_d(MO_4^-)$ (M = transition metal) with $HEP^+NO_3^-/SiO_2$ material over long contact times (greater then 20 minutes). At shorter contact times the material was highly selective towards both TcO_4^- and ReO_4^-

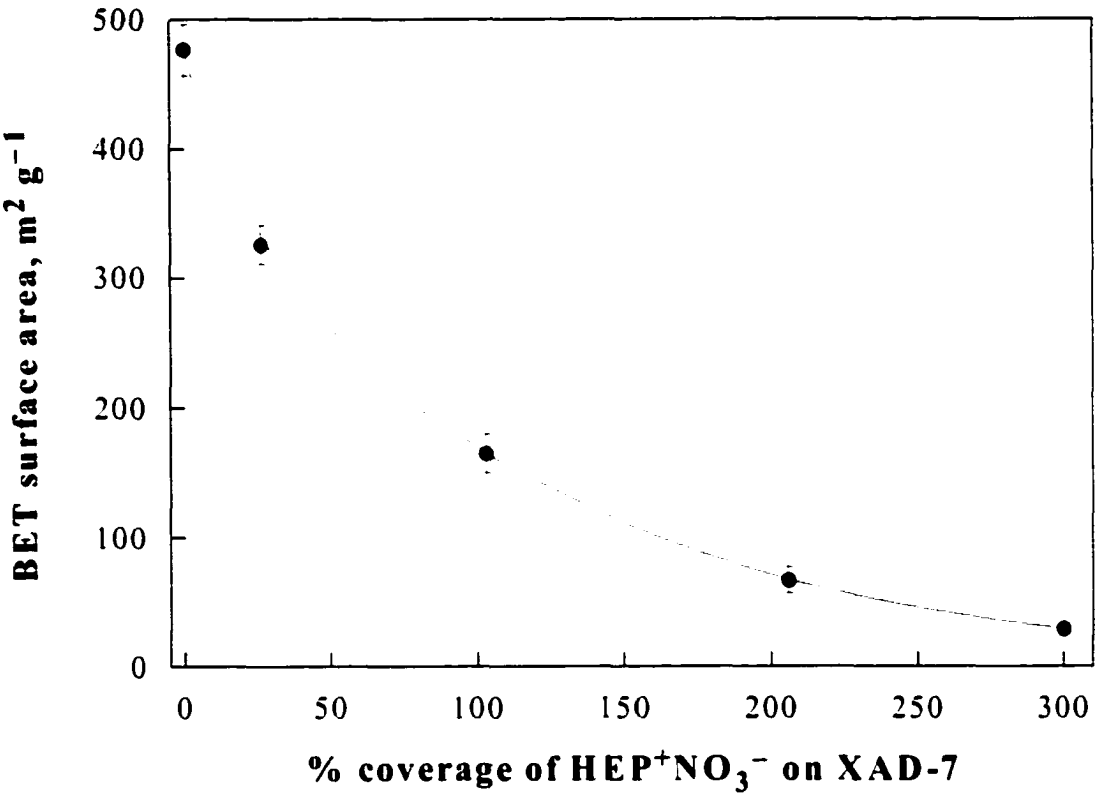

Figure 2.5. Nitrogen absorption BET surface area of increasing amounts of $HEP^+NO_3^-$ loaded onto XAD-7. Error bars for the loading of $HEP^+NO_3^-$ on XAD-7 represent an average of three samples. Error bars for the BET surface area represent and average of two measurements per sample. The data point for 300 % coverage is a single point determination. The line is a simple exponential fit to the data.

but at longer contact times there was an observed decrease in $K_d(MO_4^-)$ indicating a decrease in stability over time. Figure 2.6 shows plots of $K_d(TcO_4^-)$ versus contact time for the extraction of TcO_4^- from 0.060 M, 0.30 M and 1.00 M aqueous $NaNO_3$ using $HEP^+NO_3^-/SiO_2$. Again, at short contact times the material appears to have a higher $K_d(TcO_4^-)$ with lower $NaNO_3$ concentrations (lower concentration of competing anion). However, over longer contact times, the $K_d(TcO_4^-)$ decreases in all solutions indicating a loss in stability. The decrease in stability was attributed to the agglomeration of the $HEP^+NO_3^-$ on the surface of the silica gel. A similar study was carried out using $HEP^+NO_3^-$/XAD-7 to compare the stability of this new material to that of $HEP^+NO_3^-/SiO_2$. In this study, 0.200 g of $HEP^+NO_3^-$/XAD-7 with 0.25 mmol g^{-1} loading, was contacted for various amounts of time with aqueous solutions containing 0.10, 0.30 or 1.00 M $NaNO_3$ with 0.60 mM ReO_4^-. As can be seen in Figure 2.7, which shows $K_d(ReO_4^-)$ over time with increasing concentrations of $NaNO_3$, there is a decrease in $K_d(ReO_4^-)$ with increasing concentration of $NaNO_3$, but in every case the material reached a constant $K_d(ReO_4^-)$ at long contact times. The observed stability of $HEP^+NO_3^-$/XAD-7 at long contact times is in contrast to $HEP^+NO_3^-/SiO_2$ which showed lower effectiveness over time. The trend observed at short contact times with $HEP^+NO_3^-$/XAD-7 was similar to the behavior observed with $HEP^+NO_3^-/SiO_2$ which showed an increase in $K_d(MO_4^-)$ with decreased concentration of $NaNO_3$. This behavior was consistent with the assumption that the extraction of MO_4^- by $HEP^+NO_3^-$ is governed by the simple anion-exchange equilibrium as show below:

$$HEP^+NO_3^-/\text{support}\ (s) + MO_4^-\ (aq) \rightleftharpoons HEP^+MO_4^-/\text{support}\ (s) + NO_3^-\ (aq)$$

Increasing NO_3^- concentration in the aqueous solution should cause the equilibrium to lie further to the left (less MO_4^- extracted). These studies indicate, however, that the

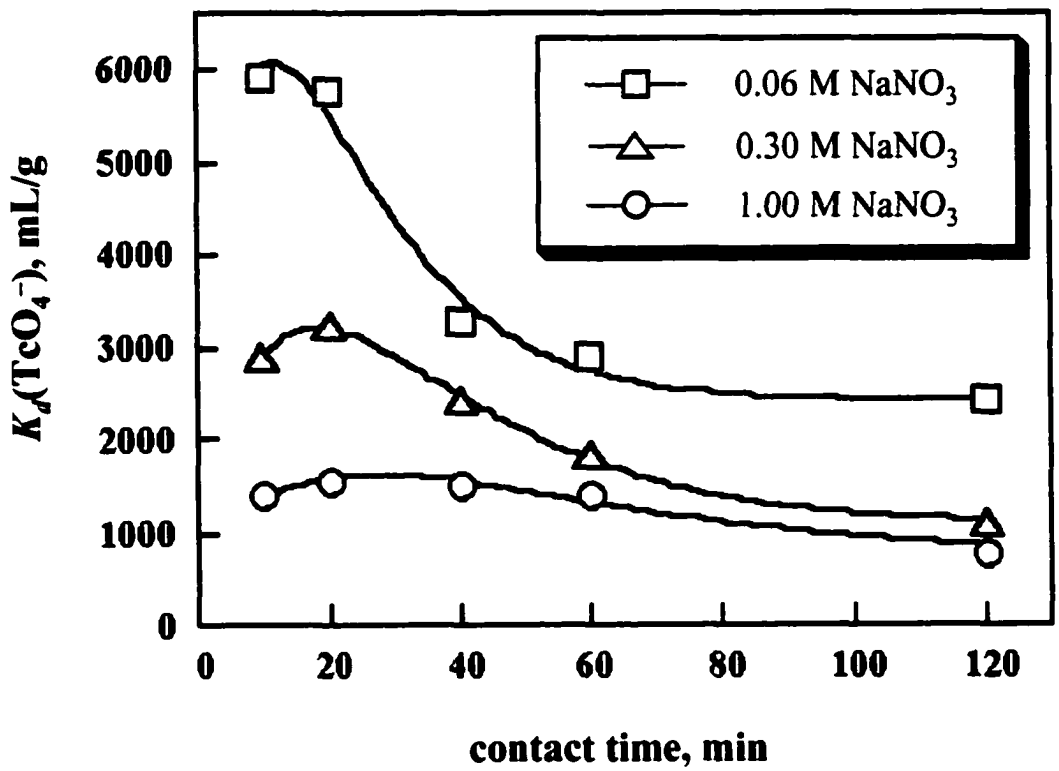

Figure 2.6. Plot of $K_d(TcO_4^-)$ vs. contact time for the extraction of 5×10^{-5} M TcO_4^- from aqueous solutions containing various concentrations $NaNO_3$ by $HEP^+NO_3^-/SiO_2$. (Reprinted with permission from reference 3. Copyright 1998 Colorado State University.)

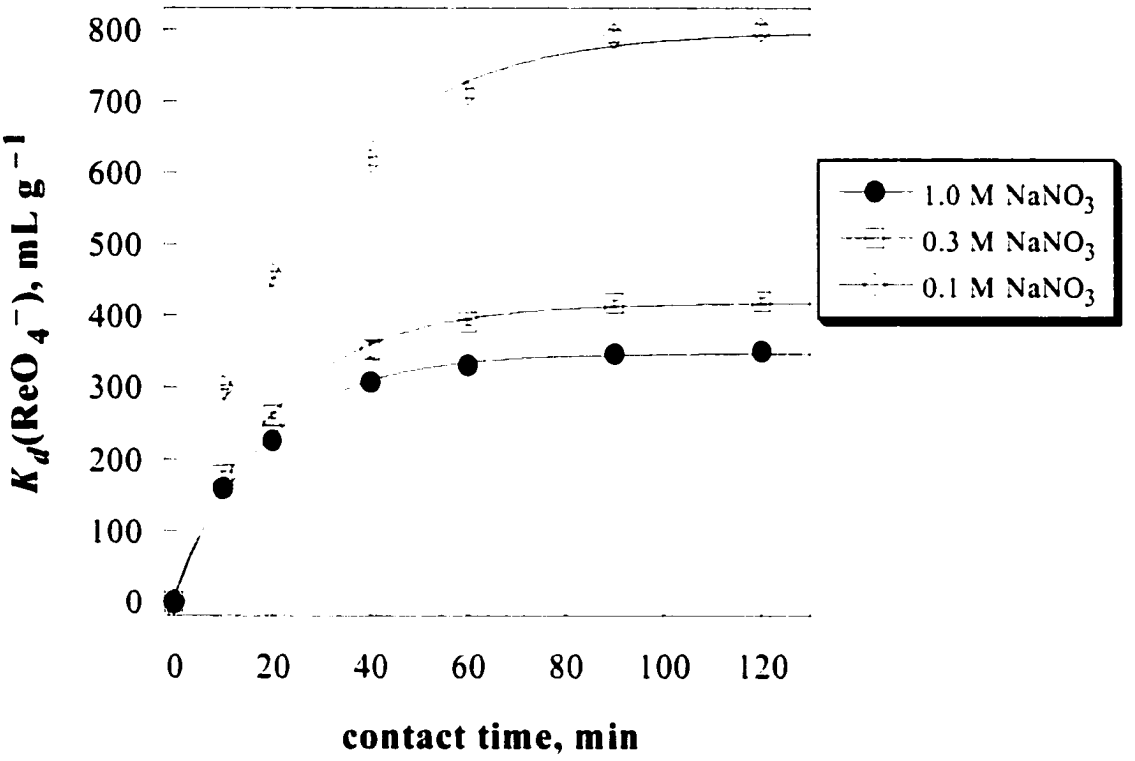

Figure 2.7. Plot of $K_d(ReO_4^-)$ vs. contact time for the extraction of 6×10^{-4} M ReO_4^- from aqueous solutions containing various concentrations of $NaNO_3$ by $HEP^+NO_3^-$/XAD-7 with 0.25 mmol g^{-1} loading. The error bars represent an average of three samples. The curves are a least-squares fit to the general exponential function $K_d^*(t) = [K_d^*][1 - e^{-kt}]$.

support used to immobilize $HEP^+NO_3^-$ plays an active role in the stability and effectiveness of the material.

Stability of $HEP^+NO_3^-$/XAD-7 in the Presence of Base. Earlier work using $HEP^+NO_3^-$ to extract $^{99}TcO_4^-$ from simulated nuclear waste with liquid-liquid extraction techniques[14] found that at short contact times $HEP^+NO_3^-$ was able to extract $^{99}TcO_4^-$ even in the presence of a strong base.[1] Although $HEP^+NO_3^-$ has been found to be a very selective extractant for ReO_4^- and $^{99}TcO_4^-$, this was a surprising result because there is literature precedence for the nucleophilic decomposition of ferrocenium compounds in the presence of base.[15] Nucleophilic decomposition has been observed with ferrocenium salts in organic solutions after contact with aqueous solutions containing 1 M NaOH. In general, 18% decomposition and 82% reduction of the ferrocenium cation occurred under these conditions.[10] Although there are several studies concerning the stability of ferrocenium in basic solutions,[15,16] the decomposition products formed are not well characterized. The following reaction shows one possible route for the nucleophilic decomposition of ferrocenium cations:

$$3\ FeCP'_2{}^+X^- + n\ OH^- \longrightarrow 2\ FeCP'_2 + Fe(OH)_3 + P \qquad (12)$$

where X = MO_4^-, CP′ = alkyl substituted ferrocenes and P = unidentified reaction products. Several factors govern the rate of decomposition including the dielectric of the solvent (tight ion-pairs usually lead to faster decomposition/reduction), the reduction potential of the ferrocenium cation, and the strength of the nuclophile.[10,15,16] Decomposition/deactivation of the ferrocenium cation could take minutes or days depending on the environment. It seemed fitting to explore the extent and rate of decomposition/deactivation of $HEP^+NO_3^-$ once loaded onto a polymeric support. The extraction of ReO_4^- by $HEP^+NO_3^-$/XAD-7 was studied in the presence of a strong base

consisting of 1.0 M $NaNO_3$, 0.1 M NaOH and 0.3 mM $KReO_4$. This type of study was not possible for the $HEP^+NO_3^-/SiO_2$ material because of the instability of silica gel (i.e., solid support) in basic solutions. Figure 2.8 shows a plot of $K_d(ReO_4^-)$ as a function of contact time. Initially, the K_d increases, but after 40 minutes the K_d starts to decrease, suggesting the material loses effectiveness over time. After 20 hours in contact with the highly basic solution, the material showed little capacity for ReO_4^-. At the end of the experiment, there was a color change observed in the $HEP^+NO_3^-$/XAD-7 material from a dark green to a light orange-green color. Recall that the green color indicates oxidized (active) extractant material, whereas, orange indicates reduced (deactivated) material. It is reasonable to assume that the decrease in K_d over time was caused by the decomposition/deactivation of $HEP^+NO_3^-$ by OH^- present in the aqueous solution as described by equation 12. It is possible that the decrease in K_d could also be caused by agglomeration or elution off of the solid support of the extractant material, but the color change of the material at the end of the experiment suggests that deactivation/degradation had occurred. A portion of the extractant material that had been in contact with the basic solution for 20 hours was washed with dichloromethane, which desorbed the extractant from the material. A UV-Vis spectrum was taken of this solution and it was found that the peak at 686 nm (the major peak for oxidized $HEP^+NO_3^-$) had decreased and that the peak at 486 nm (the major peak for reduced HEP) had increased compared to the original material. This experiment showed about 80% of the $HEP^+NO_3^-$/XAD-7 material had been deactivated after 20 hr in the presence of base. In order to determine if the extractant had decomposed or simply deactivated a portion of the material that was in contact with the basic solution for 20 hr was re-activated using $Fe(NO_3)_3$. The material was than washed, dried, and the extractant desorbed using dichloromethane. A UV-Vis spectrum was taken of this solution and the peaks at 686 nm and 486 nm compared to the peaks observed for the original material. It was found that the material lost 15% of its

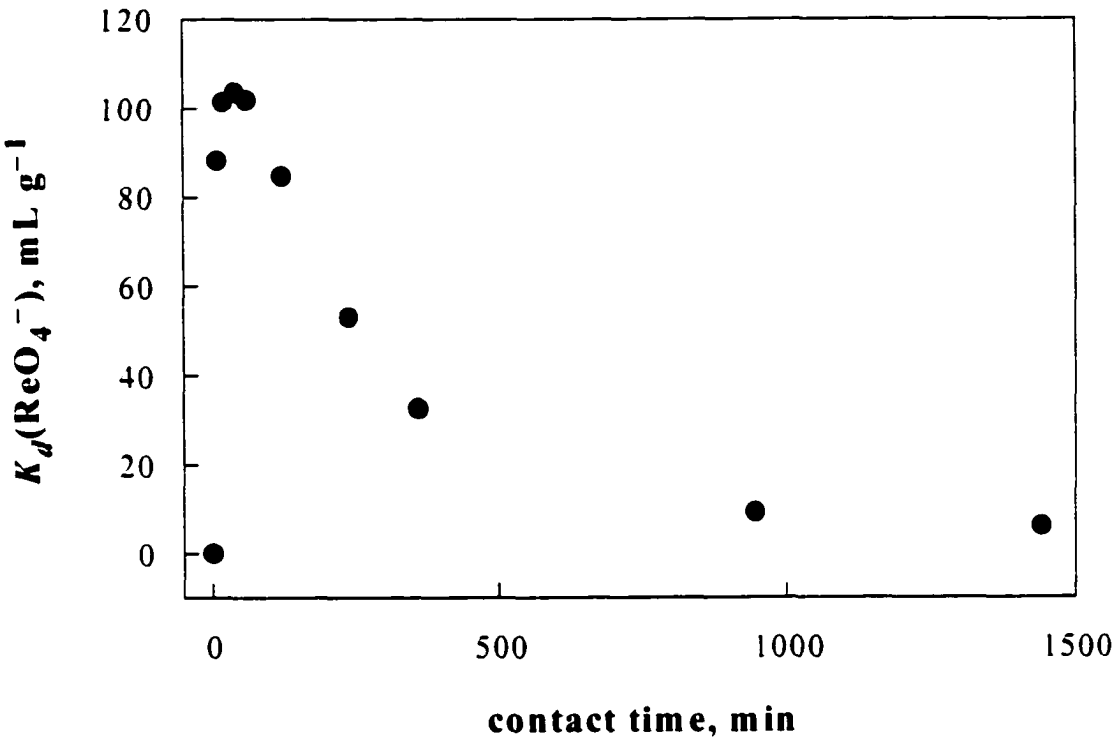

Figure 2.8. Batch distribution coefficients (K_d) for extraction of 3×10^{-4} M ReO_4^- from 1.0 M $NaNO_3$ and 0.1 M NaOH using $HEP^+NO_3^-$/XAD-7. Each sample contained ~0.2 g of $HEP^+NO_3^-$/XAD-7 and 10 mL of simulant and was shaken horizontally in a scintillation vial for time indicated. Errors in the K_d measurements are ±5%.

original capacity after contact with a basic solution. Therefore, it appears that both deactivation and decomposition are occurring with a basic solution. Even though the material decreases in capacity over time in the presence of base, the extractant could conceivably be used in basic solutions as long as the contact time in the aqueous solution was limited to less then 40 min. Figure 2.9 shows a comparison between the extraction of ReO_4^- from a 1.0 M $NaNO_3$ solution and from a solution containing 1.0 M $NaNO_3$ and 0.1 M NaOH. There was a dramatic difference in $K_d(ReO_4^-)$ between the two matrixes indicating the majority of the extractant in the basic solution was deactivated or degraded. This study suggests that $HEP^+NO_3^-$ undergoes nucleophilic decomposition/deactivation in the presence of strong base even when physisorbed onto a solid support.

Selectivity Dependence of $HEP^+NO_3^-$/XAD-7 on pH. The distribution coefficients K_d^* were measured with varying pH in aqueous solutions containing known concentrations of NO_3^- and ReO_4^- for three ion-exchange materials. The initial pH was varied by adjusting the aqueous concentration of HNO_3 while maintaining constant ionic strength of 1.0 M NO_3^- with $NaNO_3$. As shown in Figure 2.10, the value of $K_d^*(ReO_4^-)$ approached a limiting value of ~750 mL $mmol^{-1}$ as the pH was increased from 0.0 to 7.8, indicating the selectivity of $HEP^+NO_3^-$/XAD-7 for ReO_4^- increases with increasing pH. A similar behavior was observed with $HEP^+NO_3^-/SiO_2$.[2] The actual values of the distribution ratio for the samples with initial pH 0.0, 0.9, 1.9, 3.0 and 7.8 were 303, 539, 718, 768 and 750 mL $mmol^{-1}$, respectively. The cause of the increase in K_d^* with increasing pH is presently unknown. It is unlikely that the $HEP^+NO_3^-$ is desorbing from the polymeric support during the extraction experiment. The same behavior was observed with $HEP^+NO_3^-$ loaded on silica gel with both ReO_4^- and TcO_4^- therefore it is unlikely that the support is causing the decrease in K_d^* with lower pH. One possible explanation is that there is protonation of the MO_4^- anion in the aqueous solution. This

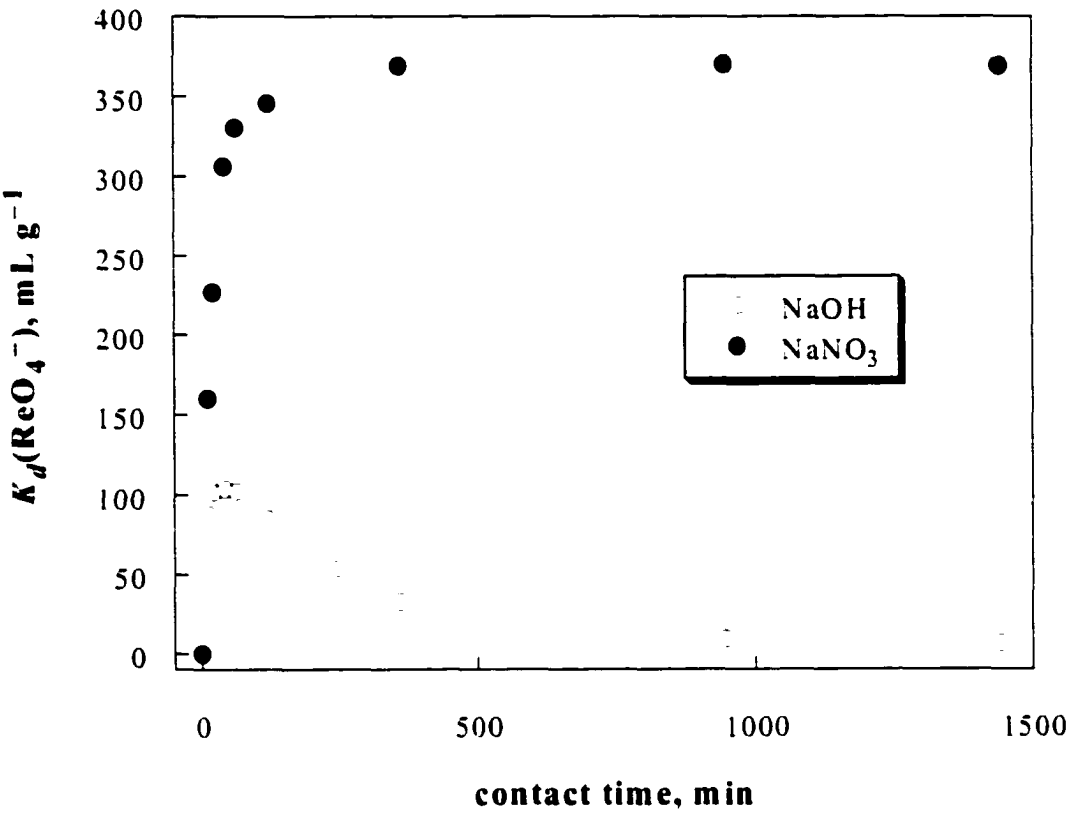

Figure 2.9. Comparison of $HEP^+NO_3^-$/XAD-7 distribution ratios, $K_d(ReO_4^-)$, from 1.0 M $NaNO_3$ and from a solution containing both 1 M $NaNO_3$ and 0.1 M NaOH. Each sample contained ~0.2 g of $HEP^+NO_3^-$/XAD-7 and 10 mL of simulant and was shaken horizontally in a scintillation vial for time indicated.

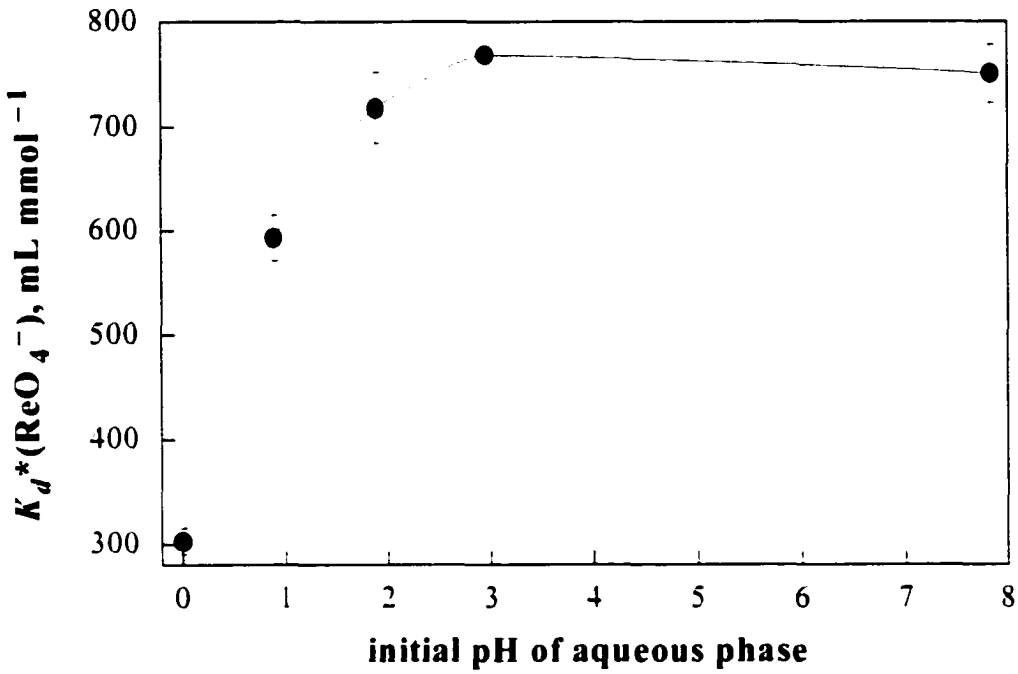

Figure 2.10. Plot of $K_d^*(ReO_4^-)$ vs. initial pH of the aqueous phase. The distribution ratios (K_d^*) were measured for the extraction of 0.5 mM ReO_4^- from aqueous HNO_3 by the 0.32 mmol g^{-1} $HEP^+NO_3^-$/XAD-7 material. The line is a simple best fit to the data. The pH was adjusted with HNO_3 and the total concentration of NO_3^- was maintained at 1.0 M by adding the appropriate amount of $NaNO_3$.

type of phenomenon has been noted in the literature.[3–5,17,18] It is possible that protonation follows the equilibrium process shown below:

$$H_3O^+(aq) + MO_4^-(aq) \rightleftharpoons HMO_4(aq) + H_2O(l) \qquad (13)$$

The neutral species is presumed to not be extracted through anion-exchange. Thus, the presence of a form of the target anion that can not be extracted ($HReO_4$ or $HTcO_4$) would cause a decrease in the observed distribution ratio. However, this type of protonation has not been observed for either TcO_4^- or ReO_4^- even at 6 M H_3O^+.[19,20] One possible explanation that was put forth by Chambliss[3] suggested that at lower pH values a hydrogen dinitrate anion species could be formed ($H(NO_3)_2^-$) which could effectively compete with MO_4^- for the exchange sites on $HEP^+NO_3^-$/support. The net effect of this competition would decrease the equilibrium constant and thus the $K_d(MO_4^-)$. Whatever the case, the overall effect of decreasing pH decreases the $K_d(MO_4^-)$ and appears to be independent of the solid support used to immobilize $HEP^+NO_3^-$.

Comparison of Commercial Polymers Used as Solid Support for $HEP^+NO_3^-$. To evaluate the effect of solid support on the selectivity of the anion-exchange material, $HEP^+NO_3^-$ was physisorbed onto a variety of commercially available polymeric resins. In this set of experiments the extractant ($HEP^+NO_3^-$) was physisorbed at nominal monolayer loadings onto the polymeric supports. Table 2.1 lists the physical characteristics and chemical nature of the polymers used in this experiment. As can be seen in Table 2.1 the polymers vary in their chemical nature and also in physical nature including surface area, pore size, and polarity. To evaluate extraction performance of the new materials, the kinetic as well as the thermodynamic selectivity were measured by determining $K_d^*(ReO_4^-)$ at 20 min and 48 hr contact times. The loading of $HEP^+NO_3^-$ ranged from 0.13 to 0.45 mmol g^{-1} depending on the surface area of the polymer (see

Table 2.1. Physical Characteristics of Polymers[22] Used as Solid Supports for $HEP^+NO_3^-$.

trade name	polymer type[a]	chemical nature[b]	mean surface area, $m^2\ g^{-1}$	mean pore diam., Å	size of beads
XAD-2	aromatic	NP, PHO	300	90	20–60 mesh
XAD-4	aromatic	NP, PHO	725	40	20–60 mesh
XAD-16	aromatic	NP, PHO	800	100	20–60 mesh
XAD-1180	aromatic	NP, PHO	600	300	20–60 mesh
XAD-2000	aromatic	NP, PHO	580	42	20–60 mesh
SP207	bromostyrene	NP, PHO	650	105	20–60 mesh
XAD-7	acrylic ester	MP, PHI	450	90	20–60 mesh
DAX-8	acrylic ester	MP, PHI	160	225	40–60 mesh
S-761	phenol-formaldehyde[c]	P, PHI	300	600	16–50 mesh

[a] Aromatic = co-polymer of divinylbenzene and various styrenes. [b] NP = nonpolar; IP = intermediate polarity; MP = moderately polar; P = polar; PHO = hydrophobic; PHI = hydrophilic. [c] This resin has methylol functional groups.

Experimental Section for loadings of all polymers). To compare each material equally K_d* (mL $mmol^{-1}$) was used instead of K_d (mL g^{-1}) in order that the loading of $HEP^+NO_3^-$ could be taken into consideration, not just the weight of the material and the amount of ReO_4^- extracted per unit volume. Table 2.2 lists the distribution ratio, K_d*, for the extraction of ReO_4^- from 1.0 M $NaNO_3$. In every case the 20 min K_d* was lower then the 48 hr K_d*, but it is interesting to note that the $\%K_d(ReO_4^-)_{48hr}$ after 20 min varies depending on both the chemical nature of the polymer and the physical nature of the polymer. Figure 2.11 is a plot of extraction rate expressed here as $\%K_d(ReO_4^-)_{48hr}$ after 20 min vs. the polarity of the support. The trend observed in this plot indicates that the rate of extraction increases with increasing polarity of the polymeric support.

Wu and Dekker[22] derive the polarity (χ^p) of polymers using the following equations:

$$\gamma = \gamma^d + \gamma^p \quad (13)$$

$$\chi^p = \gamma^p/\gamma \quad (14)$$

where, γ is the surface tension and depends on the surface chemical composition and density of the material, γ^d is the dispersion component arising from the dispersion-force interactions, and γ^p, the polar component arising from various dipolar and specific interactions. The polarity χ^p is independent of temperature. Polysytrene co-polymers (XAD-2000, XAD-16, XAD-1180, XAD-2 and XAD-4) are known to have polarities in the range of 0.15–0.17,[23] polyacrylate co-polymers (XAD-7 and DAX-8) have polarities in the range of 0.21–0.28.[23] Although no specific numbers were found for phenol-formaldehyde (S-761) it can be assumed that the polarity is above 0.29. Exact polarities are not know for the polymer resins used in this study, but according to the manufacture, styrene divinylbenzene polymers are considered non-polar (0.10–0.19), the acrylic ester

Table 2.2. Distribution Ratio (K_d*, mL mmol^{-1}) for ReO_4^- Extraction from 1.0 M $NaNO_3$ Using $HEP^+NO_3^-$ on Various Solid Supports.

anion-exchange material[a]	K_d* 20 min[b]	K_d* 48 hour[b]	(rate) $\%K_d$*$_{48hr}$ after 20 min	polarity[c]
$HEP^+NO_3^-$/XAD-2000	4	1610	0.2	NP
$HEP^+NO_3^-$/XAD-16	58	1840	3.2	NP
$HEP^+NO_3^-$/SP207	41	948	4.3	NP
$HEP^+NO_3^-$/XAD-2	50	682	7.3	NP
$HEP^+NO_3^-$/XAD-4	123	1325	9.3	NP
$HEP^+NO_3^-$/XAD-1180	188	1308	14.4	NP
$HEP^+NO_3^-$/XAD-7	724	1441	50.2	MP
$HEP^+NO_3^-$/DAX-8	771	1426	54.1	MP
$HEP^+NO_3^-$/S761	192	216	89.3	P

[a] Coverage of $HEP^+NO_3^-$ was 82–100% of monolayer for all materials. [b] Extraction of ReO_4^- from 1 M $NaNO_3$. Relative standard deveation ≤ 5%. [c] Polarity of polymers: NP = nonpolar, MP = moderately polar, P = polar. See Table 2.1 for more information on the physical characteristics of the polymers.

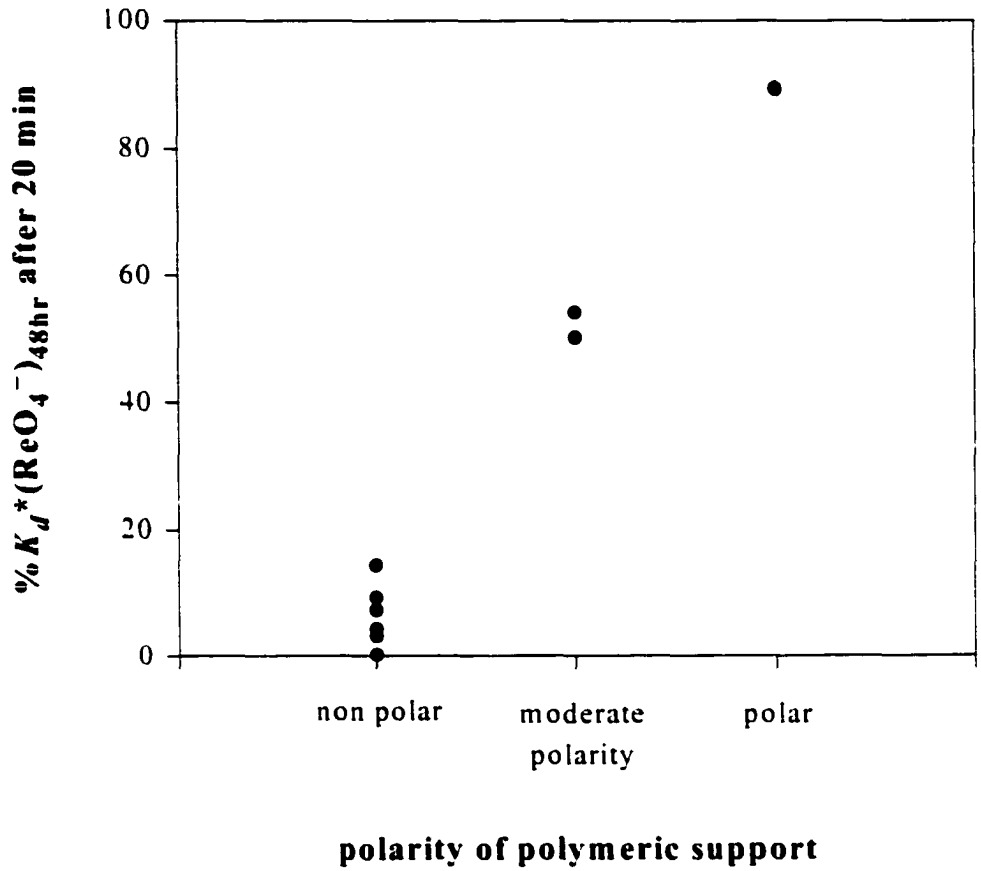

Figure 2.11. Plot of rate of extraction of ReO_4^- from 1.0 M $NaNO_3$ by $HEP^+NO_3^-$ expressed as $\%K_d$* of 48 hr after 20 min verses polarity of polymeric support. The polarity units are arbitrary, the actual polarity of the polymeric supports are unknown.

polymers are considered moderately polar (0.20–0.28) and the phenol-formaldehyde polymer is considered polar (0.29 and higher).

Taking a closer look at the polyaromatic resins (XAD-2000, XAD-16, XAD-1180, XAD-2 and XAD-4), the major differences in these polymers were the surface area and porosity. A comparison of surface area verses $\%K_d(ReO_4^-)_{48hr}$ after 20 min shows no real correlation. Likewise, a comparison of pore size verses $\%K_d(ReO_4^-)_{48hr}$ after 20 min indicates no real correlation but the ratio of surface area to pore size compared to the rate of extraction does produce a trend. Figure 2.12 shows a plot of $\%K_d(ReO_4^-)_{48hr}$ after 20 min verses the ratio of surface area to pore size expressed as m g^{-1}. It is assumed that both surface area and pore size effect the rate of extraction and by taking the ratio of surface area to pore size, both affects are taken simultaneously into account. The plot in Figure 2.12 indicates that materials with large pores (100 Å), and relatively small surface areas, allow faster ion-exchange kinetics. Whereas materials with small pores (42 Å) and larger surface areas, tend to slow down the exchange rate. This is presumably due to the small pores becoming clogged with $HEP^+NO_3^-$, effectively blocking access, or at least fast access, to the extractant molecules buried within the pores. It is possible that at higher loadings the material with larger pores will also have relatively slower anion-exchange rates due to the pores becoming blocked. This same trend was observed when $HEP^+NO_3^-$ was loaded onto a variety of silica gels. It was observed that $HEP^+NO_3^-$ on silica gel with a 40 Å pore diameter had a lower K_d and took longer to recycle (oxidize and reduce), as compared to the 100 Å pore diameter material.[2]

Comparison of $HEP^+NO_3^-$/XAD-7 Material with Commercial Resins. As was described earlier in this chapter, the selectivity towards a target anion depends on factors such as the differences in hydration energy of the perspective anions, the dielectric of the system, and the size of the extractant. One of the conclusions presented

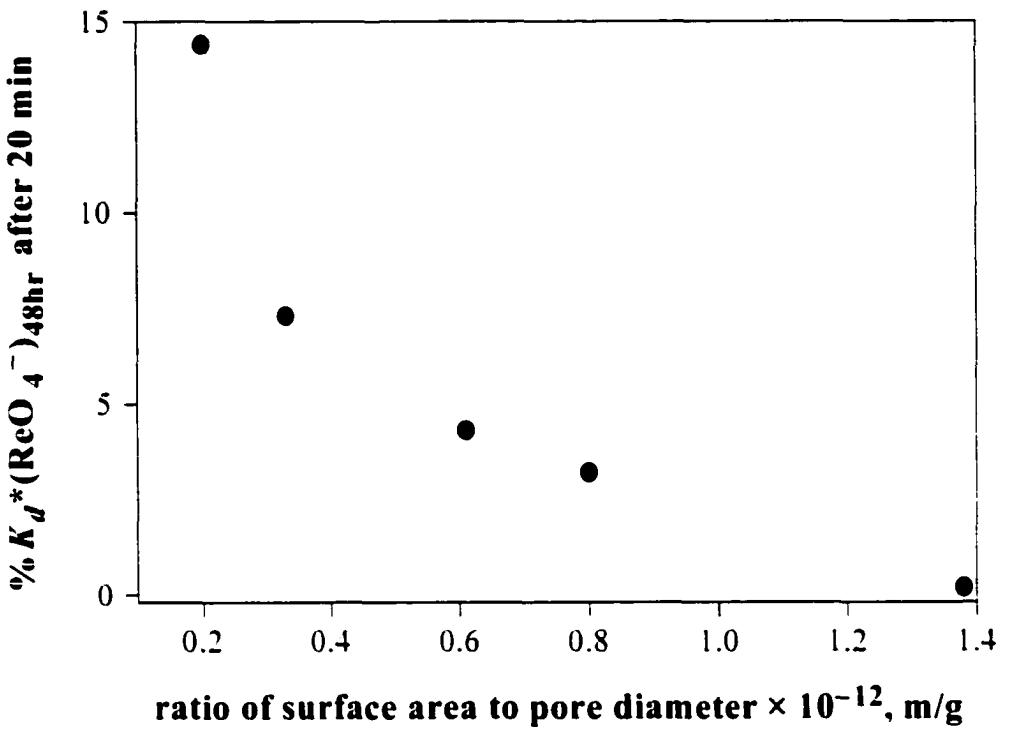

Figure 2.12. Plot of rate of extraction expressed as %K_d*(48hr) after 20 min vs. surface area divided by the pore diameter. In general, a low ratio reflects a polymer with large pore size and low surface area.

by Moyer et al. was that there is a point of "diminishing returns" on selectivity when increasing the size of the extractant. This conclusion was supported by Chambliss,[3] where modeling predicted minimal selectivity increases using cations with radii larger then 0.600 nm. Studies using commercially available anion-exchange resins showed an increase in selectivity as the size of the exchange site increased which supports the assumption that the size of the exchange site (up to a certain point) has a large effect on selectivity. It is important to note that the time needed to reach equilibrium becomes greater as the size of the exchange site in the resin becomes larger. Work performed by Chambliss[7,24] measured the selectivity of four commercially available anion-exchange resins for TcO_4^-. The resins increased in size of cation ion-exchange site from P–NMe_3^+, to P–NEt_3^+, to P–NPr_3^+, to P–NBu_3^+, where P denotes polymer backbone and Me, Et, Pr, and Bu are methyl, ethyl, propyl and butyl groups respectively. Figure 2.13 is a plot of the percentage of the $K_d^*(TcO_4^-)_{48h}$ value observed for a 20 min contact for commercial anion-exchange resins with increasing size of exchange sites. The observed trend was that the equilibrium $K_d^*(TcO_4^-)$ increased as the size of the cationic ion-exchange site increased. The increase in selectivity was consistent with a systematic decrease in the contribution of Gibbs free energy of ion-pairing terms to the overall free energy for extraction with increasing cation size, as described by equations 1 and 7. Another trend observed in Figure 2.13 was that the more selective the resin, the slower the rate of anion-exchange. The optimal case for ion-exchange resins would be to have high selectivity (high $K_d^*(MO_4^-)$) with fast kinetics (large % $K_d^*(MO_4^-)_{48hr}$ after 20 min). A comparison of the commercial anion-exchange resins with $HEP^+NO_3^-$/XAD-7 under similar extraction conditions shows this material does not follow that trend (Figure 2.14). The $HEP^+NO_3^-$/XAD-7 material was approximately three times more selective than Sybron®-Ionac SR-6 after 48 hr, but reached 39% of its $K_d^*(TcO_4^-)_{48hr}$ after 20 min. In comparison Sybron®-Ionac SR-6 reached only 23% of its $K_d^*(TcO_4^-)_{48hr}$ after

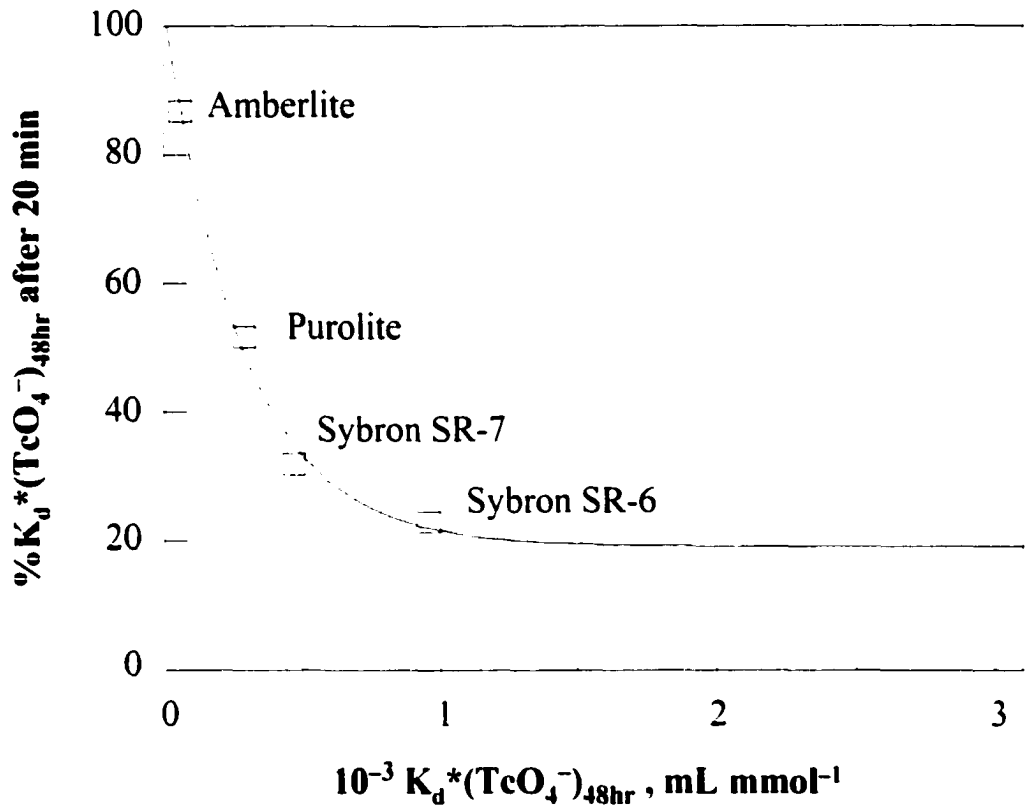

Figure 2.13. Plot showing the relationship between anion-exchange rate (i.e., fractional attainment of K_d*($^{99}TcO_4^-$)$_{48hr}$ for a 20-min contact) and anion-exchange selectivity for the extraction of 1.0 x 10^{-5} M $^{99}TcO_4^-$ from aqueous 1 M $NaNO_3$ for four commercial anion-exchange resins (Amberlite = Amberlite® IRA-900 (P–NMe_3^+), Purolite = Purolite® A-520E (P–NEt_3^+), Sybron SR-7 = Sybron®-Ionac SR-7 (P–NPr_3^+), Sybron SR-6 = Sybron® Ionac SR-6 (P–NBu_3^+)). (Reprinted with permission from reference 3. Copyright 1998 Colorado State University.) The line is a simple exponential fit to the four data points.

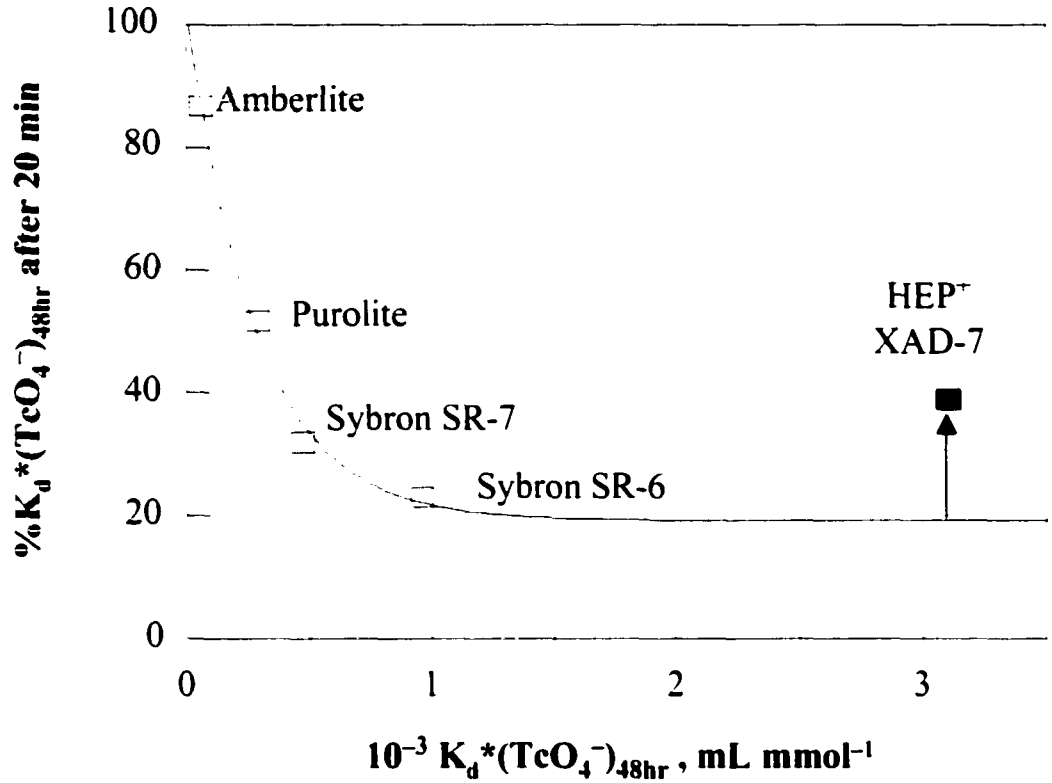

Figure 2.14. Plot showing the relationship between anion-exchange rate (i.e., fractional attainment of $K_d^*(^{99}TcO_4^-)_{48h}$ for a 20-min contact) and anion-exchange selectivity for the extraction of 1.0 x 10^{-5} M $^{99}TcO_4^-$ from aqueous 1 M $NaNO_3$ for four commercial anion-exchange resins (Amberlite = Amberlite® IRA-900 ($P–NMe_3^+$), Purolite = Purolite® A-520E ($P–NEt_3^+$), Sybron SR-7 = Sybron®-Ionac SR-7 ($P–NPr_3^+$), Sybron SR-6 = Sybron® Ionac SR-6 ($P–NBu_3^+$)) and the redox-recyclable anion-exchange material 0.25 mmol g^{-1} $HEP^+NO_3^-$/XAD-7. (Reprinted with permission from reference 3. Copyright 1998 Colorado State University.) The line is a simple exponential fit to the first four data points.

20 min. A tentative conclusion is that the new redox-recyclable material $HEP^+NO_3^-$/XAD-7 exhibits both faster ion-exchange kinetics and greater selectivity due to the interfacial nature of the anion-exchange sites.

Determining Selectivity of Various Sized Tetraalkylated Ferrocenium Cations. The ability to easily adjust the size of alkylated ferrocenes by altering the length of the alkyl chains lends a unique opportunity to study the effect of cationic size on the selectivity of the material. A variety of tetraalkylated ferrocenes ranging from BUT^+ to DEC^+ (see Experimental Section) were evaluated for their selectivity towards ReO_4^- in order to better understand the effect of size of the ferrocenium cation on selectivity. In this study, $BUT^+NO_3^-$, $PENT^+NO_3^-$, $HEX^+NO_3^-$, $HEP^+NO_3^-$, and $DEC^+NO_3^-$ were loaded onto XAD-7 and were used to extract ReO_4^- from 1.0 M $NaNO_3$. Figure 2.15 shows a plot of $K_d^*(ReO_4^-)_{24hr}$ for the extraction of ReO_4^- from 1.0 M $NaNO_3$ with $BUT^+NO_3^-$/XAD-7, $PENT^+NO_3^-$/XAD-7, $HEX^+NO_3^-$/XAD-7, $HEP^+NO_3^-$/XAD-7, and $DEC^+NO_3^-$/XAD-7. As expected, the $K_d^*(ReO_4^-)_{24h}$ increased as the size of the tetraalkylated ferrocenium cation increased. The actual values were 330, 600, 680, 840 and 1000 mL $mmol^{-1}$ for $BUT^+NO_3^-$/XAD-7, $PENT^+NO_3^-$/XAD-7, $HEX^+NO_3^-$/XAD-7, $HEP^+NO_3^-$/XAD-7, and $DEC^+NO_3^-$/XAD-7, respectively. The trend in Figure 2.15 shows that the magnitude of the selectivity increase becomes smaller as the size of the cation becomes larger. The selectivity increase between BUT^+ and $PENT^+$ was 270 mL $mmol^{-1}$, whereas, the increase between HEP^+ and DEC^+ was only 160 mL $mmol^{-1}$. This observation follows the concept outlined by Moyer et al.,[6] wherein there was a point of "diminishing returns" on selectivity as the size of the extractant increased. It is interesting to note that $DEC^+NO_3^-$/XAD-7 was found to be more selective then $HEP^+NO_3^-$/XAD-7. Recall that there was a predicted point of "diminishing returns" with cations larger then HEP^+ (r = 0.600 nm), but what was observed here was a higher $K_d^*(ReO_4^-)_{24hr}$ for the material with the larger DEC^+ cation

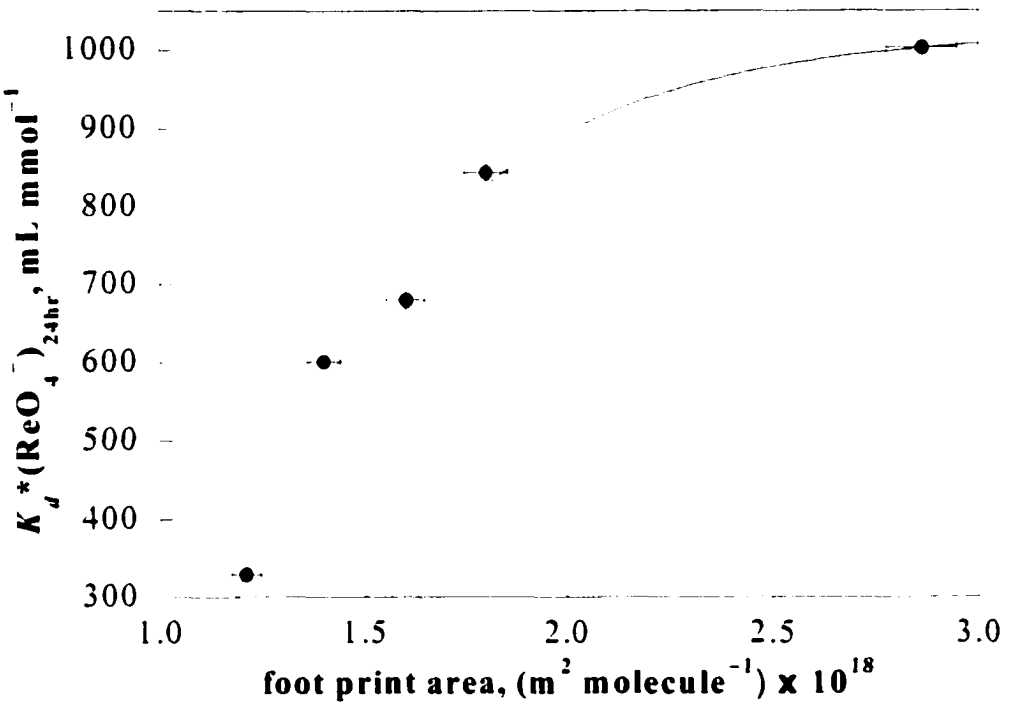

Figure 2.15. Plot of $K_d^*(ReO_4^-)$ for the extraction of ReO_4^- from 1.0 M $NaNO_3$ with increasing size of tetraalkylated ferrocenium nitrate. Error bars represent an average of three samples. The footprint size of $BUT^+NO_3^-$, $HEP^+NO_3^-$ and $DEC^+NO_3^-$ were determined from their crystal structures. The footprint size for $PENT^+NO_3^-$ and $HEX^+NO_3^-$ were derived by theoretical calculations based on the sizes of BUT, HEP and DEC. The error on the foot print size represents $\pm 3\sigma$. The curve is a least-squares fit to the general exponential function $K_d^*(t) = [K_d^*][1 - e^{-kt}]$.

(840 mL $mmol^{-1}$ for $HEP^{+}NO_3^{-}$/XAD-7 and 1000 mL $mmol^{-1}$ for $DEC^{+}NO_3^{-}$/XAD-7). It is possible that physisorbing the extractants onto a solid support allows better access to the extractants then what was allowed in organic solvents. A phenomenon that has been known to occur in organic solvents is dimerization or aggregation of the extractant at high concentrations and at high loadings. This was found to occur with $HEP^{+}NO_3^{-}$ at concentrations above 0.03 M in chlorobenzene and at loadings of greater then 0.003 M TcO_4^{-} in the organic phase.[7] This type of phenomenon causes a lowering of distribution ratio ($D(MO_4^{-})$ values, therefore, when attempting to increase capacity or selectivity in a liquid-liquid system, increasing concentration of the extractant or increasing the size of the extractant would only be effective up to the point of aggregation. It may be possible that loading the extractant onto a solid support circumvents such problems by not allowing the extractant molecules to aggregate. It has already been shown that $HEP^{+}NO_3^{-}$ agglomerates on silica gel when in contact with aqueous solutions which causes lower $K_d^{*}(MO_4^{-})$ values but this effect was not observed when $HEP^{+}NO_3^{-}$ was loaded onto polymeric supports. Another possible explanation could be that the dielectric of the surface of the polymer changes to a greater degree with larger extractants (per mmol) then with smaller extractants. In other words, a greater portion of the surface may be covered per mmol as the size of the extractant increases. A change in dielectric of the material might be just one of the effects of loading extractants onto solid supports, there might also be a decrease in surface area and pore size, which might also affect the performance of the material. Regardless of the cause, the overall effect of increasing the size of the extractant (R^{+}) loaded onto XAD-7 seems to be an increases in the selectivity of the material for ReO_4^{-}.

A more detailed examination of the change in $K_d^{*}(ReO_4^{-})_{48hr}$ with increased loadings of $HEP^{+}NO_3^{-}$ and $DEC^{+}NO_3^{-}$ onto XAD-7 is shown in Figure 2.16. The $DEC^{+}NO_3^{-}$/XAD-7 material shows a higher $K_d^{*}(ReO_4^{-})_{48hr}$ value at equal loadings of

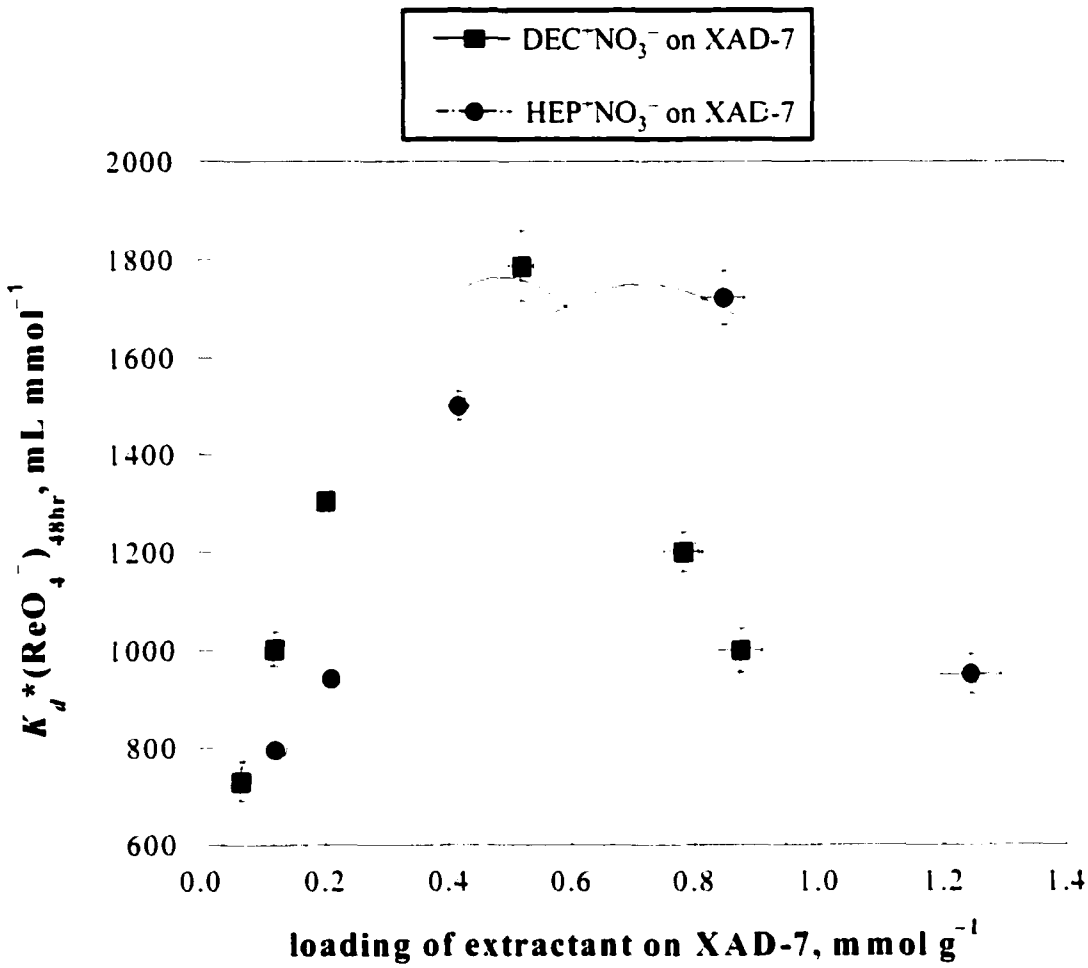

Figure 2.16. Plot of $K_d^*(ReO_4^-)$ from 1.0 M $NaNO_3$ vs. loading (mmol g^{-1}) of $HEP^+NO_3^-$ and $DEC^+NO_3^-$ on XAD-7. Note that 0.26 mmol g^{-1} and 0.41 mmol g^{-1} represent a theoretical monolayer for $DEC^+NO_3^-$ and $HEP^+NO_3^-$, respectively. Lines are a simple quadratic regression fit to the data points.

$HEP^+NO_3^-$/XAD-7 up to ~0.50 mmol g^{-1}. This observation indicates that the size and not a change in the dielectric or wettability of the surface was the major factor in the selectivity of the material. At loadings above 0.50 mmol g^{-1} for $DEC^+NO_3^-$/XAD-7 and 0.87 mmol g^{-1} for $HEP^+NO_3^-$/XAD-7 there was a decrease in K_d* suggesting that some fraction of the extractant was unable to undergo ion-exchange. However, as was mentioned earlier, DEA scans of the material showed an increase in dielectric as more $HEP^+NO_3^-$ was loaded onto XAD-7. This suggests that the addition of ionic extractants onto the surface of the polymer changes the dielectric of the material. Alternatively, if the K_d*(ReO_4^-) for each material are compared at their respective theoretical monolayer loading (0.26 mmol g^{-1} for $DEC^+NO_3^-$/XAD-7 and 0.41 mmol g^{-1} for $HEP^+NO_3^-$/XAD-7), the K_d*(ReO_4^-)'s were approximately the same. This observation would suggest that when the surface was covered in equal proportions with either $DEC^+NO_3^-$ or $HEP^+NO_3^-$, the effectiveness would be about the same for both materials.

Figure 2.17 shows the % coverage verses K_d*(ReO_4^-) for both $HEP^+NO_3^-$ and $DEC^+NO_3^-$ on XAD-7. This plot shows that the effectiveness (selectivity) was approximately the same at similar coverages for both $HEP^+NO_3^-$/XAD-7 and $DEC^+NO_3^-$/XAD-7. This would suggest that the effects of loading play a larger role in the overall selectivity of the material then the size of the extractant. Similar selectivities for both materials (up to 200% loading) agree with modeling data, which suggests that cations larger then HEP^+ will produce little increase in selectivity. At loadings above200% it appeared that the material loaded with $HEP^+NO_3^-$ had a lower K_d*(ReO_4^-). It may be that the smaller HEP^+ extractant becomes blocked within the material to a greater extent compared to the larger DEC^+ extractant, which might cause a lower K_d*. It is interesting to note that a drop in K_d* was not observed until the loadings were well above theoretical monolayer coverages. The assumption that the extractant molecule adheres to the surface in only one orientation would most likely not be an

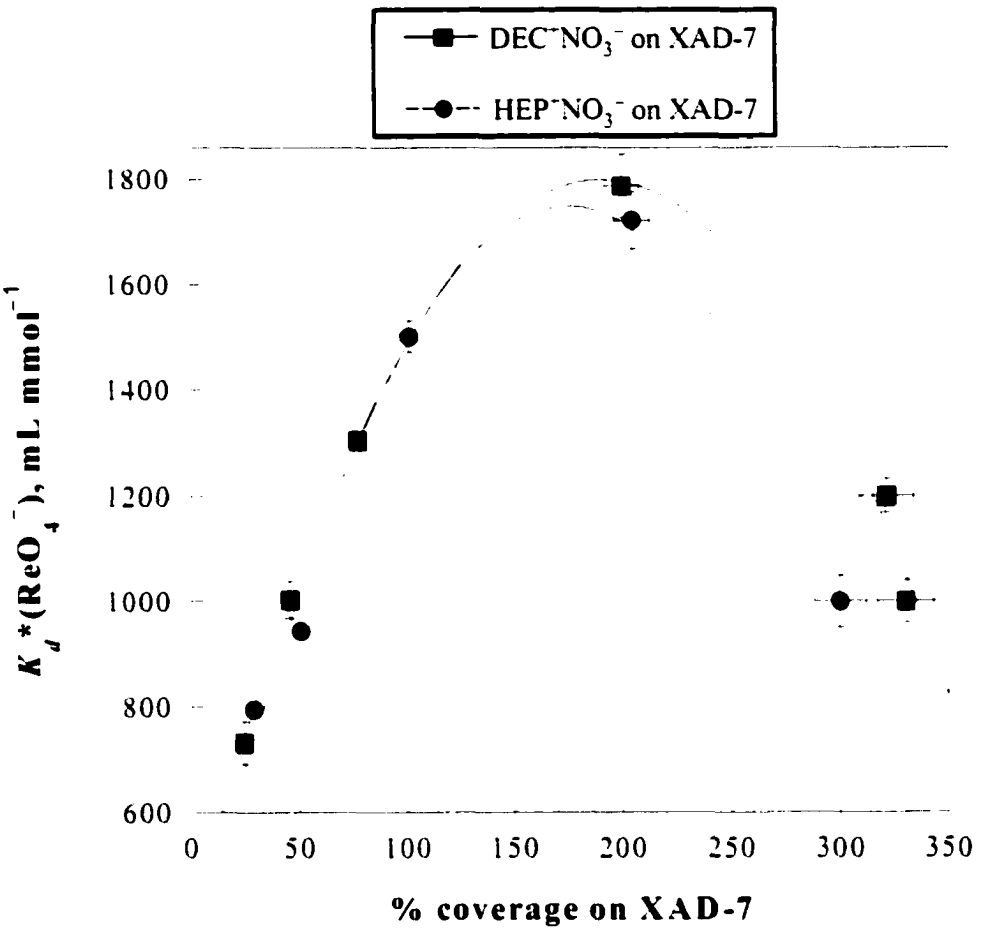

Figure 2.17. Plot of $K_d^*(ReO_4^-)$ from 1.0 M $NaNO_3$ vs. % coverage of $HEP^-NO_3^-$ and $DEC^-NO_3^-$ on XAD-7. Error bars represent an average of three samples. Lines are a simple quadratic regression fit to the data points.

accurate portrayal of the physisorption process. There are several orientations of the extractant on the surface that could occur, which could cause variations in coverage. However, useful information can be obtained by assuming one type of orientation with which to compare various materials. Whatever the case might be, there was an increase in selectivity for both $DEC^+NO_3^-$/XAD-7 and $HEP^+NO_3^-$/XAD-7 as more extractant was loaded onto the polymer up to ~200% loadings, at which point the selectivity per mmol extractant decreased. As was shown in Figure 2.15, the $K_d^*(ReO_4^-)$ measured for $BUT^+NO_3^-$, $PENT^+NO_3^-$, $HEX^+NO_3^-$, $HEP^+NO_3^-$, and $DEC^+NO_3^-$ (increasing foot print area) indicated an increase in selectivity for ReO_4^- as the size of the extractant increased. In that study, the % coverage was not held constant; therefore, the coverage and not the size of the extractant might cause the selectivity to change. Figure 2.18 shows the foot print area of the ferrocenium cation and % coverage verses $K_d^*(ReO_4^-)_{24hr}$ for each material. When $K_d^*(ReO_4^-)_{24hr}$ was plotted against % coverage for DEC^+ and HEP^+ (Figure 2.17) the observed trend was an increase in K_d^* for both materials with increasing coverage. As can be seen in Figure 2.18, DEC^+ had a higher coverage compared to HEP^+ and it also had a higher K_d^*, which follows the trend shown in Figure 2.17 below 200% coverage. However, the loading for HEX^+ and HEP^+ were similar, yet HEP^+ had a higher K_d^*. Also, $PENT^+$ had a much higher loading compared to HEX^+ but $PENT^+$ still had a lower K_d^*. This would suggest that at low loadings (~50% or less), the size of the extractant does indeed affect the selectivity of the material.

Breakthrough Study. One of the most common methods employed to evaluate the extraction performance of solid ion-exchange materials is to measure breakthrough of a target ion. The composition of the effluent and its change with time is dependent on the properties of the ion exchanger (selectivity for the target ion and capacity), the composition of the simulant, and operating conditions (flow rate, packing and column dimensions). The breakthrough capacity (i.e., the amount of target anion taken up prior

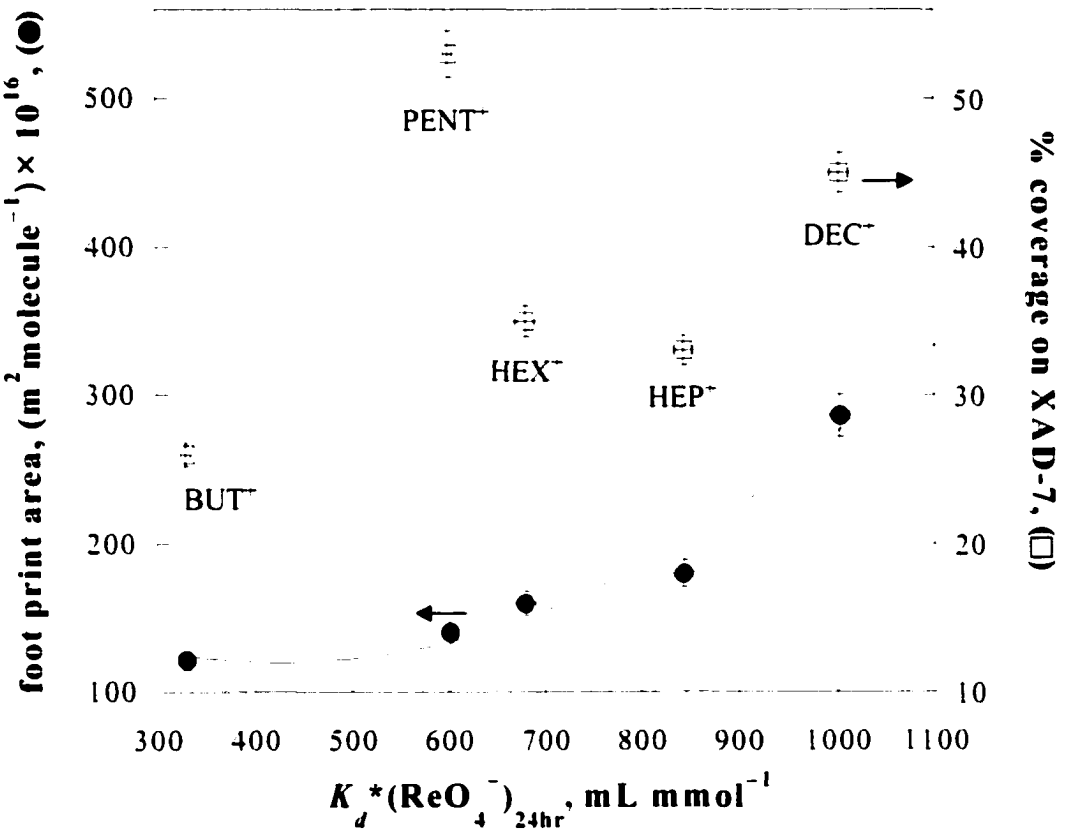

Figure 2.18. Plot of foot print size and % coverage vs. K_d*(ReO_4^-)$_{24hr}$. Error bars for the % coverage are an average of three samples. Error bars for the foot print area are ±3σ. Error bars for the K_d* are an average of three samples. The line is a simple quadratic regression fit to the foot print data.

to breakthrough) is less than the over-all anion-exchange capacity of the column. The breakthrough capacity depends on the nature of the ion-exchange process and the operating conditions, not the overall capacity of the material. The breakthrough capacity has been defined as the volume of simulant treated before 1% of the original target ion concentration was measured in the effluent. In general the greater the selectivity for a particular target anion the sharper the boundary at the breakthrough point. Several factors besides the operating conditions can affect the shape of the breakthrough curve including competing equilibria, rate of migration of the ions through the material, and initial concentration of the target ion.[25]

A series of experiments were performed measuring the uptake of ReO_4^- (as the target ion) and measuring breakthrough capacity for $HEP^-NO_3^-$/XAD-7 through multiple R^2ER cycles. A column measuring 1 cm i.d. × 9 cm in length was packed with 1.8 g of 0.38 mmol g^{-1} $HEP^-NO_3^-$/XAD-7 and a simulant solution containing 0.5 M $NaNO_3$ and 1.0 mM $KReO_4$ was pumped at 3.5 mL min^{-1}. The effluent was collected in 10 mL fractions and analyzed by ICP-AES for total Re concentration. The bed volume (volume of solution contained within the packed column) was 1.0 mL. The simulant was pumped through the column until the desired percent breakthrough had been achieved at which point the extractant material was reduced and reoxidized (put through a complete R^2ER cycle) then fresh simulant pumped through the column to start the next cycle. The column was put through a total of three R^2ER cycles, and the results of the column breakthrough experiments are shown in Figure 2.19. The first and second cycles showed a 1% breakthrough at about 55 bed volumes, whereas, the third cycle had a 1% breakthrough at 65 bed volumes (recall that each sample is an average of 10 bed volumes). The slight variation between the cycles could be due to insufficient conditioning of the material, which might cause the material to perform better over subsequent cycles as the material becomes fully conditioned. Importantly, there was no

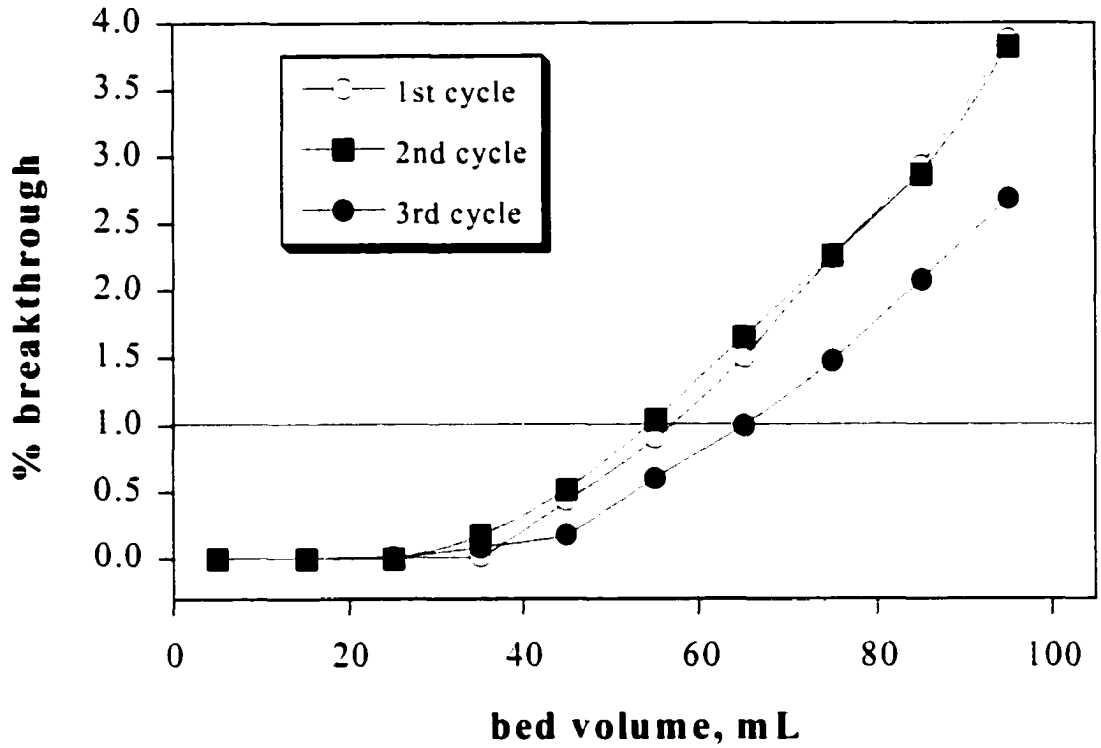

Figure 2.19. The % breakthrough of ReO_4^- vs. bed volume of simulant passed through a column. The column was packed with 1.8 g of 0.38 mmol g^{-1} $HEP^+NO_3^-$/XAD-7. The simulant consisted of 0.5 M $NaNO_3$ and 1.0 mM ReO_4^-. Each plot is a scatter plot with the points connected by a line. The material was regenerated by first reducing with aqueous $Na_2S_2O_4$ and then re-oxidizing with aqueous $Fe(NO_3)_3$. The column was washed with 0.5 M $NaNO_3$ between each cycle.

decrease in bed volumes of simulant treated before 1% breakthrough was observed over several cycles, indicating complete or near complete regeneration of the material. However, as can be seen in Figure 2.19 there is a gradual approach towards breakthrough capacity. A sharp breakthrough point would indicate high selectivity and favorable extraction conditions; however, the slow approach towards equilibrium indicates competing equilibria or less favorable extraction conditions. In this experiment, 10% of the anion-exchange capacity was accessed under these conditions before 1% breakthrough. A sharper breakthrough point (i.e., a higher fraction of the total capacity being accessed before 1% breakthrough) could be achieved by slowing down the pump speed, lowering the concentration of competing anion ($NaNO_3$), by using a material with less than a monolayer loading of $HEP^+NO_3^-$, or using a column with a greater aspect ratio. However, with this material and under these conditions, over 55 bed volumes of simulant were treated before 1% breakthrough and if we assume that ReO_4^- could be recovered in one bed volume (1 mL), then the secondary waste volume would be 1.8% or lower of the primary waste volume.

Complete Extraction-Deactivation/Recovery-Reactivation Cycles. The complete extraction-deactivation/recovery-reactivation cycles were examined to test the materials under operational column redox-recyclable conditions. The redox-recyclable ion-exchange materials $HEP^+NO_3^-$/DAX-8 (0.29 mmol g^{-1} loading) and $HEP^+NO_3^-$ /XAD-7 (0.37 mmol g^{-1} loading) were examined under similar R^2ER conditions used to study $HEP^+NO_3^-/SiO_2$. Each column was treated with samples of $KReO_4$ in aqueous nitric acid (0.316 mM ReO_4^-, 1.0 M HNO_3). The complete R^2ER cycle for the materials packed into a column is shown in Figure 2.20. The complete cycle consists of the following six steps (times for each step are shown in parentheses; flow rate = 3.5 mL min^{-1}): (1) K_d* measurement (50 min); (2) flush with 0.5 $NaNO_3$ (5 min); (3)

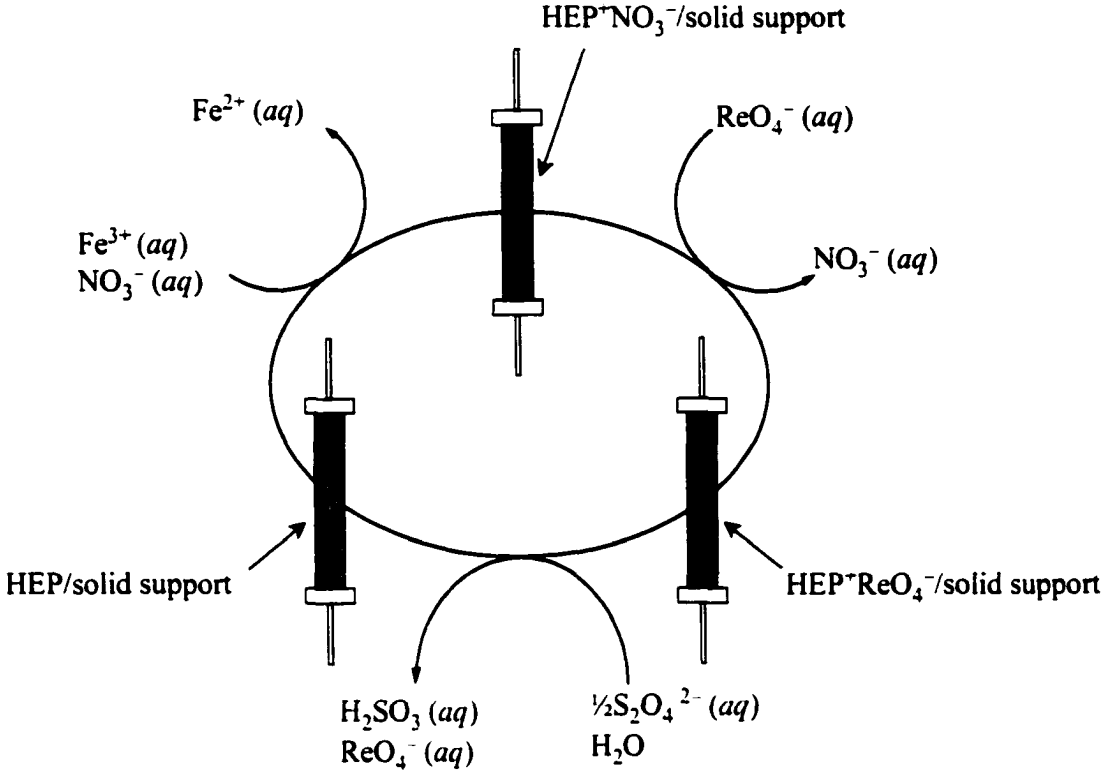

Figure 2.20. The R^2ER cycle as it applies to the extraction and recovery of ReO_4^- from aqueous solution. Aqueous dithionite ion ($Na_2S_2O_4$) was used as the deactivation/recovery reagent and aqueous $Fe(NO_3)_3$ was used as the reactivation reagent.

deactivation/recovery with $Na_2S_2O_4$ (10 min); (4) flush with 0.5 $NaNO_3$ (5 min); (5) reactivation with Fe^{3+} (10 min); (vi) flush with 1 M HNO_3 (5 min). The total duty-cycle time was 85 min. The duty-cycle for the $HEP^+NO_3^-/SiO_2$ was 94 min.[2] At least five complete cycles, giving five successive K_d* values, were carried out for each material. The successive K_d* values are listed in Table 2.3. It was found that the K_d* remains constant over the first 5 cycles for the $HEP^+NO_3^-$/DAX-8 and $HEP^+NO_3^-$/XAD-7 materials. These studies suggested that $HEP^+NO_3^-$ was stable on polymeric supports over a series of cycles in an acidic media. The constant K_d* with subsequent cycles also indicates that each reactivation of the material was essentially complete. A steady decrease in K_d* over the five cycles, from ~380 mL $mmol^{-1}$ to ~300 mL $mmol^{-1}$ was observed for $HEP^+NO_3^-/SiO_2$. The cause of this decrease in K_d* was believed to be due to agglomeration of the $HEP^+NO_3^-$ on the silica gel.[5] Compared to $HEP^+NO_3^-$ on silica gel where K_d* actually decreased over five cycles, the $HEP^+NO_3^-$/polymer material remains constant and even slightly increases over subsequent cycles, which demonstrates an improvement in stability. The K_d* for $HEP^+NO_3^-$/DAX-8 was slightly higher then the K_d* for $HEP^+NO_3^-$/XAD-7. This observation was consistent with earlier batch extractions studies where the K_d*(ReO_4^-) for $HEP^+NO_3^-$/DAX-8 was slightly higher then the K_d*(ReO_4^-) observed for $HEP^+NO_3^-$/XAD-7 under similar extraction conditions. In a separate study, a column packed with 0.76 g $HEP^+NO_3^-$/XAD-7 (0.30 mmol g^{-1} loading) was cycled seven times. The simulant used in that study contained 1.0 mM $KReO_4$ and 1.0 M $NaNO_3$. The K_d*(ReO_4^-) was 976, 1193, 1285, 1290, 1279, 1265 and 1290 for cycles 1–7 respectively. The low K_d*(ReO_4^-) observed for the first cycle was attributed to incomplete conditioning of the column. There was relatively little change in K_d*(ReO_4^-) between cycles 3 and 7, suggesting that once the column becomes fully conditioned there will be little change in effectiveness. Again, there is no observed decrease in K_d*(ReO_4^-) over multiple cycles under these conditions indicating improved

Table 2.3. K_d*(ReO_4^-) Values for $HEP^+NO_3^-$ on SiO_2, DAX-8, and XAD-7 Supports Over Multiple R^2ER cycles.[a]

cycle	$HEP^+NO_3^-/SiO_2$[b]	$HEP^+NO_3^-$/DAX-8[c]	$HEP^+NO_3^-$/XAD-7[d]
1	381	321	253
2	373	337	294
3	354	337	287
4	307	350	300
5	300	362	298
6			300

[a] Each cycle consisted of treating a packed column of $HEP^+NO_3^-$/support with (i) the waste simulant to determine K_d*. (ii) 1.0 M $Na_2S_2O_4$ to reduce $HEP^+NO_3^-$/support and recover ReO_4^-, and (iii) 0.1 M $Fe(NO_3)_3$ in 1 M HNO_3 to reoxidize HEP/support to $HEP^+NO_3^-$/support. [b] 0.26 mmol g^{-1} loading. [c] 0.24 mmol g^{-1} loading. [d] 0.37 mmol g^{-1} loading.

stability over silica gel based materials.

Conclusions

The data presented in this chapter demonstrate that effective anion-exchange materials can be prepared by simple adsorption of tetraalkylated ferrocenium salts onto polymeric supports, instead of the more difficult and more expensive alternative of covalently grafting redox active moieties onto a solid support. The polarity, pore size and surface area of the polymer used as a support have a dramatic affect on the effectiveness of the resulting anion-exchange materials. The more polar polymers (S-761, XAD-7 and DAX-8) achieved faster anion-exchange kinetics compared to the non-polar polymers. The polymer beads with larger pores and lower surface area were found to give an overall higher $K_d^*(ReO_4^-)$. This change in effectiveness was attributed to variations in loading, where some of the extractant may become buried within the smaller pores, preventing the extractant from coming in contact with the aqueous solution. The same behavior was observed when $HEP^+NO_3^-$ was adsorbed onto silica gels. Silica gels with small pores and lower surface area took longer to reduce and re-oxidize and had a lower K_d^* compared to silica gels with larger pores. Although $HEP^+NO_3^-/SiO_2$ had a higher K_d^* at short contact times, $HEP^+NO_3^-$/polymer shows greater stability over several extraction-deactivation/recovery-reactivation cycles. An additional advantage of the polymeric material is that the supports are stable under alkaline as well as acidic conditions (anion-exchange materials based on silica gel cannot, of course, be used with alkaline waste). Finally, it should be noted that efforts are being made to develop electrochemically-recyclable ion-exchange materials by adsorbing redox-active organometallic complexes on conductive supports (e.g., glassy carbon, indium tin oxide, etc.). The development of such materials would be advantageous because extraction-recovery processes would no longer require chemical reagents for the R^2ER process.

References

(1) Clark, J. F.; Clark, D. L.; Whitner, G. D.; Schroeder, N. C.; Strauss, S. H. *Environ. Sci. Technol.* **1996**, *30*, 3124.

(2) Chambliss, C. K.; Odom, M. A.; Morales, M. L.; Martin, C. R.; Strauss, S. H. *Anal. Chem.* **1998**, *70*, 775-765.

(3) Chambliss, C. K. Ph.D. Dissertation, Colorado State University, Fort Collins, CO, 1998.

(4) Ashley, K. R.; Cobb, S. L.; Ball, J. R.; Abney, K. D.; Schroeder, N. C. *Solv. Extr. Ion Exch.* **1995**, *13*, 353.

(5) Ashley, K. R.; Ball, J. R.; Pinkerton, A. B.; Abney, K. D.; Schroeder, N. C. *Solv. Extr. Ion Exch.* **1994**, *14*, 401.

(6) Moyer, B. A.; Bonnesen, P. V. Physical Factors in Anion Separation. In *Supramolecular Chemistry of Anions;* A. Bianchi, K. Bowman-James, and E. Garcia-España, Eds.; VCH, New York, 1997; Chapter 1.

(7) Chambliss, C. K.; Martin, C. R.; Strauss, S. H.; Moyer, B. A. *Solv. Extr. Ion Exch.* **1999**, *17*, 553.

(8) Baes, C. F., Jr.; Moyer, B. A.; Case, G. N.; Case, F. I. *Sep. Sci.Technol.* **1990**, *25*, 1675.

(9) Clark, J. F. Ph.D. Dissertation, Colorado State University, Fort Collins, CO, 1999.

(10) Gansle, K. M. R. Ph.D. Dissertation, Colorado State University, Fort Collins, CO, 1998.

(11) Siekierski, S. *In Extraction Chromatography*; Braun, T., Ghersini, G., Eds.; Elsefier: Amsterdam, 1975; pp 55–56.

(12) Jelinek, Z. K. Adsorption Methods: Particle Size Analysis; Bryce W. A.; Wiley & Sons: New York, 1974; Chapter 8.

(13) Brunauer, S.; Emmet, P. H.; Teller, E. *J. Am .Chem. Soc.* **1938**, *60*, 309.

(14) Rydberg, J.; Musikas, C.; Choppin, G. R. *Principles and Practices of Solvent Extraction*; Marcel Dekker, Inc.: New York, 1992.

(15) Prins, R.; Kirswagen, A. B.; Kortbeek, A. G. *J. Organomet. Chem.* **1972**, *39*, 335.

(16) Pendin, A. A.; Leont'evskaya, P. K.; Bundina, T. K. *Kin. Catal.*, **1977**, *18*, 1087.

(17) Rohal, K. M.; Van Seggen, D. M.; Clark, J. F.; Van Egeren, M. K.; Chambliss, C. K.; Strauss, S. H.; Schroeder, N. C. *Solv. Extr. Ion Exch.* **1996**, *14*, 401.

(18) Nakashima, T.; Lieser, K. H. *Radiochim. Acta* **1985**, *38*, 203.

(19) Covington, A. K.; Freeman, J. G.; Lilley, T. H. *Trans. Faraday Soc.* **1969**, *65*, 3136.

(20) Boyd, G. E. *Inorg. Chem.* **1978**, *17*, 1808.

(21) Supelco™ catalog, *Chromatography Products for Analysis and Purification*, 2001.

(22) Wu, S. *Polymer Interface and Adhesion*; M. Deeker; New York, 1982.

(23) Surface and Interfacial Tensions of Polymers, Oligomers, Plasticizers, and Organic Pigments. In *Polymer Handbook*; Brandrup, J.; Immergut, E. H.; Grulke, E. A., Eds.; 4th Ed., Wiley & Sons, 1999; p VI 521.

(24) Chambliss, C. K.; Martin, C. R.; Moyer, B. A.; Strauss, S. H. *Inorg. Chem.* **1998**, *1*, 435.

(25) Helfferich, F.; Ion Exchange in Columns. In Ion Exchange; Hume, D. N.; King, E. L.; Pople, J. A.; Stork, G.; Williams, H. H.; Herschbach, D. R., 2nd ed., McGraw-Hill Inc., New York, 1962, Chapter 9.

Chapter 3

Detection, Extraction, and Recovery of Perfluoroalkylsulfonate Salts from Aqueous Solutions

Introduction

Perfluoroalkylsulfonates (PFS's) and their derivatives are important components in two widely used commercial formulations: Scotchgard protection and repellant products[1,2] and Light Water® brand aqueous film-forming foams (AFFF's) used in fire suppression.[2–4] AFFF's are especially effective at extinguishing liquid-fuel fires and have been used extensively at military and civilian fire-fighting training facilities as well as at military airfields and municipal airports.[3,5–9] In a recent seminal study, Moody and Field detected several perfluoroalkylcarboxylate (PFC) anions at concentrations ranging from 125 $\mu g\ L^{-1}$ to 7.1 $mg\ L^{-1}$ in groundwater contaminated with untreated AFFF wastewater at Naval Air Station Fallon, NV and at Tyndall Air Force Base, Panama City, FL.[10] Their study confirmed two earlier reports that tentatively identified "fluorinated surfactants" in groundwater at the Tyndall site.[11,12] In a recent study by Moody et al. both PFC and PFS anions were detected in groundwater samples from Wurtsmith Air Force Base, Oscoda, MI, six years after the cessation of fire-training activities.[13] These studies demonstrate that fluorinated surfactants are not rapidly degraded in the environment and can persist for several years in a contaminated area.

The 3M Company recently announced that it is discontinuing production and distribution of perfluorooctylsulfonate-based products because of the toxicity of $C_8F_{17}SO_3^-$ (PFOS),[1,2,14–18] and the persistence of some PFOS-based chemicals in workers and in the environment.[1–4,18–21] The single-dose LD_{50} of $[NEt_4][PFOS]$ for Wistar rats has long been known to be 190 mg kg^{-1}.[16] In a recent 3M study, however, more than one-third of the rat pups, whose mothers were fed only 1.6 mg kg^{-1} per day during pregnancy, died within four days of birth.[1] Although the mechanism(s) of toxicity is not known, the persistence of PFOS in the environment may be related to the inert nature of C–F bonds in perfluoroalkyl chains.[22-24] For example, PFOS was not metabolized by *Pseudomonas* sp. strain D2.[25] Laboratory rats, however, were able to metabolize ^{14}C-labeled PFOS.[26]

One of the goals of this work was to develop new methods for the detection of AFFF in aqueous environments. Several methods for the detection and quantification of AFFF components have been explored. These include negative-ion-electrospray ion mass spectroscopy ((–)ES-MS), attenuated-total-reflectance Fourier transform infrared spectroscopy (ATR-FTIR), and a colorimetric assay. Although each is distinctive in its method of detection, each can be used to detect the anionic surfactants that are contained in AFFF. Also, new methods for the selective extraction and recovery of perfluoroalkylsulfonate surfactants were investigated.

Experimental Section

Materials and Reagents. Distilled water was purified and deionized to 18 MΩ with a Barnstead NanoPure purification system. The following chemicals were purchased from Aldrich and used as received: sodium triflate, bromothymol blue, methyl orange, acid blue #9, indigodisulfate, xylenol orange, and fast red tetraheptylammonium bromide. Potassium perfluorooctylsulfonate, K(PFOS), was synthesized from

perfluorooctylsulfonyl fluoride (3M) by adding it to KOH in water. K(PFOS) is the major product from this reaction; other chain lengths (C7, C6) are also present at lower concentrations. Three recrystallizations were done from hot water to take advantage of the lower solubility of K(PFOS) relative to shorter chain lengths in cold water. The purity of K(PFOS) was determined to be >99% by (–)ES-MS and by ^{19}F NMR spectroscopy. The extractant material $HEP^{+}NO_3^{-}$/XAD-7 was prepared according to literature methods[27] and had a loading of 0.22 or 0.25 mmol $HEP^{+}NO_3^{-}$ per gram of material (see chapter 2 for more detail on the preparation of this material).

Colorimetric Assay Material. To exchange the bromide ion from tetraheptylammonium (THA^{+}) bromide with a colored anion, 100 mL of 10 mM $THA^{+}Br^{-}$ in toluene was mixed thoroughly with an equal volume of a saturated aqueous solution containing one of the following colored anions: bromothymol blue, methyl orange, acid blue #9, indigodisulfate, xylenol orange, or fast red. The two layers were allowed to separate and the organic layer containing THA^{+} ion paired with one of the colored anions were transferred to a separate vial. This process was repeated a total of three times for each colored anion.

Quantifying AFFF. Varying concentrations of AFFF were made by dissolving 0.55, 1.10, 1.65, and 2.75 μL of FC-203CF Light Water® brand aqueous film forming foam (AFFF concentrate), lot # 236-2B-01, in 10 mL of water. A glass syringe was used to transfer all volumes of AFFF concentrate. Each of the solutions were then mixed with 1 mL of 10 mM tetraheptylammonium FastRed (THA-FR) (colorimetric ion-exchange material) in toluene and shaken for 10 min. The solutions were then allowed to sit, and the layers to separate. The aqueous layer was separated and analyzed by a Perkin Elmer Lambda 400 UV-visible spectrometer for the presence of fast red. The maximum absorbance for fast red in the aqueous solution was found to be 523 nm ($\varepsilon = 5240$ L mol^{-1} cm^{-1}).

Tetraheptylammonium-FastRed/XAD-7 Material. 30 mL of a 10 mM toluene solution of tetraheptylammonium FastRed (THA-FR) in toluene were added to 5.0 g of dry XAD-7 and the solvent removed under reduced pressure while being stirred (see Experimental Section for preparation of THA-FR). The material was then dried on a Shlenk line under reduced pressure for 15 min and used without further modification. To determine loading, a portion of the material was placed in 10 mL of dichloromethane, and the THA-FR was desorbed. The concentration of THA-FR was determined from a calibration curve that was linear over the range of 0.05 to 1.00 mM. The amount of THA-FR adsorbed onto the XAD-7 was then quantified by UV-Vis, and was found to be 0.06 mmol/g THA-FR/XAD-7. A calibration curve for PFOS using THA-FR/XAD-7 was generated by contacting 5 mL portions of 0.05, 0.26, 0.60 and 1.00 mM PFOS diluted from a stock solution with 0.1 g of the colorimetric material, shaking for 15 minutes and analyzing the aqueous portion with UV-vis.

Extraction and Recovery of the PFS Components of FC-95. An Ace glass column measuring 2.5 cm i.d. × 10 cm in length with #7 Ace-Thread connectors was used for the bench top system. It held 10.0 grams of the material $HEP^{+}NO_3^{-}$/XAD-7 (0.25 mmol g^{-1} loading). A saturated solution of FC-95 (recall that FC-95 contains five different PFS anions) was made by dissolving 2.5 g of powdered FC-95 in 2000 mL of heated, distilled, and deionized water. The solution was allowed to cool to room temperature (RT); precipitate was observed due to the decrease in solubility of PFS anions in cooler water (K_{sp} for NaPFOS is 2.0×10^{-6} in RT water). The RT solution was filtered through #4 Whatman filter paper to remove the precipitate. After filtration, 1500 mL was pumped through the column containing $HEP^{+}NO_3^{-}$/XAD-7 at a rate of 3.5 mL min^{-1}. A relatively large volume of FC-95 solution was used to ensure that all the accessible ion-exchange sites were ion-exchanged with PFS anions (i.e., to form $HEP^{+}PFS^{-}$/XAD-7). The column was then flushed with distilled deionized water for 10

min, at a pump rate of 3.5 mL min^{-1}, to remove the excess FC-95 solution. The material was then deactivated by passing 100 mL of a 0.1 M pH 9 $Na_2S_2O_4$ solution through the column. Once the deactivation solution had passed through the column, it was diverted through a cold trap which was cooled using a Cryocool^{TM} immersion cooler set to 0 °C to collect PFS anions that might have dissolved in solution. Hot water (85°C) was then pumped through the column for 30 min at a rate of 3.5 mL min^{-1}. Once the hot water had passed through the column, it was directed through the cold trap. A white solid was observed in the cold trap after 15 min. The cold trap was washed out and a portion of the crystalline solid was redissolved in water at 24 °C. This solution of PFS salts was analyzed by (–)ES-MS using a 4:1 (v:v) acetonitrile:water matrix. The saturated solutions of FC-95 before and after the extraction were also analyzed by (–)ES-MS.

Preparation of PFOS Solution. Saturated solutions of PFOS in distilled deionized water were prepared in the following manner. To 2 L of water heated to a boil, 3 g of K(PFOS) was added. The solution was boiled for 5 minutes and then allowed to cool to room temperature (24°C) at which point solid K(PFOS) was observed in the solution. The solution was then filtered using #4 Whatman filter paper to remove the excess K(PFOS). Weighing the dry K(PFOS) that was removed by filtration and subtracting that weight from the initial amount added to the solution determined the concentration. It was determined that 24°C water contains 0.72(2) g of K(PFOS) per liter. In a similar fashion, the saturation point of K(PFOS) at 0 °C was determined. The room temperature water was cooled to ~0 °C in an ice bath during which time white crystals formed. The crystals where quickly filtered through a chilled filter flask. The crystalline solid was then dried and weighed. This weight was subtracted from that of the room temperature water saturation weight (0.72 g L^{-1}). The concentration was determined to be 0.40(2) g L^{-1}.

Extraction and Recovery of PFOS. In a 3.5 cm i.d. × 28 cm in length Ace Glass column equipped with #11 Ace-Thread joints, 31.8 g of 0.22 mmol g^{-1} $HEP^{+}NO_3^{-}$ /XAD-7 material was dry packed. The column was conditioned with distilled and deionized water pumped at 10 mL min^{-1} for 20 min. The column was loaded with PFOS by passing two liters of a PFOS saturated solution continuously for 15 hr at a pump rate of 3.5 mL min^{-1} using a Fluid Metering Model QSY pump equipped with a low-flow isolation kit (1/16-in.-i.d.). The material was then reduced by passing a solution containing 0.1 M $Na_2S_2O_4$ saturated with PFOS through the column for 15 min at a pump rate of 3.5 mL min^{-1}. Once the material was reduced (deactivated) Na(PFOS) was then recovered by flowing hot water (85 °C) through the column and then directing the effluent through a cold trap. The water was heated by pumping the recovery solution through heating coils which where immersed in 85 °C water. The column was also heated externally using heating tape, which was set at 85 °C. The hot solution containing Na(PFOS) was directed through cooling coils which were immersed in an ethylene glycol bath that was cooled using a Cryocool™ immersion cooler set to 0 °C. Upon cooling, white crystals of Na(PFOS) were collected in a course filter frit and the filtrate was circulated back through the heating coil before being pumped through the column. The recovery solution was circulated through the column for 5 hr. The solid Na(PFOS) captured in the cold trap was then dried in an oven (100 °C) for 2 hr, cooled and weighed. After the column cooled to room temperature, a regeneration solution, containing 0.1 M $Fe(NO_3)_3$ in 0.3 M HNO_3, was pumped through the column at 3.5 mL min^{-1} for 15 min. The column was conditioned with distilled deionized water before repeating the procedure.

Results and Discussion

Colorimetric Assay. One of the simpler analysis techniques for detecting anionic surfactants is spectrophotometric detection of a colored compound that has been ion-paired or ion-exchanged with the surfactant.[28–32] Some of the criteria for a suitable colored anion are (1) chemical inertness in aqueous solution and (2) specific interactions with the surfactant with low probability of false indication of the presence of PFS anions. In other words, the colorimetric test should only be sensitive to the presence of surfactants in solution. Current methods for spectrophotometric detection of surfactants are based on liquid-liquid extraction of an ion association complex, formed between a cationic dye and an anionic surfactant. Cationic dyes that are commonly used for spectrophotometric determination of anionic surfactants in aqueous solutions include Methylene Blue, Ethyl violet, Malachite Green, Rhodamine B (pH 5), 4-nitrobenzyl-4-(4-diethylaminophenylazo)pyridinium bromide (NDPP), *N*-alkyl-naphthylazo pyridinium salts, and Safranin T. Neutral dyes include Rhodamine 6G and 4-dimethylamino-phenylazo-2-methylquinoline. The basic steps for anionic surfactant detection include (1) the introduction of the sample into an aqueous phase containing a dye, (2) mixing the resulting aqueous phase with an organic phase, (3) extraction of the ion-pair into the organic phase, and (4) separation of the phases and subsequent detection of the ion-pair by spectrophotometry.

Agudo et al. have developed a method for continuous liquid-liquid extraction with on-line monitoring for the determination of anionic surfactants in water.[29] An aliquot of an organic phase (e.g., chloroform) was injected into a cuvette positioned such that a spectrophotometer beam could be directed through it for quantitative analysis. The aqueous phase was passed through the system carrying the dye (Methylene Blue) and a background absorbance recorded. A sample containing an anionic surfactant was than injected and allowed to mix with the dye. As the sample-dye mixture entered the cuvette,

a gradual enrichment of the organic phase by the ion-pair was monitored over time. The throughput for this system was 20 samples hr^{-1}. With this method there were two ways in which the surfactant concentration was determined: rate of enrichment and final absorbance. The detection limit for the model surfactant sodium dodecylsulfate (SDS) was 20±1 $\mu g\ L^{-1}$.

Another common system was one that utilizes a reaction coil for phase separation after the ion-pair has been formed in the aqueous phase.[30] Most reaction coils are made of porous poly(tetrafluoroethylene) membranes. The advantage of this type of system was the versatility of detection after phase separation. For example, spectrophotometric experiments as well as spectrofluorimetric determinations could be performed on the same system. Rhodamine B was one dye used for spectrofluorimetric determinations. The carrier stream, which consists of a buffered solution and a dye, was pumped through the apparatus and the background recorded. The sample was then injected and mixed with the carrier stream at the segmenter. The mixture was pumped through the extraction coil at which point the phases were separated. The organic phase carrying the ion-pair passed through the extraction coil and enters the detector. The detection limit using SDS as a model surfactant was 2 μM (577 $\mu g\ L^{-1}$) for this system.

Anionic surfactants are naturally accumulated in sediments. One procedure used to determine the concentration in sediments was the extraction of anionic surfactants from sediments into water using ultrasound. A colorimetric assay based on Ethyl Violet was used to quantitate the amount of surfactant extracted into water. The authors claimed that their procedure gave recoveries between 80% and 100%. Microwave radiation has also been used to aid in the determination of surfactant concentration in sediments.[28]

There are also electrochemical methods that have been employed to determine anionic surfactant concentrations. One example of such a method involves mixing bis(ethylenediamine)copper(II) with an aqueous sample containing a surfactant.[31] After

the compound was mixed the surfactant/copper ion-paired complex was extracted into chloroform. The complex was then back-extracted into 0.1 M aqueous nitric acid, which dissolved the $[Cu(en)_2]^{2+}$ cation and destroyed the ion-pair. The acidic aqueous solution was then monitored by voltammetric analysis; an electrode is scanned between –0.2 and –0.1 V vs. Ag/AgCl. The voltammetric peak height and shape was used to quantify the amount of Cu^{2+} and thus the amount of anionic surfactant originally in solution. The detection limit with this system was found to be 5 $\mu g\ L^{-1}$.

Finally, there are methods for detection of anionic surfactants that do not involve liquid-liquid extraction.[32] The detection and quantification of anionic surfactants was determined by mixing buffered solutions containing the surfactants and Rhodamine 6G in test tubes made from different materials. The mixtures were shaken at 25 rpm in a temperature-controlled shaker for 5 min; during that time surfactant/dye ion-pairs adsorb to the test tube walls. The aqueous buffer was then discarded and the test tube air-dried. An organic solvent was then added to dissolve the ion-pair for spectrophotometric assay. The detection limit for sodium dodecylsulfate with this procedure was 720±30 $\mu g\ L^{-1}$.

In most cases the detection and quantification of anionic surfactants requires a multi-step process that can be both time consuming and prone to error. The spectrophotometric method developed in our labs was aimed at eliminating the multi-step process while maintaining high sensitivity with low occurrence of false positives. The method involves exchanging the colorless surfactant quantitatively with a colored anion, followed by subsequent spectrophotometric detection. The colorimetric method is better compared to other methods mentioned in that it is a one step ion-exchange process with no organic solvents contacting the aqueous solution before spectrophotometric analysis.

To explore the method's selectivity towards fluorinated anionic surfactants, a series of liquid-liquid extraction experiments, testing the selectivity of tetraheptylammonium (THA^+) ion-paired with various colored anions, were performed.

The cation tetraheptylammonium, a bulky colorless cation, was chosen to ion-pair with the colored anions because of its similar size to HEP^+, its insolubility in water, and its ability to take on the characteristic color of the anion with which it is ion-paired. In this experiment, solutions of toluene containing the extractant ion-paired with various colored anions were put in contact with each of the following aqueous solutions: pure water, pure water saturated with FC-95 (a mixture of 5 PFS anions), seawater simulant, and seawater simulant saturated with FC-95. If an aqueous solution that did not contain PFS anions exhibited a color change (i.e. false positive test), that colored anion was not considered suitable. Table 3.1 lists the anions studied and the results of the colorimetric test.

All the anions tested indicated a positive test for PFS anions when the PFS surfactants were dissolved in pure water. When contacted with seawater, however, many of the anions showed a false positive (i.e. change in the aqueous solution's color) indicating a low selectivity towards PFS anions. Only two colored anions were found to be suitable as a colorimetric test for PFS anions in seawater or water that has a high salt content. Indigodisulfonate indicated some color when in contact with seawater, but only a slight hint of blue. When in contact with a solution that contained PFS anions, the aqueous solution turns a dark blue. The colored anion, Fast Red, showed a positive test (i.e. a red colored aqueous solution) only for solutions that contain PFS anions. Fast Red (2,7-napthalenedisulfonic acid) is a red tri-anion, available as the trisodium salt (Na_3FR). It has many common names, including Fast Red, acid red 27, acid amaranth, and food red No. 2. To test the pH sensitivity of Fast Red, an aqueous solution of Fast Red was made by dissolving 0.01 g in 1 L of water. 10 mL portions were then adjusted to pH 1, 3, 5, 7, 10, and 12 (adjusted with HCl and NaOH) and monitored by UV-Vis. It was found that no appreciable change in wavelength occurred in this pH range, indicating low sensitivity to pH. Due to the low sensitivity to pH and the high selectivity towards PFS

Table 3.1. Results of Colorimetric Test with Several Colored Anions.

anion[a]	pure water[b] with no PFS	pure water with PFS anions	seawater[c] with no PFS	seawater with PFS anions
bromothymol blue	colorless	blue	blue	blue
methyl orange	colorless	orange	orange	orange
acid blue # 9	colorless	blue	blue	blue
xylenol orange	colorless	violet	violet	violet
Indigodisulfonate	colorless	blue	light blue	dark blue
fast red	colorless	red	colorless	red

[a] Organic solvent used was toluene. [b] Barnsted Nanopure purification system was used to purify the water. [c] See Table A.1 in Appendix A for the analytes used to make the seawater simulant.

anions, it was determined that the colored anion Fast Red ion-paired with tetraheptylammonium would serve as the best colorimetric material for detecting the anionic components contained in AFFF mixtures. The goal of this study was to develop a colorimetric material that would accurately test for AFFF contamination.

To test the validity of the colorimetric system varying concentrations of AFFF were made ranging from 55 to 275 μg L^{-1} AFFF concentrate (FC-203CF) in water. Table 3.2 shows the UV-Vis absorbance results of the AFFF solutions after contact with THA-FR. Figure 3.1 is a plot of absorbance vs. concentration of AFFF. The linear regression has a correlation coefficient of 0.9937 suggesting that the colorimetric ion-exchange compound THA-FR has a linear response to increasing amounts of AFFF in aqueous solutions. This suggests that THA-FR could be used accurately for the detection and possible quantification of solutions containing AFFF. One of the primary components of AFFF, sodium dodecylsulfate (DDS), could possibly exchange for Fast Red along with the PFS anions contained in AFFF. A test was performed in which a 0.01 mM solution of DDS contacted with an equal volume of 10 mM THA-FR in toluene and shaken for one minute. The aqueous solution turned red indicating DDS does indeed exchange for Fast Red. This test demonstrated the low selectivity of THA-FR towards PFS surfactants. This low selectivity could be problematic because a wide variety of products contain DDS and could pose a significant source of false positive detection for AFFF. The THA-FR material was not sensitive towards the common ions found in seawater, however, it was not selective enough to distinguish between fluorinated and non-fluorinated surfactants of similar size and similar hydration energy.

After establishing a liquid-liquid extraction method utilizing THA-FR for the detection of surfactants found in AFFF mixtures, a solid-liquid method was explored. The advantage of developing a solid-liquid method is that the aqueous solution does not

Table 3.2. Extraction of AFFF by THA-FR.

absorbance at 523 nm[a]	μg L^{-1} AFFF	dilution factor[b]
0.048	55	18000
0.158	110	9000
0.288	165	6000
0.468	275	3600

[a] Absorbance of fast red in aqueous phase after extraction with solution containing AFFF.

[b] Dilutions from AFFF concentrate lot number FC-203CF.

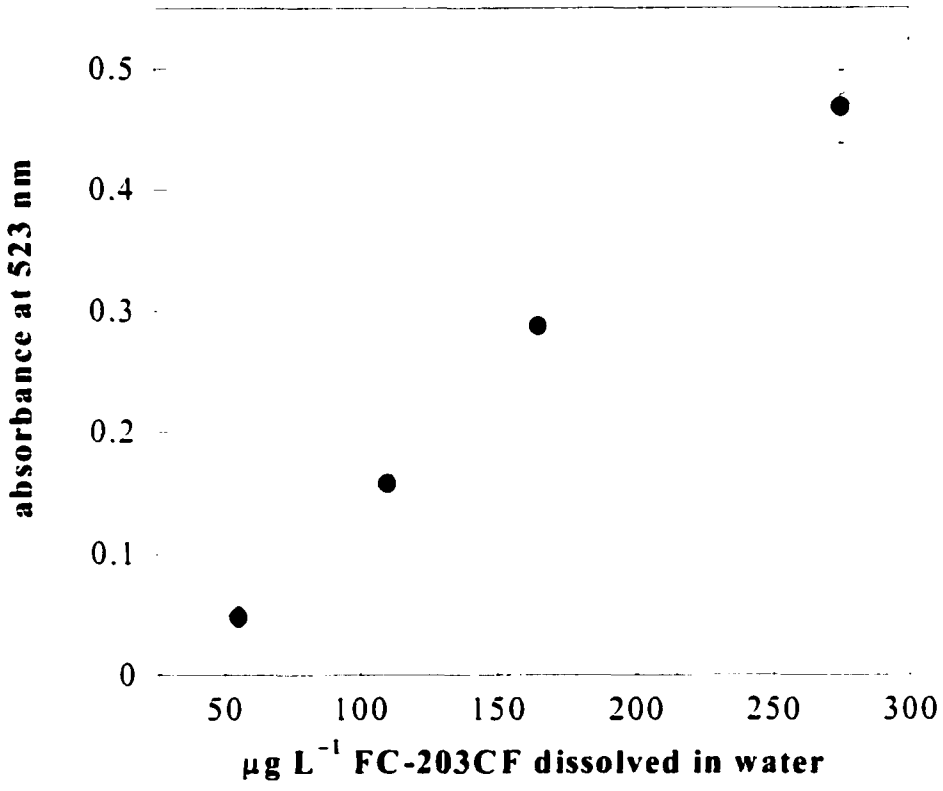

Figure 3.1. Detection of increasing amounts of AFFF concentrate (FC-203CF) in water by THA-FR. The error bars represent ±3σ with each point run in triplicate. The line is a linear regression analysis of the four points with a least square fit (r^2) of 0.99.

come into contact with an organic solvent, and the time needed to separate the indicating material from the aqueous solution is greatly reduced. To determine if the material THA-FR/XAD-7 (see experimental section for the fabrication of this material) could be used to indicate the presence of PFOS, a portion of the dry beads (0.1g) was added to 5-mL portions of 0.05, 0.26, 0.60, and 1.00 mM PFOS diluted from a stock solution. The solutions were shaken for 15 min at 100 RPM on a constant temperature shaker bath. 3 mL portions were pipetted into quartz quvet cells and analyzed by UV-vis. Figure 3.2 is a graph plotting the concentration of PFOS verses absorbance at 520 nm. Although there was only a single point determination for each concentration, the least squares fit to the curve (r^2) was 0.99, suggesting a linear response to the increasing concentration of PFOS in solution using this material. Thus, by simply adsorbing the colorimetric compound, THA-FR, onto an acrylic ester polymeric support, a colorimetric material was made that could be used as a simple test for the presence of surfactants in aqueous solutions. Although the colorimetric method could be used to detect and even quantify surfactants it has not proven selective enough to identify which surfactants were being extracted.

Detection of Anionic Surfactants using Negative Ion Electrospray Mass Spectroscopy ((–)ES-MS). In the previous section, a colorimetric assay was described for the detection of anionic surfactants, but the material was not selective enough to distinguish between fluorinated and non-fluorinated surfactants. To date, there have been only two published methods, besides that of Moody and Field,[3,4] for the identification of fluorinated surfactants in water, and neither is suitable for the quantitative determination of sub-ppm amounts of individual PFS anions. In the two published methods, PFS anions were identified, but not quantified, using fast-atom-bombardment and collision-activated-dissociation mass spectrometry.[33] In one study, two commercially available mixtures of PFS anions (3M products FC-95 and FC-93) were quantitatively measured by ion chromatography at concentrations between 5 and 50 mg/L in aqueous acid.[34]

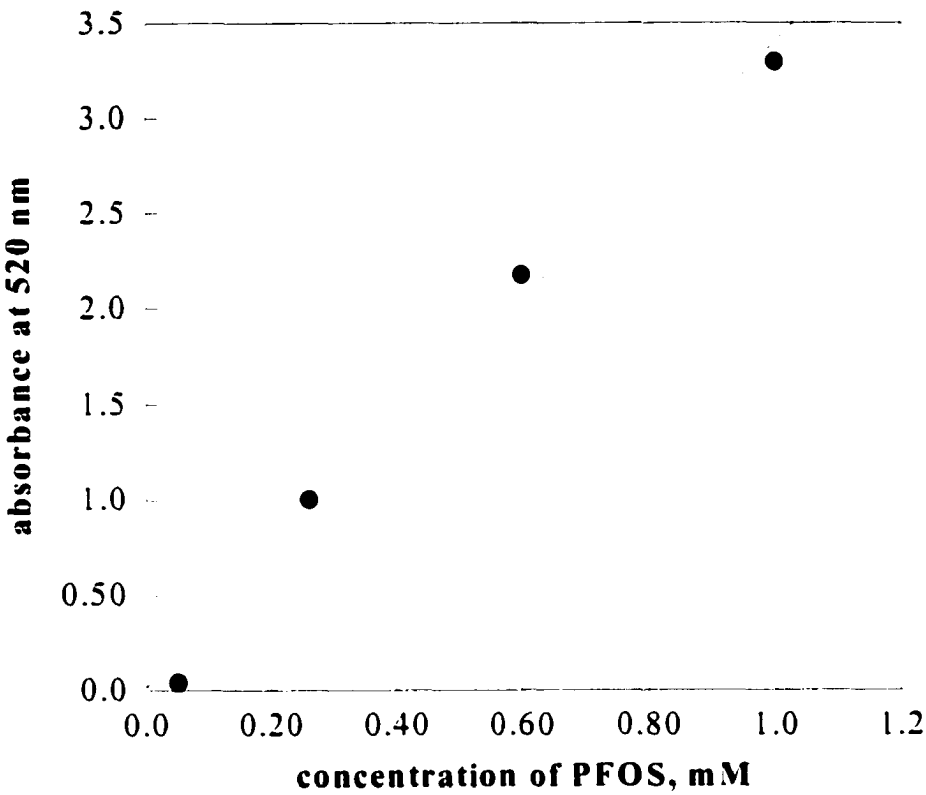

Figure 3.2. Calibration curve of PFOS using THA-FR/XAD-7. Each point is a single point determination. The line is a linear regression analysis of the four points with a least square fit (r^2) of 0.99.

Although total concentration of fluorinated surfactant was measured, PFS anions were not individually quantified by this method.

Hansen et al. reported a mass spectral method for determining concentrations of PFOS and other fluorochemical anions in blood serum and whole liver tissue.[35] Due to the complex nature of these matrixes, their method requires (1) extraction of PFOS (and the other fluorochemical anions) into an organic solvent using an ion-pairing reagent, (2) evaporation of the solvent and reconstitution in another solvent, (3) HPLC separation of the anions on a Betasil C_{18} column, and (4) negative ion *tandem* mass spectrometry (the latter was necessary because of possible biological interferences).[36] This important new method, albeit complex, has now been used to determine the accumulation of PFOS in marine mammals[36] and the global distribution of PFOS in wildlife.[37]

A significant portion of AFFF, according to the MSDS, is a mixture of anionic surfactants. When AFFF is used in fire training exercises both by the government and by local fire stations, ground contamination is a real concern. Recently, Moody and co-workers have determined that AFFF is highly mobile in the environment.[4] Detection and quantification of AFFF has proven to be a challenge due to the complex mixture that makes up AFFF. One of the goals of this project was to develop procedures for measuring ppm levels of certain perfluoroalkylsulfonate (PFS) anions, $C_nF_{2n+1}SO_3^-$, in water contaminated with AFFF. Currently under development in the Strauss group, is a method employing negative ion electrospray mass spectroscopy ((–)ES-MS) capable of detecting and quantifying anionic surfactants. Figure 3.3 shows a portion of the (–)ES-MS of 10 μL of AFFF concentrate dissolved in 1 mL of 1:1 (v:v) acetonitrile:water solution. The peak at m/z 237 belongs to $C_{10}H_{21}OSO_3^-$, one of the two alkylsulfate anions present in AFFF (the other, more abundant, anion is $C_8H_{17}OSO_3^-$; it's much more intense peak at m/z 209 is not shown in this portion of the spectrum). The peaks at m/z 299, 349, 399, 449 (not labeled), and 499 belong to the PFS-4, PFS-5, PFS-6, PFS-7, and

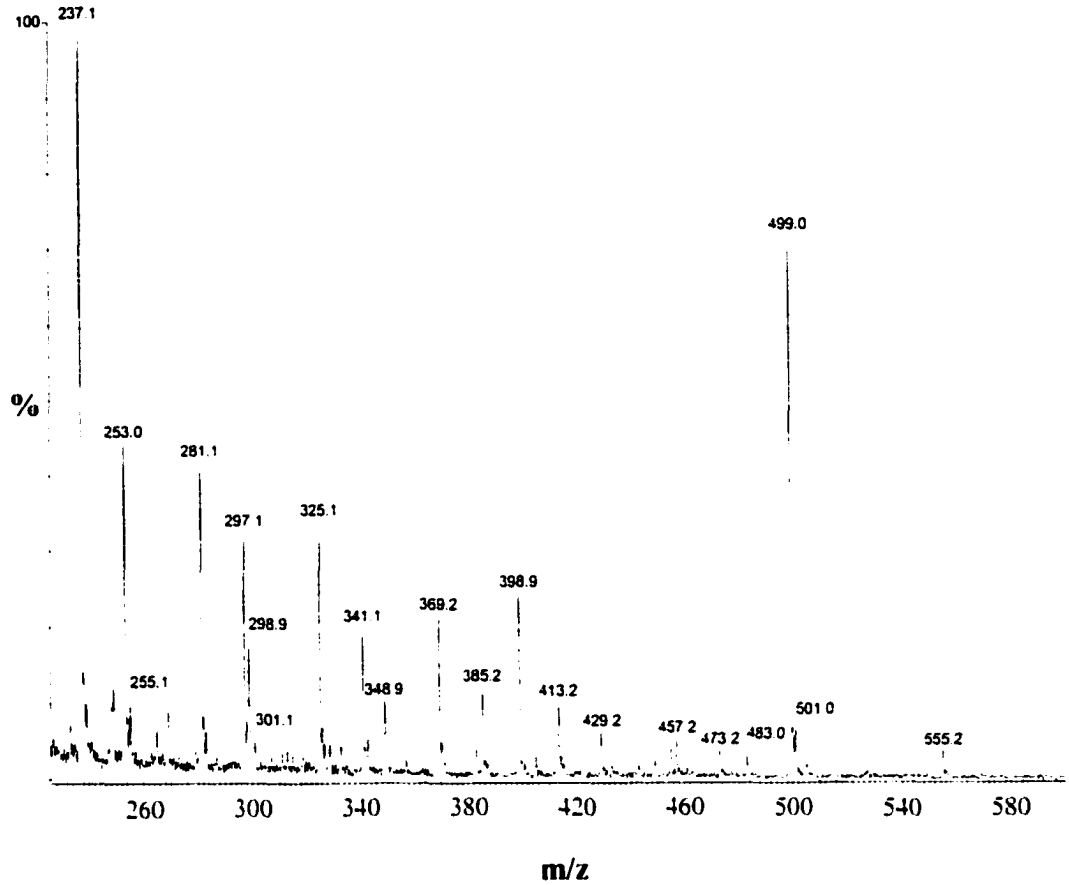

Figure 3.3. Negative-ion electrospray mass spectrum of a dilute sample of AFFF in 1:1 (v:v) acetonitrile:water. Note that there are peaks at m/z 269 and 313 (very weak), which belong to PFC-6 ($C_5F_{11}^-$ and $C_5F_{11}CO_2^-$, respectively), and at m/z 369 and 413, which belong to PFC-8 ($C_7F_{15}^-$ and $C_7F_{15}CO_2^-$, respectively).

PFOS (PFS-8) anions. Note that there are weak peaks at m/z 269 and 313, which are attributed to PFC-6 fragmentation (i.e., $C_5F_{11}^-$ and $C_5F_{11}CO_2^-$), and at m/z 369 and 413, which belong to PFC-8. These are the same two PFC anions discovered in AFFF-contaminated groundwater by Field and Moody.[3]

The mass spectrum of 3M's FC–95 FLUORAD Brand Fluorochemical Surfactant is shown in Figure 3.4. It is likely that the PFS salt component in 3M's AFFF concentrate is the 3M product FC–95 or a very similar product. According to the 3M patent on various AFFF formulations, the only perfluoroalkylsulfonate used in AFFF is K(PFOS). Nevertheless, the MSDS for FC–203CF indicates that five perfluoroalkylsulfonate salts are present, not just one.

The mass spectrum of FC–95 in Figure 3.4 exhibits peaks that belong to the five PFS anions (PFOS, PFS-7, PFS-6, PFS-5, PFS-4). In addition, it exhibits peaks at m/z 249 and 199, which may belong to PFS-3 and PFS-2. More importantly, it exhibits peaks at m/z 413, 369, 313, and 269. Therefore, FC–95 also contains K(PFS-3), K(PFS-2), K(PFC-8), and K(PFC-6). Furthermore, although the relative intensities of the peaks cannot be used to precisely calculate the concentrations of the different species, it appears that the concentrations of the PFC anions in AFFF is a significant fraction, perhaps as much as 5–10%, of the concentration of PFOS in AFFF (see Figure 3.3).

A series of experiments were performed in order to more accurately quantify the anions contained in AFFF. Sodium dodecylsulfate (DDS) was used as an internal standard in all (–)ES-MS samples to allow for the quantification of PFS anions. In general, it is important that an ES-MS internal standard has properties similar to the analyte, so that both species will tend to form ions under similar conditions. Several researchers have used an isotopically labeled form (i.e., a perdeuterated or polydeuterated isotopomer) of their analyte as an internal standard,[38–40] but that method was not convenient for perfluorinated compounds. Keeping the internal standard similar to the

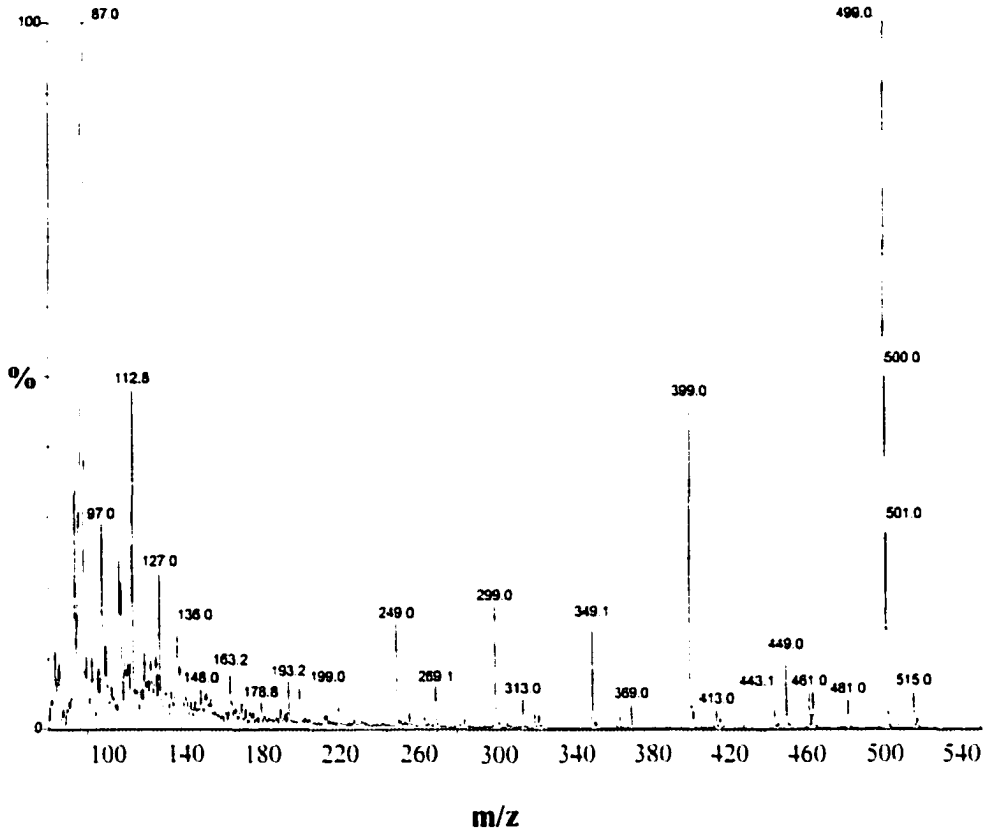

Figure 3.4. Negative-ion electrospray mass spectrum of a dilute sample of FC–95 FLUORAD (3M) in 1:1 (v:v) acetonitrile:water. Note that there are peaks at m/z 269 and 313 (very weak), which belong to PFC-6 ($C_5F_{11}^-$ and $C_5F_{11}CO_2^-$, respectively), and at m/z 369 and 413, which belong to PFC-8 ($C_7F_{15}^-$ and $C_7F_{15}CO_2^-$, respectively). Note also that there are peaks at m/z 199 and 249, which may belong to PFS-2 and PFS-3, respectively.

analytes structure and mass ensures it will produce a similar sensitivity coefficient to the analyte. The sensitivity coefficient is a constant that is related to the efficiency of a molecule to form ions in the electrospray source.[39,40] The ratio of anion intensities is equal to the ratio of sensitivity coefficients when the concentrations of the anions are equal.[39,40] The anions PFOS and DDS have different sensitivity coefficients, which were manifested by two different (–)ES-MS intensities for the same concentration of the two ions. However, work performed by Gretchen Hebert in the Strauss group found that the ratio of these intensities, I(499)/I(265), was relatively constant (to within experimental error) at 1.4–2.2 over the concentration range 0.01 μM to 50 μM for equal concentrations of the two surfactant anions, making DDS an appropriate internal standard for PFOS.

Each sample was prepared so that only one dilution from the original bottle of AFFF concentrate would take place before the sample was submitted for (–)ES-MS analysis. These dilutions correspond to a 1:5000 fold dilution directly from the AFFF concentrate into 1:1 (v:v) ACN:water. The average concentration and standard deviation from twelve separate dilutions are reported in Table 3.3. The samples also contained perfluoroalkylcarboxylic acids and their fragments from the ionization process, however these concentrations are not reported. All of the anions listed had peak intensities that were at least three times greater than the background intensity. By analyzing AFFF solutions for PFOS (499 m/z) and using Table 3.3, the detection limit (3 times signal to noise) for AFFF was 6 μg L^{-1}.

Remediation of AFFF Contaminated Water. One of our goals, along with identifying contaminated areas, was to find ways to remediate or remove AFFF from those contaminated areas. We investigated whether or not UV photolysis of hydrogen-peroxide-containing aqueous solutions of AFFF or PFS salts would result in degradation of the PFS anions. To our knowledge no one has reported similar experiments.

Table 3.3. Quantification of AFFF by (–)ES-MS Using DDS Internal Standard.[a]

anion	m/z ratio	concentration		percent error
		mM	ppm	
$C_8H_{17}OSO_3^-$	209	259 ± 17[b]	53000 ± 3000	6
$C_{10}H_{21}OSO_3^-$	237	11.7 ± 0.6	2700 ± 100	5
PFS-3	249	4.2 ± 0.3	1010 ± 70	7
PFS-4	299	6.8 ± 0.6	2000 ± 200	9
PFS-5	349	4.2 ± 0.4	1400 ± 100	9
PFS-6	399	9.9 ± 0.8	3800 ± 300	8
PFS-7	449	1.0 ± 0.2	450 ± 70	15
PFOS	499	37 ± 5	18000 ± 2000	12

[a] Concentrations were determined through spiked additions of DDS. [b] The error is derived from an average of 12 separate samples.

In one experiment a dilute solution of AFFF was made by dissolving 3 mL of AFFF concentrate in 500 mL of water. A 10:1 molar ratio of H_2O_2 to all organic components was added to the AFFF solution. The solution was photolyzed with UV light using a Hg lamp for 150 min after the addition of hydrogen peroxide. The solution was stirred at 10 rpm and the temperature was held at 20°C by circulating water through the lampwell for the duration of the experiment. The solution was analyzed by (–)ES-MS before and after photolysis. Prior to analysis each sample was diluted by taking 450 μL of the sample and adding 0.955 mL of distilled deionized water. The (–)ES-MS results are listed in Table 3.4.

The most significant result is that the two alkylsulfate anions are almost completely destroyed by photochemical conditions, whereas the PFS anions are not. The small change in concentrations of PFS anions may or may not be due to photochemical degradation in the presence of other organic radicals that are formed as the organic components of AFFF are destroyed. However, the larger changes in PFS anion concentrations could be due to the surfactant properties of the longer-chain PFS anions and the significant amount of foaming that occurred when this experiment was performed (i.e., foaming may have caused the concentrations of various PFS anions to have changed by differential adhesion to, for example, the walls of the reactor). In fact we have found that fluorinated surfactants do indeed adhere to surfaces at varying extents depending on the type of surface.[41] These experiments show that photochemical conditions virtually eliminate the anionic alkylsulfate surfactants in AFFF, but do not eliminate the anionic PFS surfactants in AFFF.

A solution containing 5.7 μg L^{-1} AFFF concentrate still foamed after 150 min of photolysis, which indicates that PFS anions alone can cause significant foaming. To quantify this phenomenon, the foaming of AFFF solutions was investigated in more detail (there are no published data that we are aware of). The foaming properties

Table 3.4. (–)ES-MS Results for AFFF Photolysis Experiments.

anion	peak intensity before photolysis ($\times 10^{-7}$)[a]	peak intensity after photolysis ($\times 10^{-7}$)[b]	percent removed
PFOS	6.65(5)	4.4(3)	34
PFS-6	1.94(2)	2.0(2)	0
PFS-5	0.77(2)	0.54(4)	29
PFS-4	1.00(2)	0.99(3)	0
$C_{10}H_{21}OSO_3^-$	2.92(4)	baseline noise	99
$C_8H_{17}OSO_3^-$	44.80(9)	1.41(3)	97

[a] Each sample prepared for (–)ES-MS analyses contained 450 μL of sample and 0.955 mL of water. Peak intensity is an average of three samples. [b] Foaming occurred during the experiment, which might cause a variation in anionic surfactant peak intensities.

of the two solutions before and after photolysis was monitored by a simple foam measuring apparatus consisting of a glass cylinder (15 in. × 1 in.) with a medium glass frit at the bottom through which argon gas was bubbled at a rate of 1-2 sccm. For each foaming experiment, 10 mL of solution was added to the cylinder and the height of the foam at equilibrium was measured from the frit to the top of the column of foam. The results are listed in Table 3.5. It is concluded that AFFF solutions that originally contain 1.9 μg L^{-1} or less AFFF concentrate (as well as the corresponding amounts of the other PFS surfactants) will not foam after a photochemical treatment.

An experiment was performed to determine whether $HEP^{+}NO_3^{-}$/XAD-7 could be used to remove the PFS surfactants after the photochemical reaction. This is an important experiment for the following reason. It has been demonstrated that $HEP^{+}NO_3^{-}$/XAD-7 can remove PFS anions from "relatively clean" aqueous solutions (see Chapter 4), the photochemically-treated solution originally containing AFFF may contain chemical species that could interfere with the R^2ER process.

A 20-mL sample of photochemically-treated AFFF solution that was originally 2.85 mL AFFF concentrate in 500 mL of water was contacted with 0.42 g of 0.26 mmol/g $HEP^{+}NO_3^{-}$/XAD-7 for 45 min. The concentrations of anionic surfactants before photolysis, after photolysis, and after contact with $HEP^{+}NO_3^{-}$/XAD-7 were determined by (–)ES-MS and are listed in Table 3.6. After the photolysis, and extraction with $HEP^{+}NO_3^{-}$/XAD-7, the aqueous solution did not foam. In other words, even though a dilute AFFF solution containing 0.11 mM $C_8F_{17}SO_3^{-}$ will still foam after photochemical treatment (see Table 3.5), it will not foam after treatment with $HEP^{+}NO_3^{-}$/XAD-7. It was assumed that the $HEP^{+}NO_3^{-}$/XAD-7 material extracted the remaining foaming agents which were the PFS surfactants. Attenuated total reflectance (ATR) FTIR spectra of the aqueous solution was recorded before photochemical treatment and after treatment and are shown in Figure 3.5. Spectrum 3.5 A is a dilute solution containing 5.7 g L^{-1}

Table 3.5. Results of Foaming Experiments with AFFF Solutions.

$\mu g\ L^{-1}$ AFFF in solution	height of foam column before photochemical process (in.)	height of foam column after photochemical process (in.)
1.90	7	0[a]
5.70	>15[b]	2

[a] No foaming observed above the solution. [b] Foamed out of the cylinder.

Table 3.6. (–)ES-MS Results for AFFF Photolysis and Extraction Experiments.

anion	conc. before photolysis (mM)[a]	conc. after photolysis[b] (mM)	conc. after photolysis and extraction[c]
$C_8F_{17}SO_3^-$	0.25	0.11	baseline noise
$C_6F_{13}SO_3^-$	0.07	0.06	baseline noise
$C_5F_{11}SO_3^-$	0.03	0.03	baseline noise
$C_4F_9SO_3^-$	0.05	0.05	baseline noise
$C_{10}H_{21}OSO_3^-$	0.07	baseline noise	baseline noise
$C_8H_{17}OSO_3^-$	1.63	0.01	baseline noise

[a] Concentrations determined using DDS as an internal standard (error = 5%). [b] The AFFF solution was photolyzed with a 450 W UV lamp for 150 min with 10:1 molar ratio H_2O_2. [c] 20 mL sample of the photolyzed solution was contacted with 0.42 g of 0.26 mmol g^{-1} $HEP^+NO_3^-$/XAD-7 and shaken for 45 min in a shaker bath at 150 rpm set at 24 °C.

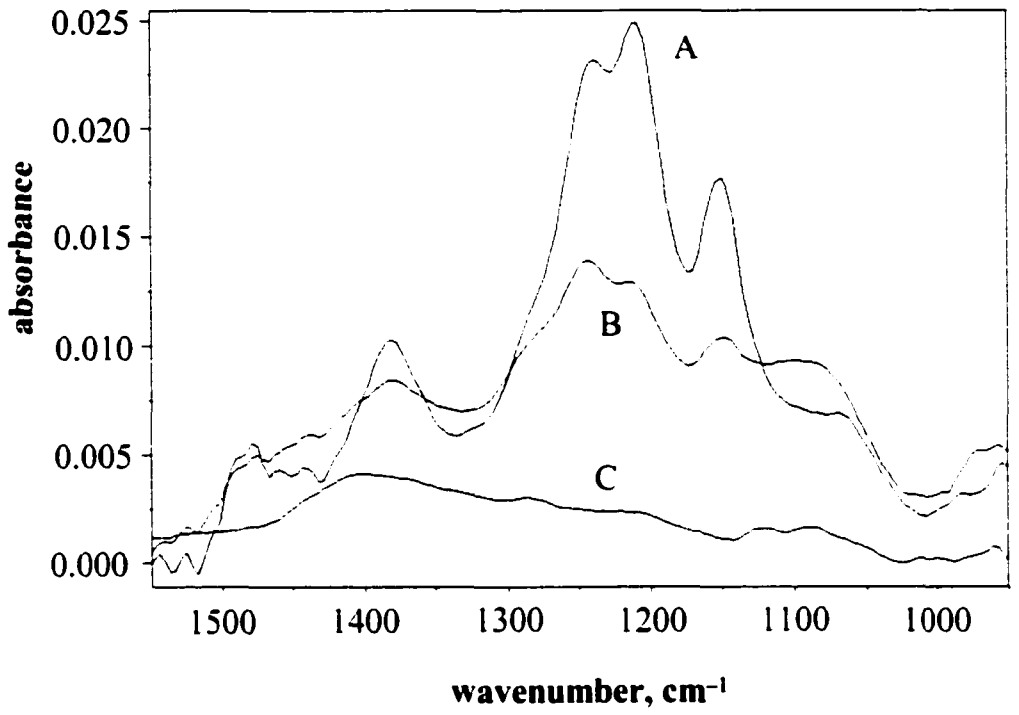

Figure 3.5. Aqueous ATR-FTIR spectra of aqueous solutions of AFFF before treatment (A), after photochemical treatment (B), followed by treatment with $HEP^{+}NO_3^{-}$/XAD-7 (C).

AFFF concentrate (2.85 mL AFFF concentrate in 500 mL water). Spectrum 3.5 B is the same solution after the photochemical treatment described above. Note the decrease in overall intensity in the 1300–1100 cm^{-1} region, commensurate with the virtual elimination of alkylsulfate anions and the persistence of PFS anions. Spectrum 3.5 C is the same solution after contact with $HEP^{+}NO_3^{-}$/XAD-7. Note the complete absence of any peak between 1300-1100 cm^{-1}, signaling the virtually complete extraction of PFS anions by the $HEP^{+}NO_3^{-}$/XAD-7 material.

Extraction and Recovery of PFS Surfactants. Although our initial goal was to develop methods for the identification of AFFF contaminated sites, we also investigated ways to selectively extract and recover the PFS anions contained in AFFF as possible routes for remediation of those sites. We began by using a new redox-recyclable extraction and recovery (R^2ER)[42,27] system that employs a hot-water/cold-water recovery process developed as part of this work. This process efficiently removes PFS anions using $HEP^{+}NO_3^{-}$/XAD-7 and recovers them as crystalline salts after deactivation of the extractant material. This system takes advantage of the high selectivity of $HEP^{+}NO_3^{-}$ loaded onto a polymeric support ($HEP^{+}NO_3^{-}$/XAD-7) towards PFS anions and the recyclability of this extractant material. Due to the low solubility of salts of PFS surfactants in water at room temperature, deactivation of the extractant material resulted in the PFS salts immediately precipitating within the column. Many column volumes of distilled and deionized water were needed to purge the column of PFS salts. The large volume of water required to purge the column almost equaled the volume of waste simulant treated. The precipitation of the PFS salts was initially perceived to be a problem for the recovery of the pollutant in a small volume but this disadvantage was turned into an advantage. The solubility of PFS salts dramatically increases at the Krafft point.[43] For example, the Krafft point for potassium perfluorooctylsulfonate is ~ 80 °C. PFS salts could be efficiently washed from the reduced column and recovered as a solid

in a cold trap by heating the recovery solution to temperatures above the Krafft point of the PFS salts. This technique allowed the recovery of the PFS pollutant as a solid, resulting in a volume reduction of 99.99%.

The new R^2ER process consists of four steps: the extraction of PFS anions by $HEP^+NO_3^-$/XAD-7, the deactivation of the extraction material by a reducing agent, the recovery of the PFS anions by flushing with hot water with subsequent precipitation in a cold trap, and reactivation of the extractant material using an oxidizing agent. The low solubility of PFS anions in chilled aqueous solutions allows for a recovery scheme in which the PFS anions are washed off the column with water heated above the Krafft point and collected as a precipitate in a chiller. The recirculation (recovery) loop includes the following elements: (1) a heater to reheat the recovery water to ca. 90°C just before it enters the insulated column; (2) a chiller to cool the water to ca. 0°C after it exits the column; (3) a filtration element to collect the crystalline Na(PFS) salts; and (4) a circulating pump. This scheme results in the collection of solid Na(PFS) (and/or other salts of PFS anions) by filtration. *Note that solid Na(PFS) represents one of the smallest possible volumes of secondary waste for PFS anions.* Figure 3.6 is a schematic of the recirculating recovery loop. The ability to easily cycle the extractant material from a high affinity extractant to a low affinity extractant makes it possible to recover the extracted waste in a much smaller volume. PFOS and the 3M material FC-95 were used to evaluate the selectivity of the $HEP^+NO_3^-$/XAD-7 material as well as the efficiency of the hot-water/cold-water recovery system.

To investigate the selectivity of the ion exchange material towards a mixture of fluorinated surfactants, the material was used to extract FC-95. Figure 3.7 shows the differences in (–)ES-MS PFS anion peak intensities for the FC-95 solution before extraction with $HEP^+NO_3^-$/XAD-7 and after extraction (See Experimental Section). It is important to note that the amount of PFS used in this experiment exceeded the amount of

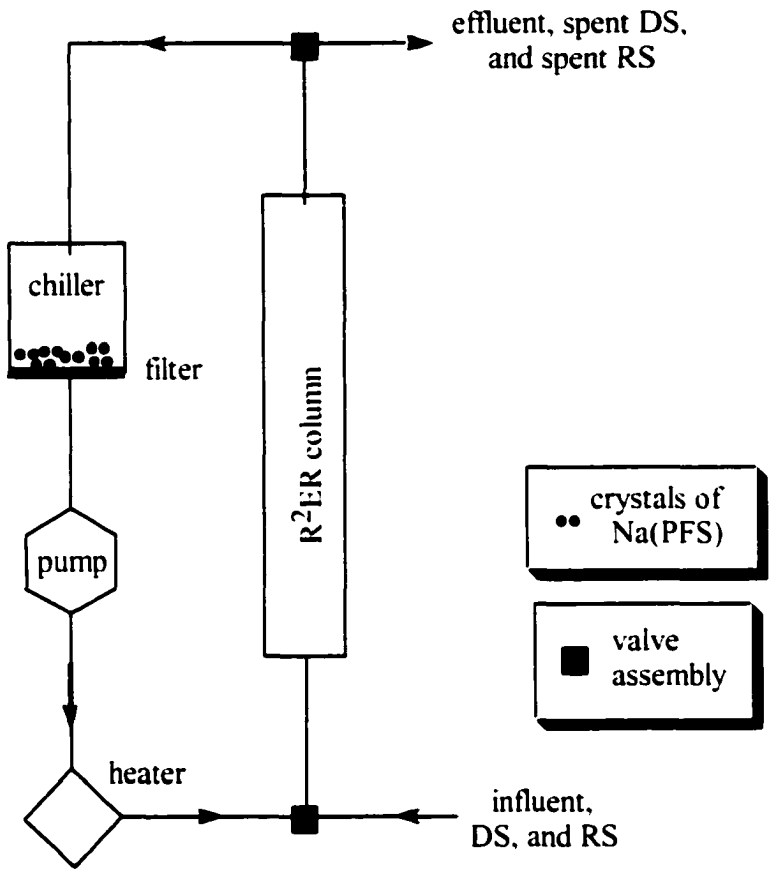

Figure 3.6. R^2ER set up with a hot-water/cold-water recovery system. The deactivating solution (DS) and reactivating solution (RS) are introduced through the bottom of the column. The deactivating solution is diverted through the chiller. The recovery solution is cycled through the column and through both the chiller and heater.

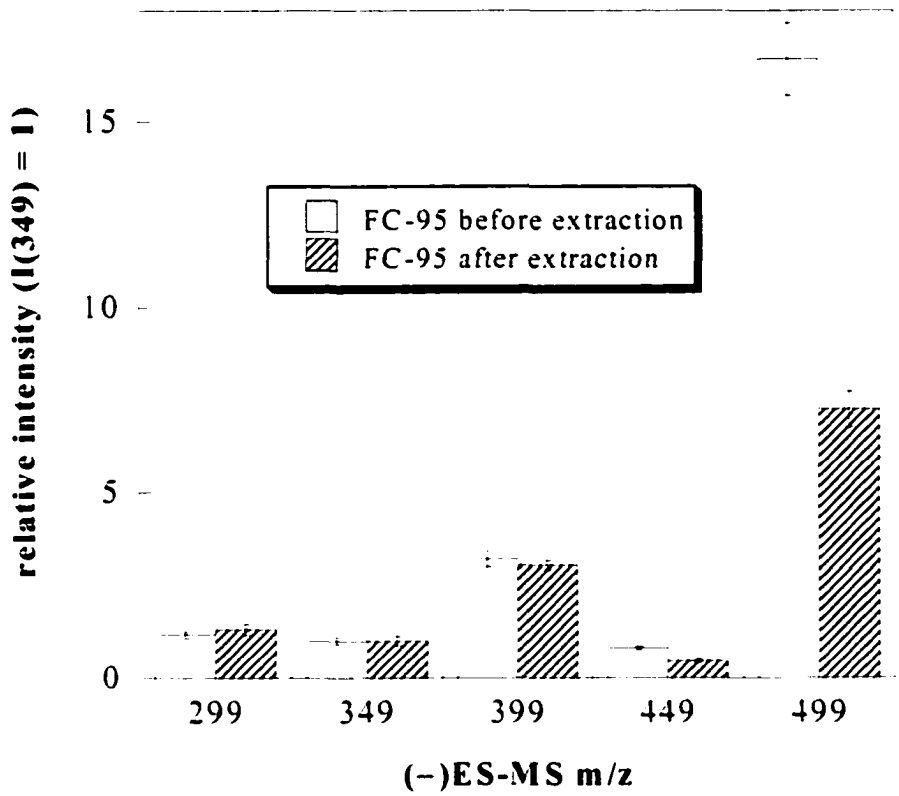

Figure 3.7. Relative (–)ES-MS intensities of PFS anions before and after extraction with $HEP^{+}NO_3^{-}$/XAD-7. The m/z values for PFS-4, PFS-5, PFS-6, PFS-7, and PFOS are 299, 349, 399, 449, and 499, respectively (PFOS = $C_8F_{17}SO_3^{-}$). Error bars represent and average of three (–)ES-MS samples.

$HEP^+NO_3^-$ (per mole) used to extract the PFS anions. More than half the amounts of PFOS (PFS-8) and PFS-7 in the original solution were extracted by $HEP^+NO_3^-$/XAD-7. In contrast, negligible amounts of PFS-6, PFS-5 and PFS-4 were extracted. This is an important result, although it is not unexpected. The extraction equilibrium, shown below, is governed by the relative hydration energies of NO_3^- and the PFS anion:

$$HEP^+NO_3^-/XAD\text{-}7\,(s) + PFS^-\,(aq) \rightleftharpoons HEP^+PFS^-/XAD\text{-}7\,(s) + NO_3^-\,(aq)$$

The more weakly hydrated the PFS anion, the larger the equilibrium constant for this ion exchange. Accordingly, the equilibrium constant for the reaction will always be greater than 1 as long as Y > X (X and Y are integers such as 5, 6, 7, and 8).

$$HEP^+(PFS\text{-}X)^-/XAD\text{-}7(s) + (PFS\text{-}Y)^-(aq) \rightleftharpoons HEP^+(PFS\text{-}Y)^-/XAD\text{-}7(s) + (PFS\text{-}X)^-(aq)$$

Therefore, longer-chain PFS anions (i.e., PFS-7 and PFOS) will be extracted preferentially over shorter-chain PFS anions because longer-chain PFS anions have lower hydration energies than shorter-chain PFS anions. The recovery process was investigated by analyzing FC-95 dissolved in room temperature water and FC-95 that had precipitated at ice bath temperatures from an aqueous room temperature solution. Figure 3.8 shows the (–)ES-MS intensities of PFS anions collected as their potassium salts in a cold trap from a solution of FC-95 and PFS anions from FC-95 dissolved in room temperature water. It is important to note that the samples analyzed by (–)ES-MS had concentrations of PFS well below the saturation point to ensure all available PFS anions were dissolved. PFOS was the most abundant anion found in the cold trap. Significantly, the relative concentrations of PFS anions decrease as the chain length of the PFS anion decreases.

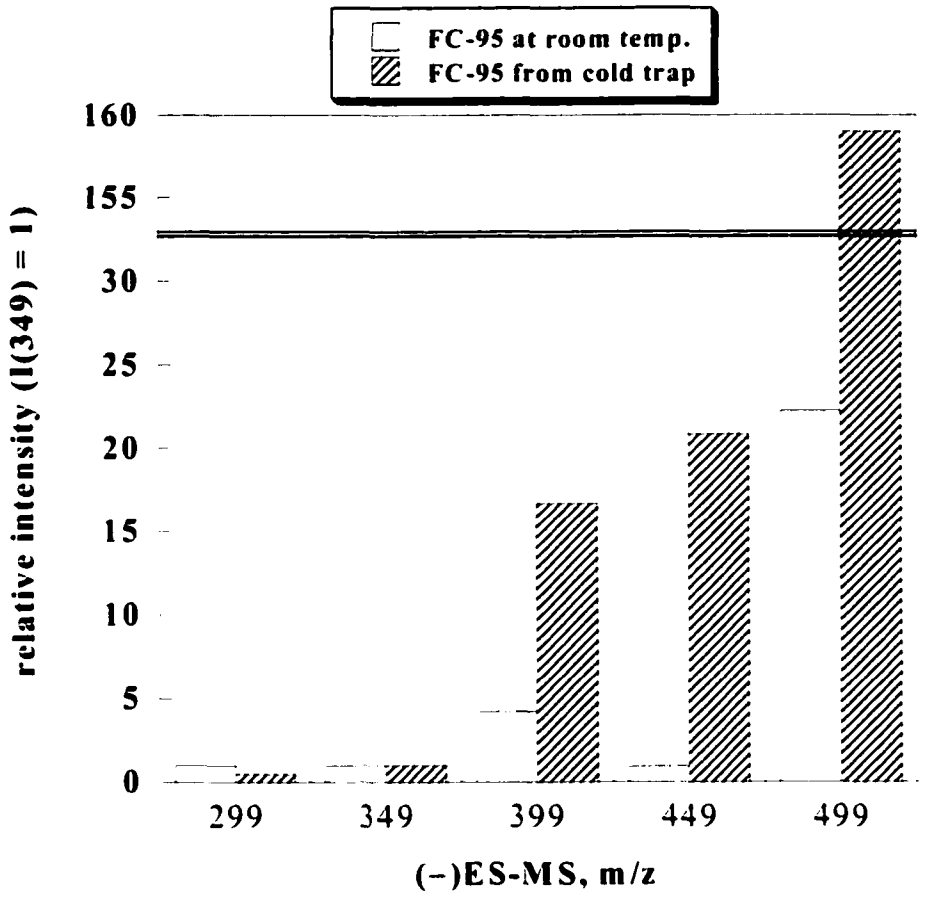

Figure 3.8. Relative (–)ES-MS intensities of PFS surfactants dissolved in room temperature water and PFS surfactants collected from 5 °C water. Note that the relative intensity increases as m/z increases in the cold-water sample indicating longer chain PFS surfactants preferentially precipitate at cooler temperatures compared to shorter chain length PFS surfactants.

This suggests that larger PFS anions precipitate to a greater extent at colder temperatures then smaller chain PFS anions. From this result, it can be concluded that the hot-water/cold-water treatment results in the recovery of crystalline PFS salts that are enriched in longer-chain PFS anions. This follows the general trend as dictated by the Krafft point of the PFS salts. This result, too, is not unexpected; salts of long-chain PFS anions are expected to be less soluble in water than the corresponding salt of a shorter-chain PFS anion. So, not only does the extraction process favor longer chain PFS anions, but the recovery process does as well. One can envision a purification scheme in which long chain surfactants are separated from short chain surfactants using this process.

Extraction and recovery of PFOS Over Four R^2ER Cycles. One PFS salt (PFOS) was chosen to test the selectivity of the material as well as the recovery process over many cycles. In a batch study, a 20-fold molar excess of $HEP^+NO_3^-$/XAD-7 was treated with a 50-ppm solution of PFOS. The solution was contacted for a certain period of time and then analyzed by (–)ES-MS. After 10 min [PFOS] = ~ 3 ppm; after 1 h, [PFOS] = 0.09(3) ppm (99.8% removal); after 24 hr, [PFOS] = 0.012(2) PPM; (99.97% removal). These data indicate that the $HEP^+NO_3^-$/XAD-7 material efficiently extracts PFOS and is nearly complete after 24 hr. An ion-exchange column packed with 37 g of $HEP^+NO_3^-$/XAD-7 was treated with aqueous solutions of PFOS so that 50% of the ion-exchange sites were loaded with the PFOS anion. Once the column was loaded, the material was deactivated and washed with 85 °C water, which was then passed through a cold trap to precipitate the PFOS that was extracted (see Figure 3.6). The amount of solid PFOS collected in the cold trap was compared to the initial amount of PFOS contained in the aqueous solution. Table 3.7 lists the results of four R^2ER cycles. The recovery of crystalline PFOS from the loaded column was 88% or greater in each case. This result suggests that the $HEP^+NO_3^-$/XAD-7 material maintains its selectivity over many cycles and that there was efficient recovery of PFOS over each cycle. Note that this is a volume

Table 3.7. Extraction and Recovery of PFOS by $HEP^{+}NO_3^{-}$/XAD-7.[a]

initial[b] concentration mg mL^{-1}	final[c] concentration mg mL^{-1}	PFOS recovered g	% recovery
0.72	<0.01	1.27	88
0.72	<0.01	1.37	97
0.72	<0.01	1.27	88
0.72	<0.01	1.43[d]	101

[a] The column was packed with 31.8 g of 0.22 mmol $HEP^{+}NO_3^{-}$/XAD-7. [b] Two liters of solution where continually pumped at 3 mL/min for 15 hours. [c] Final concentration was determined by (–)ES-MS using DDS as an internal standard. [d] The excess PFOS is believed to be unrecovered PFOS from the previous cycle.

reduction of greater then 2,000. This volume reduction was based on the assumption that the specific gravity for PFOS is similar to FC-95, which was 0.6. Samples of the material were observed at 120× magnification after deactivation and after being washed with 85 °C water. As can be seen in Figure 3.9, crystals of Na(PFOS) can be seen on the surface of the beads upon deactivation, but after being washed with 85 °C water, these crystals are no longer observed.

Conclusions

There are several methods outlined here for the detection, identification, and quantification of fluorinated surfactants. The colorimetric method provides a general test for the presence of anions surfactants and is quantitative between 50 and 275 $\mu g\ L^{-1}$ in the case of AFFF. Although the colorimetric material THA-FR had a low selectivity specifically for fluorinated surfactants, it was able to detect anionic surfactants in complex matrixes from a seawater simulant. The (–)ES-MS method of detection could achieve much lower detection limits compared to the colorimetric method (below 6 $\mu g\ L^{-1}$) and it had the added advantage of identification through mass analysis. The quantification of the anions contained in the AFFF concentrate was achieved by adding an internal standard. Reliable quantification data was achieved by using an internal standard with similar sensitivity coefficients to the anionic fluorinated surfactants of interest. The internal standard must have similar sensitivity coefficients so that molecules form ions in the electrospray source to similar extents. For example, triflate and hexafluorophosphorous were also used as internal standards but neither produced numbers that were accurate due to the difference in sensitivity coefficients. Although the internal standard DDS does not produce a similar peak height as PFOS at similar concentrations the ratio of peak heights does remain constant over a wide range of concentrations. This method had the added benefit of a simple sampling procedure with

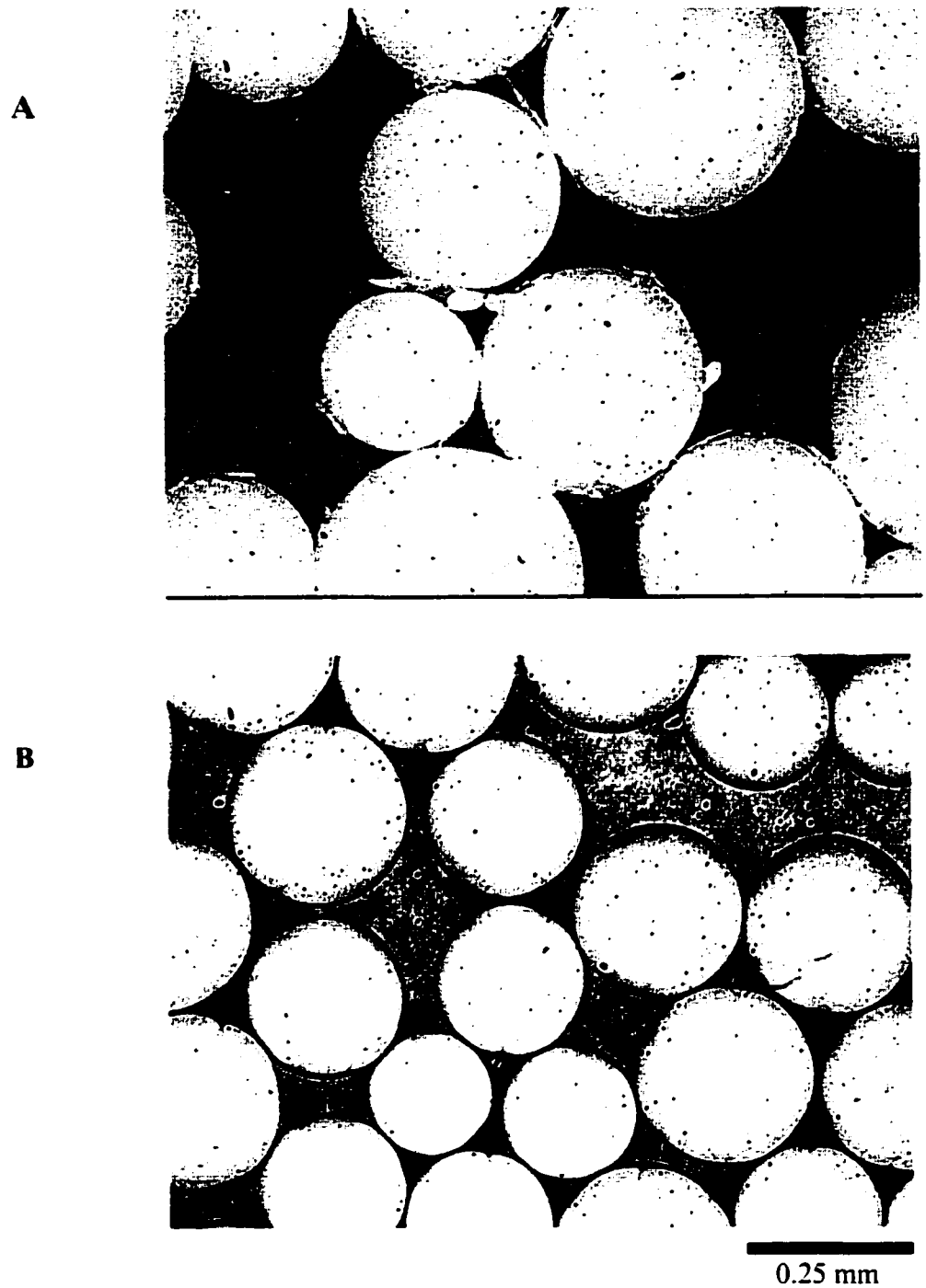

Figure 3.9. Magnified photographs (120 ×) of: **A.** Beads of HEP/XAD-7 after reduction of $HEP^{+}PFS^{-}$/XAD-7 with $Na_2S_2O_4$ before being flushed with hot water. **B.** HEP/XAD-7 after flushing with 85 °C water for three hours.

no matrix matching required. This greatly reduced the time required to run a sample.

It has been shown that the redox-recyclable $HEP^{+}NO_3^{-}$/XAD-7 material could be used to extract PFS anions and that by using the hot-water/cold-water method, the PFS surfactants could be recovered as a solid. A volume reduction of 2,000 was achieved through the extraction of PFS anions from several liters of water and recovery in a much smaller volume (1 cc) as a solid using the hot-water/cold water recovery method. This type of volume reduction would not be possible without employing the easily recyclable $HEP^{+}NO_3^{-}$/XAD-7 extractant material and using the hot-water/cold-water recovery method.

References

(1) Tullo, A. *Chem. Eng. News* **2000**, *78* (May 29), 12–13.

(2) Tullo, A. *Chem. Eng. News* **2000**, *78* (May 22), 9–10.

(3) Moody, C. A.; Field, J. A. *Environ. Sci. Technol.* **2000**, *34*, 3864–3870.

(4) Moody, C. A.; Hebert, G. N.; Strauss, S. H.; Field, J. A. *Environ. Sci. Technol.*, submitted for publication.

(5) Darwin, R. L.; Ottman, R. E.; Norman, E. C.; Gott, J. E.; Hanauska, C. P *NFPA Journal* **1995**, *May/June*, 67–73.

(6) Hashimoto, Y. *DIC Tech. Rev.* **1995**, *1*, 9–18.

(7) Szonyi, S.; Cambon, A. *Fire Saf. J.* **1990**, *16*, 353–365.

(8) Szonyi, F.; Szonyi, S.; Cambon, A. *Comun. Jorn. Com. Esp. Deterg.* **1991**, *22*, 297–304.

(9) Briggs, A. A. *Fire Technol.* **1979**, *15*, 20–24.

(10) Moody, C. A.; Field, J. A. *Environ. Sci. Technol.* **1999**, *33*, 2800–2806.

(11) Henley, M.; Mayfield, H.; Shelley, T. *Book of Abstracts, 1997 Pittsburgh Conference (Atlanta, GA)*; American Chemical Society: Washington, DC; Abstract 519.

(12) Levine, A. D.; Libelo, E. L.; Bugna, G.; Shelley, T.; Mayfield, H.; Stauffer, T. B. *Sci. Total Environ.* **1997**, *208*, 179–195.

(13) Moody, C. A.; Hebert, G. N.; Strauss S. H.; Field, J. A. *Eviron. Sci. Technol.*, accepted for publication.

(14) Sohlenius, A.-K.; Eriksson, A. M.; Hogstrom, C.; Kimland, M.; DePierre, J. W. *Pharmacol. Toxicol.* **1993**, *72*, 90-93.

(15) Schnellmann, R. G. *Toxic. in Vitro* **1990**, *4*, 71–74.

(16) Meussdoerffer, J. N.; Niderprüm, H. *Chem. Z.* **1980**, *104*, 45–52.

(17) Chan, D. B.; Chian, E. S. K. *Environ. Prog.* **1986**, *5*, 104–109.

(18) Perfluorooctyl Sulfonates; Proposed Significant New Use Rule: *Fed. Regist.* **2000**, *65 (202)*, 62319–62333.

(19) Giesy, John P.; Kannan, K. *Environ. Sci. Technol.*, in press.

(20) Kannan, K.; Koistinen, J.; Beckmen, K.; Evans, T.; Gorzelany, J. F.; Hansen, K. J.; Jones, P. D.; Helle, E.; Nyman, M.; Giesy, J. P. *Environ. Sci. Technol.*, in press.

(21) Olsen, G. W.; Burris, J. M.; Mandel, J. H.; Zobel, L. R. *J. Occup. Environ. Med.* **1999**, *41*, 799–806.

(22) Smart, B. In Hudlicky, M.; Pavlath, A. E., Eds., *Chemistry of Organic Fluorine Compounds II (ACS Monograph 187)*; American Chemical Society: Washington, DC, 1995, p 979.

(23) Gloeckner, V.; Lunkwitz, K.; Prescher, D. *Tenside, Surfactants, Deterg.* **1989**, *26*, 376–380.

(24) Kissa, E. *Fluorinated Surfactants: Synthesis, Properties, Applications*; Marcel Dekker: New York, 1994.

(25) Key, B. D.; Howell, R. D.; Criddle, C. S. *Environ. Sci. Technol.* **1998**, *32*, 2283–2287.

(26) Johnson, J. D.; Gibson, S. J.; Ober, R. E. *Fundam. Appl. Toxicol.* **1984**, *4*, 972–976.

(27) Chambliss, C. K.; Odom, M. A.; Martin, C. R.; Moyer, B. A.; Strauss, S. H. *Inorg. Chem. Comm.* **1998**, *1*, 435-438.

(28) Mecozzi, M.; Amici, M.; Pietrantonio, E. *Anal. Comm.* **1996**, *33*, 303.

(29) Agudo, M., Rios, A., and Valcarcel, M., *Analyst* **1994**, *119*, 2097.

(30) Sakai, T., *Talanta* **1998**, *45*,543.

(31) Spencer, M.; Wallace,G. G.; Crisp, P. T.; Lewis, T. W. *Anal. Chim. Acta* **1991**, *244*, 197.

(32) Kymaya, M.; Tomizawa, Y.; Nagashima, K. *Anal. Chim. Acta* **1998**, *362* 157.

(33) Lyon, P. A.; Tomer, K. B.; Gross, M. L. *Anal. Chem.* **1985**, *57*, 2984–2989.

(34) Laikhtman, M.; Rohrer, J. S. *J. Chrom. A* **1998**, *822*, 321–325.

(35) Hansen, K. J.; Clemen, L. A.; Ellefson, M. E.; Johnson, H. O. Environ. Sci. Technol. 2001, 35, 766–770.

(36) Giesy, John P.; Kannan, K. *Environ. Sci. Technol.*, in press.

(37) Kannan, K.; Koistinen, J.; Beckmen, K.; Evans, T.; Gorzelany, J. F.; Hansen, K. J.; Jones, P. D.; Helle, E.; Nyman, M.; Giesy, J. P. *Environ. Sci. Technol.*, in press.

(38) Cole, R. B. *Electrospray Ionization Mass Spectrometry: Fundamentals, Instrumentation, and Applications*; John Wiley and Sons: New York, 1997.

(39) Webb, K. S.; Baker, P. B.; Cassells, N. P.; Francis, J. M.; Johnston, D. E.; Lancaster, S. L.; Minty, P. S.; Reed, G. D.; White, S. A. *J. Forensic Sci.* **1996**, *41*, 938–946.

(40) Kebarle, P.; Tang, L. *Anal. Chem.* **1993**, *65*, 972A–986A.

(41) Hebert, G. N. Ph.D. Dissertation, Colorado State University, Fort Collins, CO. Manuscript in preparation.

(42) Chambliss, C. K.; Odom, M. A.; Morales, M. L.; Martin, C. R.; Strauss, S. H. *Anal. Chem.* **1998**, *70*, 775-765.

(42) Shinoda, K.; Hato, M.; Hayashi, T. *J. Phys. Chem.* **1972**, *76*, 909.

Chapter 4

Development of ATR-FTIR Detection Techniques for Monitoring the Extraction of Polyatomic Anions

Introduction

Attenuated total reflectance (ATR) FTIR is a well-developed spectroscopic technique that has been widely used for the analysis of solid-solid and solid-liquid interfaces due to its surface sensitivity and selectivity on a molecular basis within the penetration depth of a few micrometers.[1-7] It can deliver qualitative and quantitative information as well as monitor changes in films that have been physi- or chemisorbed at the surface of the waveguide. Common transmission spectroscopy cannot be used when investigating aqueous solutions due to the very strong absorption bands in the mid-IR region. Minimizing this effect requires the use of very small optical pathlengths which are often difficult to prepare. With ATR techniques, short pathlengths are easily realized. The phenomenon that gives rise to total internal reflectance, as described by Harrick,[8] occurs within the waveguide (e.g., silicon, diamond, ZnSe) when light is incident at the interface between two optically transparent regions of high (n_1) and low (n_2) refractive index. The angle of incident needs to be greater then the critical angle θ_c (where $\sin \theta_c = n_2/n_1$ (Snell's law)) before internal reflectance occurs. In most cases n_1 is the refractive index of the waveguide and n_2 is the refractive index of air or of the film on the waveguide. The interaction of the incident light and the reflected light results in a standing wave that penetrates a short distance above the waveguide. This standing wave

is referred to as the evanescent wave and the penetration depth beyond the crystal is described by the equation below:

$$d_p = \frac{\lambda}{2\pi\left(n_1^2 \sin^2\theta - n_2^2\right)^{1/2}}$$

where λ is the wavelength of the electromagnetic wave. The penetration depth (d_p) of the evanescent wave is thus dependent on the refractive index of the waveguide and the sample above the waveguide, and the wavelength of light passing through the waveguide. The penetration depth of the evanescent wave is usually on the order of a few microns beyond the surface of the waveguide.

Described here is the development of an ATR-FTIR method that is able to detect and identify polyatomic anions in the low micromolar concentration in water. Typically, the application of a thin film of a selective organometallic extractant to the surface of the ATR crystal affords a sensitivity increase of over 1,000 times that of the unmodified probe. Also discussed in this chapter is the use of ATR-FTIR spectroscopy (using an unmodified probe) to track and monitor the extraction of triflate ($CF_3SO_3^-$) by $HEP^+NO_3^-$/XAD-7. The technique can be used to follow the R^{2}ER process and can be used to determine column efficiencies by measuring breakthrough in real time.

There is an ongoing need to detect and quantify anionic pollutants such as cyanide (CN^-),[9,10] perchlorate (ClO_4^-),[11–14] and perfluorooctylsulfonate ($C_8F_{17}SO_3^-$; PFOS)[15–20] at low concentrations in aqueous media. The current US Environmental Protection Agency (USEPA) drinking-water standards and drinking-water reference doses for cyanide and perchlorate are 200 μg L^{-1} [21,22] and 4-18 μg L^{-1},[14] respectively. The surfactant PFOS, which was formerly used in Scotchgard®-brand fabric treatments and aqueous film-forming foams (AFFF's) used to fight liquid fuel fires,[15,16,18–20] is a

major wastewater problem in that its presence can cause excessive foaming and shutdowns of publicly-owned treatment works.[15]

Currently, the most common method used to detect aqueous ClO_4^- is ion chromatography[23] (IC), but the method relies on retention times as a means of detection and is prone to error if the matrix is unknown. IC techniques can also be used to detect CN^- but due to the weak acid nature of hydrogen cyanide (pK_a = 9.22), the detection limit is much higher than for ClO_4^-.[24] In general, strong acid anions (e.g., ClO_4^-, Cl^-) give a high conductivity and thus high detector response, but weak acids are weakly ionized and, thus, give a low detector response. Conventional separation techniques, such as distillation, precipitation, and solvent extraction, are methods used to enhance the sensitivity by means of preconcentration. Other methods of cyanide analysis include potentiometry,[25] spectrofluorometry,[26] headspace gas chromatography (HS-GC),[27] and spectrophotometry.[28] The detection of perfluoroalkylsulfonates (PFS's) has only recently been studied due to reports that point towards environmental persistence and biological toxicity of perfluoroalkylsulfonates and perfluoroalkylcarboxolates.[19,20,29–39] As was mentioned in Chapter 3, Moody and co-workers developed a mass spectrometry method for the detection of perfluoroalkylcarboxolates (PFC's), but the multi-step sample preparation is time consuming and is designed for detection of PFC's only.

Experimental Section

Materials and Reagents. The following chemicals were obtained from the indicated vendors and were used without further purification: potassium cyanide (Fisher), sodium hydroxide (Fisher); sodium chloride (Fisher), dichloromethane (Fisher), 1,3-bis(diphenylphosphino)-propanedichloronickel(II) ($NiCl_2$(dppp) (Aldrich), lithium perchlorate (G.F.S.), Hydrion buffer salt (pH 10.00 ± 0.02) sodium carbonate and sodium bicarbonate (Micro Essential Lab). Potassium perfluorooctylsulfonate, K(PFOS), was

synthesized from perfluorooctylsulfonyl fluoride (3M) by adding it to KOH in water. K(PFOS) is the major product from this reaction, while other chain lengths (C7, C6) are also present at lower concentrations. Three recrystallizations were done from hot water to take advantage of the lower solubility of K(PFOS) in cold water compared to homologous salts with shorter chain lengths. The purity of K(PFOS) was determined to be >99% by (–)ES-MS and by ^{19}F NMR spectroscopy. The polyalkylated ferrocenium salt 1,1',3,3'-tetrakis(2-methyl-2-nonyl)ferrocenium nitrate ($DEC^{+}NO_3^{-}$) was synthesized according to a literature method.[40] All aqueous stock solutions were prepared in Class A volumetric glassware using distilled deionized water that had an initial resistivity of 18 MΩ cm. All experiments were performed at 24 ± 1 °C.

FTIR Spectrometer and ATR Immersion Probe. The spectrometer used in all experiments was an ASI React IR 1000 ATR-FTIR equipped with either an 18-bounce diamond (DiComp®)or 30-bounce silicon (SiComp®) ATR crystal mated to a ZnSe optical focusing element. The spectrometer was equipped with a liquid-nitrogen-cooled MCT detector. The spectral window was 4000–650 cm^{-1}. The spectrometer was interfaced to a dedicated personal computer. Data collection and manipulation was carried out using ASI ReactIR™ software (version 2.1).

Breakthrough Experiments. A column measuring 2.5 cm i.d. × 23 cm in length with No. 11 Ace-Thread joints was dry packed with 37 g of 0.25 mmol g^{-1} $HEP^{+}NO_3^{-}$/XAD-7 (see Chapter 2 Experimental Section for development of the $HEP^{+}NO_3^{-}$/XAD-7 material). Aqueous solutions were pumped through the column (23 mL min^{-1}) using a Fluid Metering Model QSY pump equipped with a low-flow isolation kit (1/16-in.-i.d.). The column was conditioned by pumping distilled and deionized water at 23 mL min^{-1} for 1 hr (no air pockets were observed in the column after conditioning). The probe used consisted of a 30-bounce reflection silicon ATR crystal mated to a ZnSe optical focusing element and housed in a 1.5 in. long × 1-in. diameter cylindrical

stainless-steel conduit. The tip of the probe was recessed 3 mm with the silicon crystal centered in the bottom of the recess. The tip held approximately 2 mL of solution when the probe was oriented in a vertical position. The effluent was directed over the tip of the probe, which was oriented such that only 1 mL fluid could collect in the recess before flowing into a waste container. Spectra were recorded every 26 seconds at 8-cm^{-1} resolution. Sixteen scans were averaged per spectrum and the instrument gain was set at 2. Distilled and deionized water was used as the background for each experiment. At the flow rate and data interval mentioned, every 10 mL of effluent was analyzed during this experiment.

Modification of Diamond and Silicon ATR Crystals. The exposed surfaces of the ATR crystals were treated with a 0.542 g L^{-1} dichloromethane solution of $NiCl_2$(dppp) (80 μL) (silicon crystal only) or 0.804 g L^{-1} $DEC^+NO_3^-$ (20 μL) (silicon and diamond crystals). Evaporation of dichloromethane left thin-film coatings of the water-insoluble organometallic ion-exchange compounds on the surface of the ATR crystal. Film thickness was determined by ellipsometry to be approximately 0.1 μm using a WVASE 32™ ellipsometer.[41]

In a typical analysis, the coated SiComp® probe was immersed into a known volume of water and stirred at 200 rpm. The coating was allowed to equilibrate with water for 10 min, at which time a background spectrum was collected. An appropriate amount of an analyte stock solution was then added with stirring and FTIR spectra of the resulting dilute, analyte solution was collected every minute for 60 min. No spectral smoothing was used, the nominal spectral resolution was 8 cm^{-1}, 64 scans were averaged per spectrum, and the instrument gain was set to one.

Determination of Detection Limits. The detection limits listed in Table 4.2 (3 × signal/noise ratio) using the unmodified and modified SiComp® probes were determined in different manners. For the unmodified probe, an aqueous solution of the analyte was

brought into contact with the probe and a spectrum ratioed to water was recorded by signal averaging continuously for 60 min (24,576 scans). The modified probe was immersed in aqueous solutions of specific analyte concentrations which resulted in bands that were three times the signal to noise ratio at either 4 or 60 min. Each spectrum recorded was the result of signal averaging 64 scans (30 sec total collection time). Lower concentrations of analytes could be detected if the modified probe was allowed to be in contact with the solution for longer periods of time.

Results and Discussion

Monitoring Extraction of IR-Active Anions Using ATR-FTIR. As was described in Chapter 2 breakthrough experiments, although informative, were very time consuming and column performance was determined well after the conclusion of the experiment. When thinking about applying this material in an industrial setting it is beneficial to determine in real time when the column has reached its capacity so that the material can be regenerated and reused with minimal down time. The optimal case for an industrial setting would be to have several columns in series where half the columns are being used to treat waste while the other half are being regenerated. In either case knowing when the column has reached its capacity in real time is beneficial.

Although water absorbs strongly in the infrared region of the electromagnetic spectrum, IR-active analytes can be detected at millimolar concentrations in most cases. To determine if this technique could be used to monitor or confirm the extraction of IR-active anions, solutions containing dodecylsulfate (DDS), triflate or FC-95 (mixture of fluorinated anionic surfactants) were analyzed by ATR-FTIR before and after extraction with $HEP^{+}NO_3^{-}$/XAD-7. According to the following ion-exchange equilibrium, NO_3^{-} will replace the analyte being extracted from the aqueous solution.

$$HEP^{+}NO_3^{-}/XAD\text{-}7(s) + analyte(aq) \rightleftharpoons HEP^{+}analyte^{-}/XAD\text{-}7(s) + NO_3^{-}(aq)$$

An ATR-FTIR spectrum taken of the aqueous solution before extraction should only produce absorbance bands from the analyte dissolved in the solution. After extraction those bands should no longer be detectable, instead, only the band(s) due to nitrate should be observed.

A series of experiments were performed in which the ion exchange material $HEP^{+}NO_3^{-}$/XAD-7 was used to extract IR-active anions and the solutions were monitored by ATR-FTIR spectroscopy. In one experiment 0.25 mmol g^{-1} $HEP^{+}NO_3^{-}$ /XAD-7 was used to extract 10 mM triflate ($CF_3SO_3^{-}$) and IR spectra were taken of the aqueous solution before and after extraction. As can be seen in Figure 4.1, the initial spectrum (spectrum A) shows the major IR ν(CF) and ν(SO) bands of triflate at 1040, 1180 and 1255 cm^{-1} with peak heights commensurate with 10 mM triflate. After extraction with $HEP^{+}NO_3^{-}$/XAD-7 (spectrum B) those bands are no longer detected and a new band at 1355 cm^{-1} (ν(NO) for aqueous NO_3^{-}) has appeared. This suggests that the majority of the triflate anion in the aqueous solution has been replaced by nitrate indicating successful extraction of triflate from the aqueous phase. More importantly the reaction was easily monitored at these concentrations by ATR-FTIR spectroscopy. The same type of experiment was carried out for the extraction of dodecylsulfate and FC-95. In each case the IR bands commensurate with dodecylsulfate and FC-95 were no longer observed after extraction and the new band at 1355 cm^{-1} had appeared. These experiments show that ATR-FTIR can be used to monitor the extraction of IR active anions provided that the concentrations are above the detection limit of the spectrometer.

Once it was confirmed that ATR-FTIR spectroscopy could be used to monitor the ion exchange of IR active anions studies evaluating the R^2ER process were carried out by monitoring the uptake and breakthrough of $CF_3SO_3^{-}$ (triflate anion) in real time.

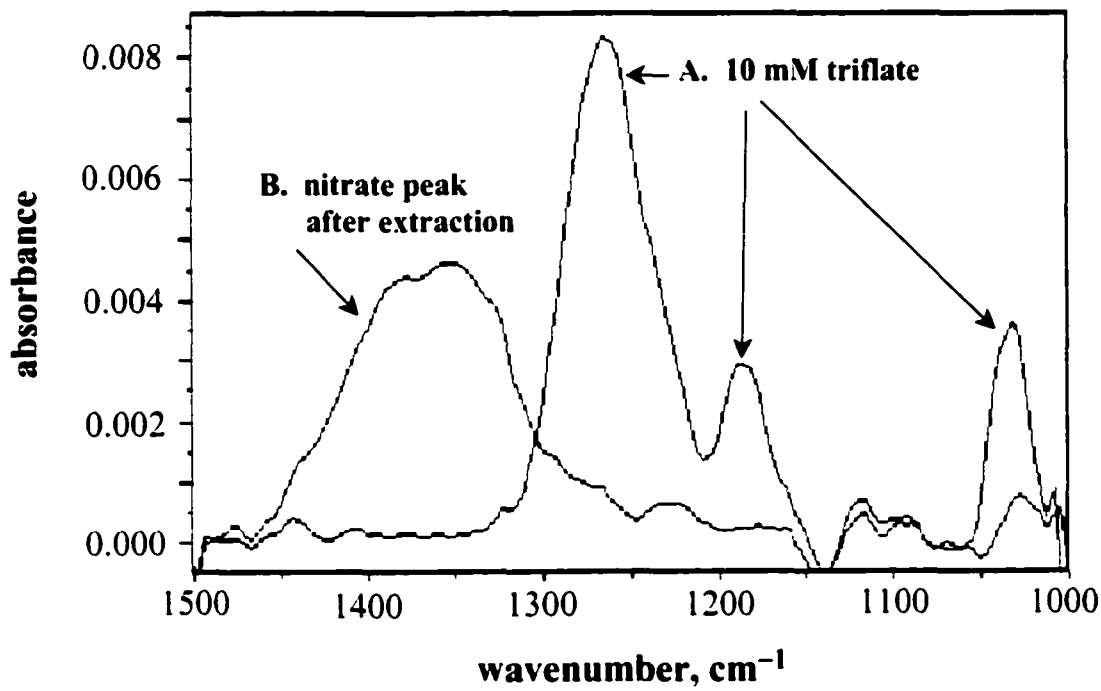

Figure 4.1. ATR-FTIR spectra of aqueous triflate before and after extraction with $HEP^{+}NO_3^{-}$/XAD-7. **A.** 10 mM lithium triflate using water as a background. The major bands of ν(CF) and ν(SO) at 1040, 1180 and 1255 cm^{-1} are observed. **B.** The triflate solution after extraction with $HEP^{+}NO_3^{-}$/XAD-7. The new band at 1355 cm^{-1} is due to NO_3^{-} that has been ion-exchanged for triflate.

Breakthrough experiments were designed to evaluate the extraction performance of a column packed with beads of $HEP^{+}NO_3^{-}$/XAD-7. This system is designed to continuously monitor the extraction process in real time. By "continuously" it is meant that a spectrum was recorded once every 26 sec for the duration of the experiment. In one set of experiments, a column containing 37 g of $HEP^{+}NO_3^{-}$/XAD-7 packed in a column measuring 2.5 cm i.d. × 23 cm in length (see Experimental Section) was used to extract 10 mM triflate with a flow rate of 23 mL min^{-1} (1.1 void volumes min^{-1}). The column was put through at least three complete R^2ER cycles. The resulting IR spectra in the 1000–1500 cm^{-1} region clearly showed that effluent from the columns contained only NO_3^- until the column became "saturated" with $CF_3SO_3^-$, at which time the band due to NO_3^- decreased rapidly over time and the bands due to $CF_3SO_3^-$ grew in until they reached the limiting absorbances commensurate with a 10 mM solution of $CF_3SO_3^-$, as shown in Figure 4.2. This behavior is exactly what is expected for the following ion-exchange equilibrium:

$$HEP^{+}NO_3^{-}/XAD\text{-}7(s) + CF_3SO_3^{-}(aq) \rightleftharpoons HEP^{+}CF_3SO_3^{-}/XAD\text{-}7(s) + NO_3^{-}(aq)$$

With this data, the percentage of capacity reached at breakthrough can be determined. Breakthrough is defined as the number of bed volumes (BV) of aqueous waste that were passed through the column before the bands due to $CF_3SO_3^-$ were clearly discernable (3 times signal to noise) in the IR spectra. Bed volume is defined as the volume of simulant contained within the packed column. In this particular experiment, breakthrough occurred at about 27 bed volumes, which corresponds to 84% of capacity. The column was then reduced and reoxidized (put through a complete R^2ER cycle) and once again a 10 mM solution of triflate was passed through the column and breakthrough monitored by ATR- FTIR spectroscopy. The column was put through a total of three R^2ER cycles

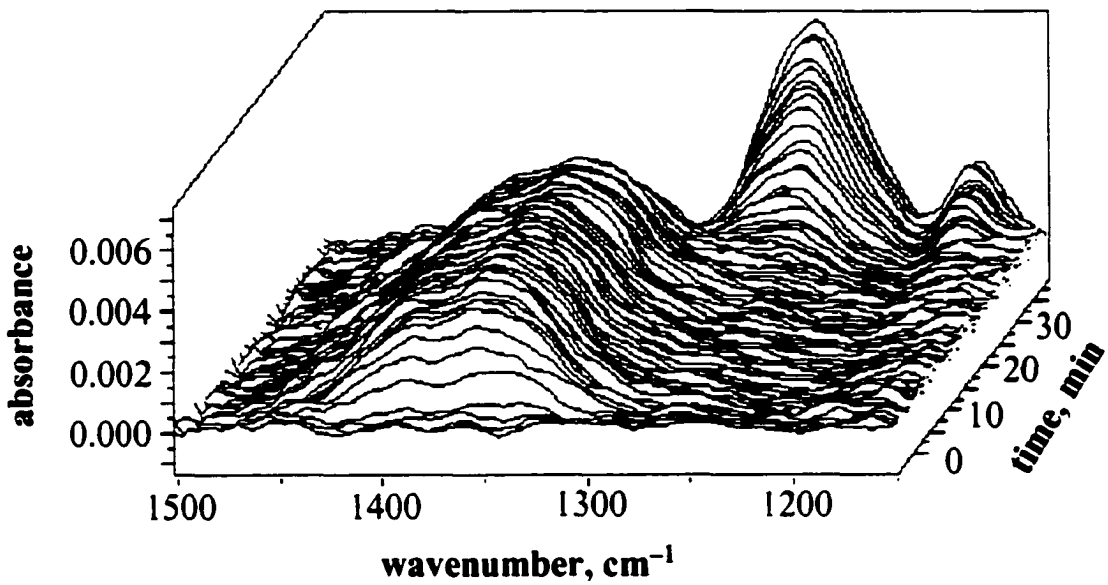

Figure 4.2. ATR-FTIR spectra of the column effluent from the extraction of 10 mM $CF_3SO_3^-$ from water using the R^2ER ion-exchange material $HEP^+NO_3^-$/XAD-7 (flow rate = 1.1 VV min^{-1}; one spectrum was recorded every 26 sec). The broad band at ca. 1355 cm^{-1} (assigned to NO_3^-) grows in early in the experiment and eventually disappears at the expense of the sharper band at ca. 1255 cm^{-1}. The 1255 cm^{-1} band is assigned to $CF_3SO_3^-$.

and the results of the column breakthrough experiments are listed in Table 4.1. Importantly, a given ion-exchange column does not seem to undergo degradation through multiple cycles. Although a majority of the material underwent ion-exchange in this experiment even greater efficiencies could be achieved by slowing the pump speed. The slower pump speed would allow longer resonance times within the column, which would allow more time for the ion-exchange process to occur.

Although ATR-FTIR spectroscopy can be used to monitor the ion exchange of IR active anions as well as evaluate column performance, the absorbance of water in the IR region prohibits the use of this technique for detection of trace analytes in solution (i.e., < 1 mg L^{-1}).[7,42] Nevertheless, there are examples of attenuated total reflectance (ATR) crystals coated with submicron-thick layers of polymeric or sol-gel materials that enhance the sensitivity of FTIR spectrometers by concentrating an analyte in the region probed by the evanescent wave (i.e., in the coating). Most analytes that have been detected in this manner are neutral organic molecules such as atrazine (3 mg L^{-1}), 1,1-bis(4-chlorophenyl)-2,2,2-trichloroethane (DDT) (50 mg L^{-1}), trichloroethylene (TCE) (100 mg L^{-1}), and benzonitrile (350 μg L^{-1}) (the lowest aqueous concentrations studied to date are shown in parentheses).[3,6,43] Only a few coatings that can concentrate ions have been reported, and none are known to detect aqueous ions at concentrations below 1000 μg L^{-1}.[44–51] Described here is the detection of CN^-, ClO_4^-, and $C_8F_{17}SO_3^-$ in water at concentrations ≤ 25 μg L^{-1} using a commercially available silicon ATR-FTIR immersion probe that has been coated with thin films of suitable organometallic ion-exchange compounds.[52–56]

The goal of this work was to demonstrate that ATR-FTIR spectroscopy could be used to detect polyatomic anions in water at concentrations three to five orders of magnitude lower than current ATR-FTIR detection limits. This has been accomplished by modifying commercially available ATR-FTIR immersion probes with thin-film

Table 4.1. Ion-Exchange Results for the Extraction of Triflate.[a]

cycle	flow rate, BV min^{-1}	number of BV[b] to breakthrough	% ion-exchange at breakthrough
1	0.78	27.70	84
2	0.78	27.03	83
3	0.78	27.37	84

[a] The simulant was 10 mM aqueous $LiCF_3SO_3$; the activated extractant was $HEP^+NO_3^-$/XAD-7 with an ion-exchange capacity of 0.261 mmol $HEP^+NO_3^-$ per g of material; experiment was run using a column of dimensions 2.5 cm i.d. × 23 cm long containing 37 g. [b] Bed volume (BV) is defined as the volume of aqueous solution contained in the packed column.

coatings of organometallic ion-exchange compounds. It is important to note that no further modification of the ATR-FTIR probe, and no sample pretreatment, were necessary for these experiments. The potential benefit of this technique is the simultaneous detection, positive identification, and quantification of IR active analytes in one measurement.

Each thin-film coating was used for only one analysis, after which it was removed from the ATR crystal by washing with dichloromethane. In other words, the ATR crystal was re-coated with a thin film of the organometallic ion-exchange compound for each sample. Even though this simple evaporation procedure does not allow film thickness and uniformity to be precisely controlled, it was found that different films of a given extractant afforded excellent reproducibility (10% or less) for multiple samples of a given aqueous analyte. By using water-insoluble but organic-soluble coatings in this manner, one is able to study several different ion-exchange compounds and aqueous analytes in a relatively brief period of time using only one ATR-FTIR probe. The rapid removal and reapplication of coatings would not have been possible if more robust, covalently-linked coatings had been used instead.

The benefit of applying an extractant film directly on the surface of the probe is two-fold. First, it partially blocks water from the surface of the probe; second, the film acts to concentrate the analyte of interest within the evanescent wave. The act of blocking water and increasing the amount of analyte being detected at the same time greatly increases the sensitivity of the instrument. A depiction of the surface modification is shown in Figure 4.3.

Detection of ClO_4^- Using a $DEC^+NO_3^-$ Coating. When the SiComp® probe coated with a thin film of $DEC^+NO_3^-$ was immersed in a solution of 3 μg L^{-1} ClO_4^- in distilled deionized water (pH 5–6), a new band at 1092 cm^{-1} was observed in 60 min. This band is the T_2-symmetry ν(ClO) band of the tetrahedral perchlorate ion, now

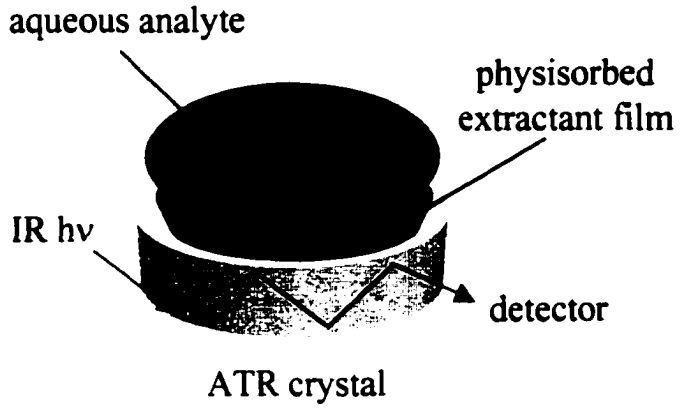

Figure 4.3. Graphic representation of the surface modified ATR crystal used to concentrate an analyte within the evanescent wave.

concentrated in the thin-film coating via the following, essentially irreversible, ion-exchange reaction:

$$DEC^{+}NO_3^{-}(s) + ClO_4^{-}(aq) \rightarrow DEC^{+}ClO_4^{-}(s) + NO_3^{-}(aq)$$

A depiction of the ion-exchange process is shown in Figure 4.4. Note that there are three different kinetic processes that could potentially govern the rate of growth of the band at 1092 cm^{-1}: (1) the diffusion of ClO_4^- from the bulk solution into the stagnant aqueous layer and concomitant diffusion of NO_3^- from the stagnant layer into the bulk solution (depicted with straight arrows); (2) the ClO_4^-/NO_3^- interchange at the surface of the film; and (3) ClO_4^-/NO_3^- ion-exchange between adjacent DEC^+ centers (depicted with curved arrows). The ion-exchange process can readily be seen in Figure 4.5, which displays IR spectra recorded after five and ten minutes when the coated probe was immersed in 15 μg L^{-1} aqueous ClO_4^-. The negative band at 1331 cm^{-1} (the E_u-symmetry ν(NO) band of the nitrate ion) represents the loss of an equivalent amount of NO_3^- from the thin-film coating (based on ClO_4^-) as the ion-exchange reaction proceeds and ClO_4^- is incorporated into the film, which gives rise to the positive band at 1092 cm^{-1}. Since the one-hour detection limit for aqueous ClO_4^- (ν(ClO) = 1104 cm^{-1}) with the unmodified SiComp® probe was found to be 288,000 μg L^{-1}, the $DEC^+NO_3^-$ coating has lowered the detection limit for aqueous perchlorate by a factor of nearly 100,000 (see Table 4.2). When the concentration of aqueous ClO_4^- was 500 μg L^{-1}, the time necessary to observe the band at 1092 cm^{-1} was only 2 min with the $DEC^+NO_3^-$ modified probe.

Detection of PFOS Using a $DEC^+NO_3^-$ Film. When the SiComp® probe coated with a thin film of $DEC^+NO_3^-$ was immersed in a solution of 25 μg L^{-1} PFOS in distilled deionized water (pH 5–6), several new bands in the fingerprint region were observed,

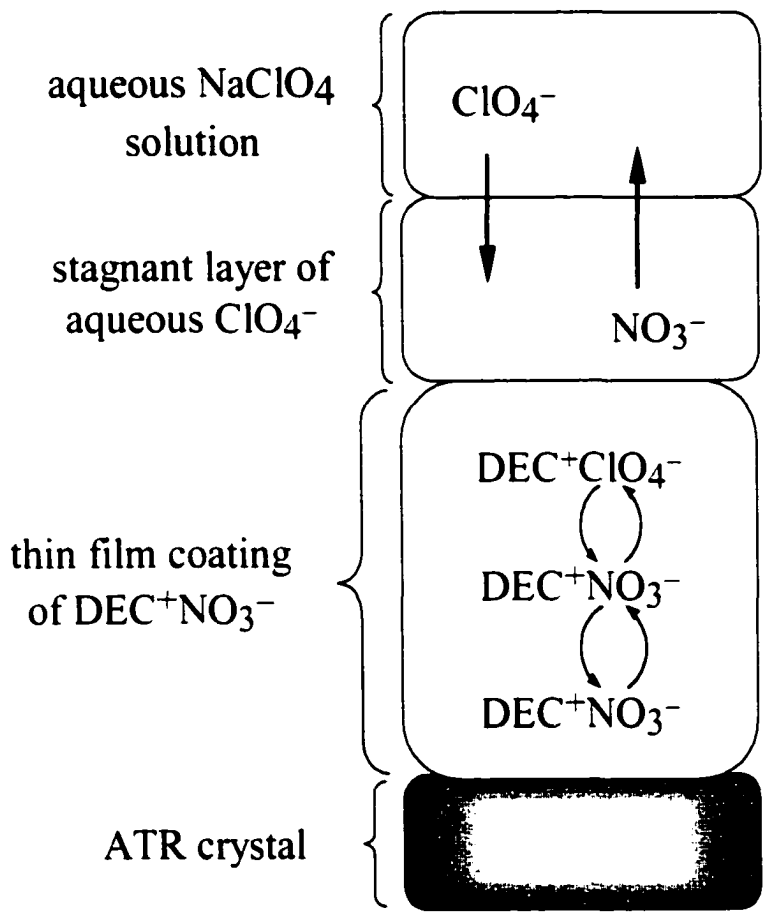

Figure 4.4. Schematic drawing of the ClO_4^-/NO_3^- ion-exchange reaction that occurs when a thin film of $DEC^+NO_3^-$ is treated with an aqueous solution of $LiClO_4$. The relative thickness of the layers is not to scale.

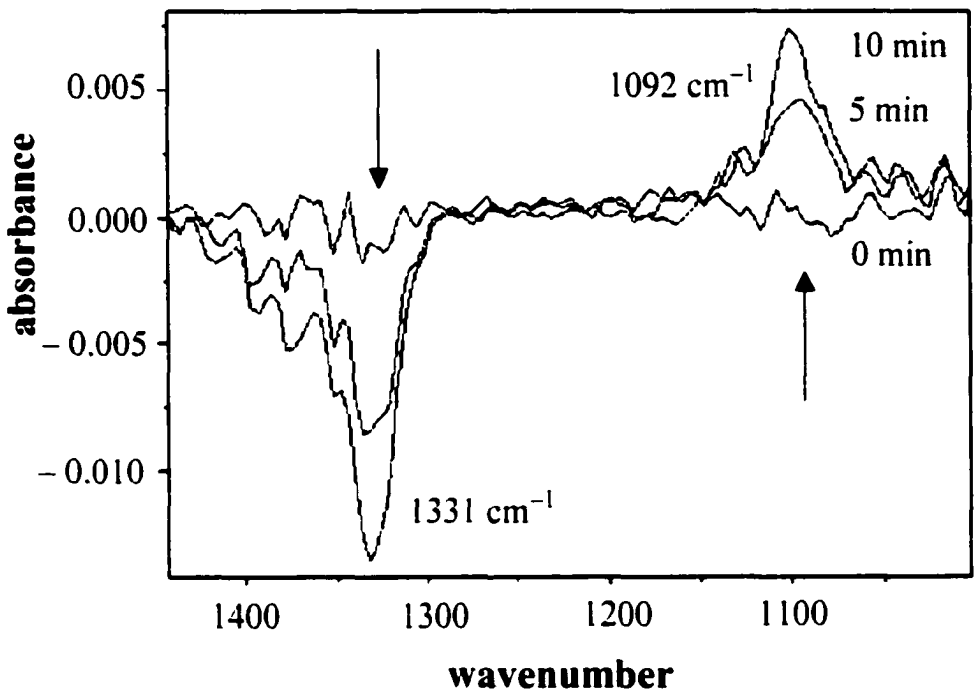

Figure 4.5. The time-dependent ATR-FTIR spectra of a thin film of water-insoluble $DEC^+NO_3^-$ on the SiComp® probe immersed in a pH 5–6 aqueous solution of $LiClO_4$ after 0, 5 and 10 min. (DEC^+ = 1,1',3,3'-tetrakis(2-methyl-2-nonylferrocenium) cation; $[ClO_4^-]$ = 15 μg L^{-1}). The positive band at 1092 cm^{-1} and the negative band at 1331 cm^{-1} that grow in over time are assigned to the water-insoluble compounds $DEC^+ClO_4^-$ and $DEC^+NO_3^-$, respectively. The appearance of $DEC^+ClO_4^-$ and the disappearance of $DEC^+NO_3^-$ throughout the film are the result of the ClO_4^-/NO_3^- ion exchange reaction.

Table 4.2. One-Hour Detection Limits for the Unmodified and Modified ATR-FTIR Probe.[a]

anion	wavenumber monitored[b]	detection limit		organometallic extractant[c]
		unmodified probe	modified probe	
CN^-	2104	130,000 μg L^{-1}	5 μg L^{-1}	$NiCl_2$(dppp)
ClO_4^-	1092	288,000 μg L^{-1}	3 μg L^{-1}	$DEC^+NO_3^-$
n-$C_8F_{17}SO_3^-$	1270	100,000 μg L^{-1}	25 μg L^{-1}	$DEC^+NO_3^-$

[a] The detection limit is defined as the concentration at which a band with a signal/noise ratio ≥ 3 was observed after 60 min. [b] The wavenumber monitored for the modified probe experiments and the unmodified probe experiments differed by a few wavenumbers in all three cases. [c] dppp = 1,3-bis(diphenylphosphino)propane; DEC^+ = 1,1',3,3'-tetrakis(2-methyl-2-nonyl)ferrocenium cation.

undoubtedly due to an ion-exchange process similar to the one described above for ClO_4^-. The most intense band, at 1270 cm^{-1}, had a signal/noise ratio of 3 after 60 min. Figure 4.6 is a plot of the absorbance at 1270 cm^{-1} as a function of time over 350 min. Even though the maximum absorbance of the PFOS bands are not achieved in 60 min, this time is sufficient for the detection of PFOS. When the concentration of aqueous PFOS was 250 μg L^{-1}, the time necessary to observe the band at 1270 cm^{-1} was only 4 min. Figure 4.7 shows FTIR spectra recorded over time of the $DEC^+NO_3^-$-coated probe immersed in an aqueous solution containing 250 μg L^{-1} PFOS. Since the one-hour detection limit for aqueous PFOS (ν = 1243 cm^{-1}) with the unmodified SiComp® probe was found to be 100,000 μg L^{-1}, the $DEC^+NO_3^-$ coating has afforded a sensitivity increase (ratio of detection limits) of 4,000 for PFOS. When a $HEP^+NO_3^-$ modified probe was used to detect triflate, the detection limit was found to be 0.1 μM (in 20 min). The detection limit with no modification was found to be 3.2 mM, therefore, using a film of $HEP^+NO_3^-$ produced a sensitivity increase of 32,000 for triflate.

The magnitude of dA(1270 cm^{-1})/dt, and not final absorbance, is concentration dependent, therefore, it might be possible to prepare a calibration curve for the quantitative determination of aqueous PFOS by FTIR spectroscopy at micromolar concentrations with little or no sample pretreatment. The functional form of dA/dt curves and the effect of competing anions on those curves are currently being studied and will be the subject of a forthcoming paper.[57]

Detection of AFFF Using a $DEC^+NO_3^-$ Film. Detection of AFFF in water was investigated using a $DEC^+NO_3^-$ modified ATR-FTIR diamond probe. The detection limit without any surface modification was found to be 4 μg L^{-1} AFFF concentrate. Figure 4.8 shows the difference ATR-FTIR spectra of the detection of 0.2 μg L^{-1} AFFF at 2, 15 and 30 min after the $DEC^+NO_3^-$ coated diamond probe was immersed in the solution. The intensity of the IR band due to the NO_3^- ion in the film decreased over

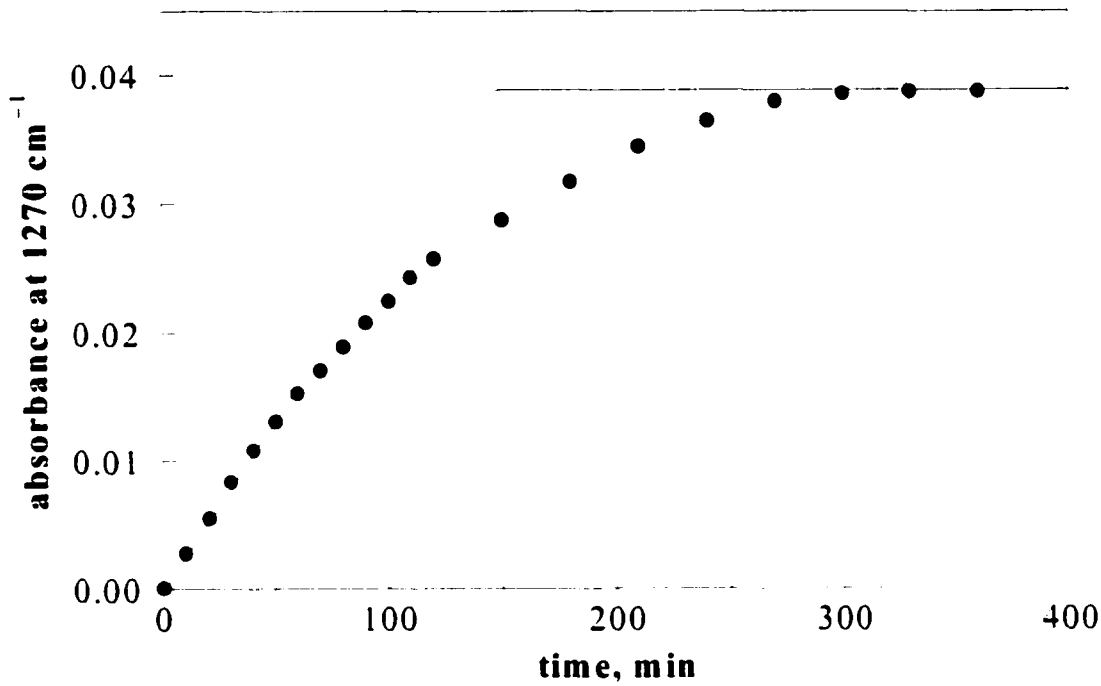

Figure 4.6. Plot of absorbance at 1270 cm^{-1} vs. time for a thin film of water-insoluble $DEC^{+}NO_3^{-}$ on the SiComp® probe immersed in a pH 5–6 aqueous solution of K(PFOS) ([PFOS] = 25 μg L^{-1}). The lines are a linear fit to the first seven and last three data points.

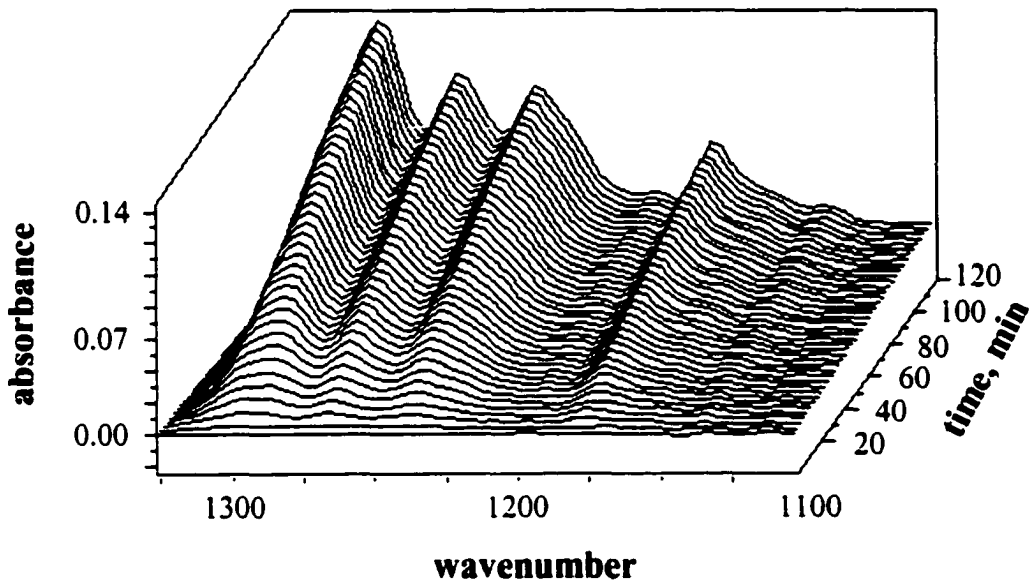

Figure 4.7. Time-dependent ATR–FTIR spectra of a thin film of water-insoluble $DEC^+NO_3^-$ on the SiComp® probe immersed in a pH 5–6 aqueous solution of K(PFOS) (DEC^+ = 1,1',3,3'-tetrakis(2-methyl-2-nonyl)ferrocenium) cation; PFOS = $C_8F_{17}SO_3^-$; [PFOS] = 250 μg L^{-1}). The bands that grow in over time are assigned to the water-insoluble compound DEC(PFOS), which is formed throughout the film by the PFOS/NO_3^- ion-exchange reaction.

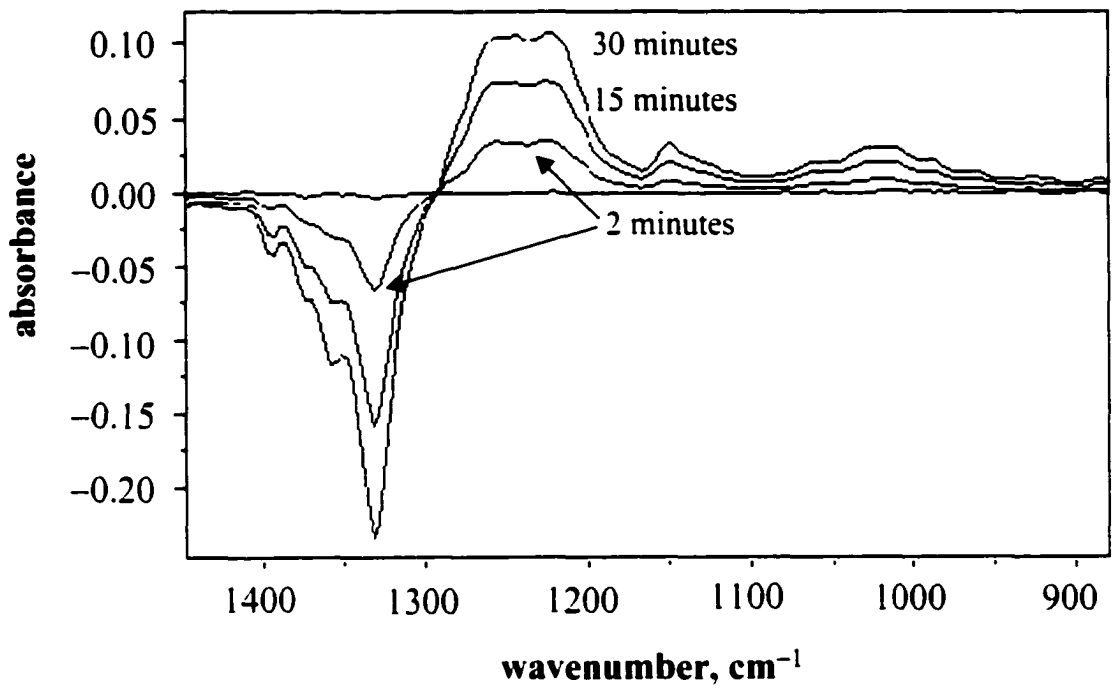

Figure 4.8. ATR-FTIR detection of 0.2 mg L^{-1} AFFF concentrate using a $DEC^{+}NO_3^{-}$ modified diamond ATR sensor. The spectra shown are after 2, 15 and 30 min of contact with the AFFF solution.

time while the ν(SO) and ν(CF) IR bands in the 1300 - 950 cm^{-1} region grew in over time. The bands in the 1300 - 950 cm^{-1} region grow in because anions from the AFFF matrix are accumulating in the film (i.e., they are undergoing selective ion exchange with NO_3^-). The negative band at 1351 cm^{-1} is the ν(NO) band of NO_3^-, which is partitioning from the film into the aqueous solution. Peaks, due to the anions in AFFF, were detectible within 2 min (i.e., signal to noise greater than 3). Since the detection limit of AFFF with the uncoated silicon ATR crystal is 4 μg L^{-1}, this example demonstrates that a lowering of the detection limit by a factor of 20 is possible using R^2ER-extractant-containing coatings on FTIR ATR crystals.

Although more recent studies have found $DEC^+NO_3^-$ to be a more stable extractant film on the surface of the probe, Table 4.3 lists the detection enhancements for eight anions that have been analyzed using $HEP^+NO_3^-$ modified ATR probes. The absorbance values without the $HEP^+NO_3^-$ film as well as the enhanced absorbance values with the $HEP^+NO_3^-$ film are also recorded in Table 4.3. The enhancement factors for triflate and PFOS were determined in quadruplicate where the variation was ±7% in both cases.

$NiCl_2$(dppp). A Non-Recyclable Extractant. When the SiComp® probe coated with a thin film of this compound was immersed in a pH 10 aqueous solution of 5 μg L^{-1} CN^-, a new band at 2104 cm^{-1} was clearly discernable above the detection limit (i.e., signal/noise ≥ 3 at 2004 cm^{-1}) in 60 min. Since the one-hour detection limit for aqueous CN^- with the unmodified SiComp® probe was found to be 130,000 μg L^{-1}, the nickel-complex coating has lowered the detection limit for aqueous cyanide by a factor of 26,000 (see Table 4.2). When the concentration of aqueous CN^- was 130 μg L^{-1}, the time necessary to observe the band at 2104 cm^{-1} was only 4 min. Figure 4.9 shows FTIR spectra recorded over time of the $NiCl_2$(dppp)-coated probe immersed in an aqueous solution containing 130 μg L^{-1} CN^-. Preliminary experiments indicate that the band at

Table 4.3. ATR-FTIR Detection Enhancements for Various Anions.

anion	wavenumber (cm^{-1})	absorbance		enhancement factor[a]
		no film	$HEP^+NO_3^-$ film	
triflate	1266	0.0002	0.3738	2000
PFOS	1266	0.0012	0.3862	300
DDS	1660	0.0018	0.1973	110
acetate	1664	0.0060	0.0998	17
perrhenate	915	0.0027	0.1689	63
sulfate	1664	0.0052	0.1255	24
iodate	1660	0.0057	0.1507	26

[a] The enhancement factors are accurate, except for triflate, to two significant figures only. The enhancement factors for triflate are accurate to one significant figure.

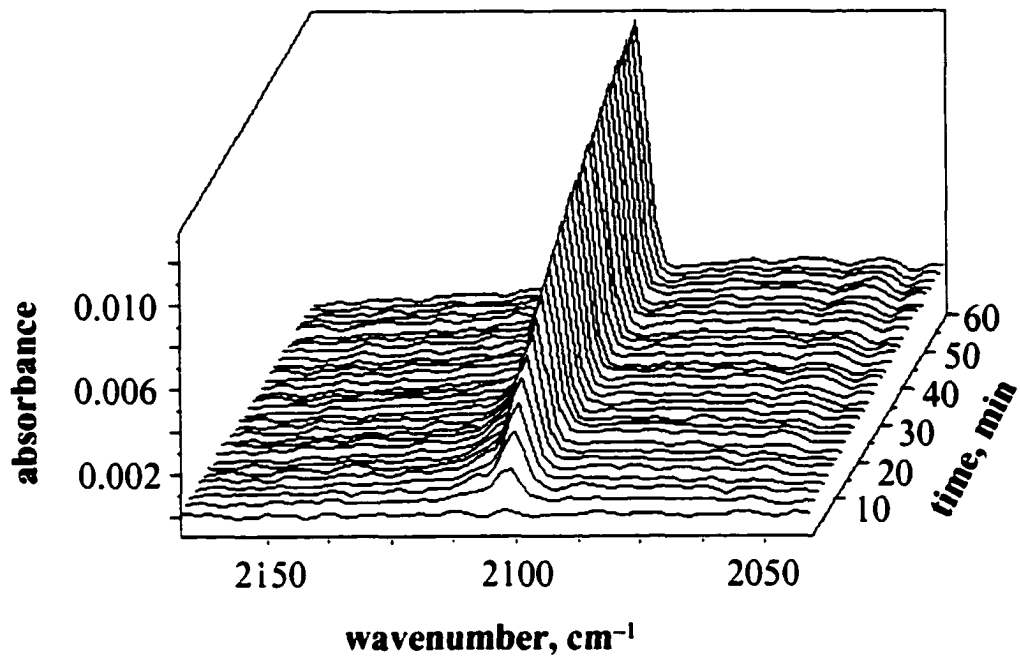

Figure 4.9. Time-dependent ATR-FTIR spectra of the water-insoluble compound $NiCl_2(dppp)$ on the SiComp® probe immersed in pH 10 aqueous KCN ($[CN^-]$ = 130 μg L^{-1}). The band that grows in over time, at 2104 cm^{-1}, is assigned to the water-insoluble compound NiCl(CN)(dppp), which is formed throughout the film by the CN^-/Cl^- ion-exchange reaction that occurs in the film.

2104 cm^{-1} is due to the formation of the new water-insoluble complex NiCl(CN)(dppp). Its formation is probably due to the following, essentially irreversible, ion-exchange reaction:

$$NiCl_2(dppp)\,(s) + CN^-\,(aq) \rightarrow NiCl(CN)(dppp)\,(s) + Cl^-\,(aq)$$

Since the appearance of the band at 2104 cm^{-1} occurred at different times for different concentrations of CN^-, kinetic process (diffusion of CN^- from the bulk solution into the stagnant aqueous layer and concomitant diffusion of Cl^- from the stagnant layer into the bulk solution) may be rate limiting under these conditions. In future work, it will be determined if a reliable calibration curve of dA(2104 cm^{-1})/dt vs. cyanide concentration can be generated.

Importantly, when the $NiCl_2$(dppp)-coated probe was immersed in an aqueous solution containing 130 μg L^{-1} CN^- and 35.5 g L^{-1} Cl^-, the band at 2104 cm^{-1} was also observed in about 4 min. Therefore, a 200,000-fold excess of the co-contaminant Cl^- does not interfere with the detection of CN^-. This demonstrates the very high selectivity of $NiCl_2$(dppp) for CN^- and suggests that cyanide might be detectable at low concentrations in sea water and other aqueous brines using $NiCl_2$(dppp)-coated ATR-FTIR probes.

Finally, it may be possible to make a highly selective extractant material for CN^- by physisorbing $NiCl_2$(dppp) onto solid supports. Although the material would not be redox-recyclable, similar techniques for evaluating the effectiveness of $HEP^+NO_3^-$/support materials could be applied towards this material.

Conclusions

The development of an ATR-FTIR technique capable of monitoring the extraction of polyatomic ions from aqueous solutions has been used to determine capacity and extraction performance of $HEP^{+}NO_3^{-}$/XAD-7 packed into columns. This technique, although limited by the strong absorbance of water in the infrared region was able to detect the breakthrough of 10 mM triflate in real time. Knowing when a column has reached capacity in real-time is important when treating large volumes of contaminated waste. Measuring breakthrough in real-time allows the full capacity of a column to be reached before replacement or, in the case of redox-recyclable materials, before regenerating the material.

As was noted earlier, the major drawback in using IR techniques in aqueous media is the strong interference by water. The enhancement in sensitivity of the ATR-FTIR spectrometer for IR active anions in aqueous solutions was investigated by physisorbing highly selective water insoluble organometallic extractants to the surface of the probe. A thin film of the organometallic extractant $NiCl_2$(dppp) applied to the tip of the ATR probe was used to detect CN^- in the low microgram per liter (ppb) concentrations. Within 4 min, 130 $\mu g\ L^{-1}$ CN^- was detectable (3 times signal to noise) and 5 $\mu g\ L^{-1}$ was detectable after only 60 min. The detection limit for an unmodified probe was 130,000 $\mu g\ L^{-1}$ CN^-, therefore, by simply applying a thin film of $NiCl_2$(dppp) the detection limit for aqueous cyanide has been lowered by a factor of 26,000. Cyanide was also detectable at 130 $\mu g\ L^{-1}$ in 4 min in the presence of 200,000-fold excess Cl^- which demonstrates the high selectivity of $NiCl_2$(dppp) for CN^-. Applying a thin film of $DEC^{+}NO_3^{-}$ afforded a sensitivity increase of 96,000 for ClO_4^- and 4000 for PFOS.

The $DEC^{+}NO_3^{-}$ modified ATR-FTIR probe was able to detect AFFF by extracting anionic components from the aqueous matrix at concentrations well below that, which was achieved using an unmodified probe. The virtue of this technique was that the

anions being extracted into the selective $DEC^{+}NO_3^{-}$ film could be identified through the unique IR-bands that were produced.

The detection limits reported here are unprecedented for infrared detection of these ions in aqueous solutions. The ability to easily switch extractant films demonstrates the versatility of the system. By simply adjusting the extractant that is physisorbed to the surface of the probe, specific analytes can be targeted for detection. The added advantage of using infrared spectroscopy was positive identification of the target analyte through the unique IR absorbance produced by the analyte. Ongoing work with this technique will determine if accurate dA/dt curves can be generated for quantification of target analytes. If a successful calibration curve can be generated the ATR-FTIR technique described here will be able to detect, identify, and quantify IR-active analytes in the low microgram per liter range simultaneously with a single, simple measurement.

References

(1) Hellstern, U.; Hoffmann, V. *J. Molec. Struc.* **1995**, *349*, 329.

(2) Han, L.; Niemczyk, T. M.; Lopez, G. P. *Appl. Spec.* **1999**, *53*, 381.

(3) Han, L.; Niemczyk, T. M.; Lu, Y.; Lopez, G. P. *Appl. Spec.* **1998**, *52*, 119.

(4) Lu, Y.; Han, L.; Brink, C. J.; Niemczyk, T. M.; Lopez, G. P. *Sens. Actuators, B* **1996**, *B36*, 517.

(5) Rosenberg, E.; Kellner, R. *Proc. SPIE-Int. Soc. Opt. Eng.* **1992**, *1575*, 346.

(6) Goebel, R.; Seitz, R. W.; Tomellini, S. A.; Krska, R.; Kellner, R. *Vib. Spec.* **1995**, *8*, 141.

(7) Urban, M. W. *Attenuated Total Reflectance Spectroscopy of Polymers. Theory and Practice.* American Chemical Society: Washington, DC, 1996.

(8) Harrick, M. J. *Internal Reflection Spectroscopy*; Wiley & Sons: New York, 1967; Chapter 2.

(9) Boening, D. W.; & Chew, C. M. *Water, Air, Soil Pollut.* **1999**, *109*, 67.

(10) Otu, E. O.; Byerley, J. J.; & Robinson, C. W. *Int. J. Environ. Anal. Chem.* **1996**, *63*, 81.

(11) Christen, K. *Environ. Sci. Technol.* **2000**, *34*, 374A.

(12) Okamoto, H. S.; Rishi, D. K.; Steeber, W. R.; Baumann, F. J.; & Perera, S. K. *Jour. AWWA* **1999**, *91:10*, 73.

(13) Susarla, S.; Collette, T. W.; Garrison, A. W.; Wolfe, N. L.; & McCutcheon, S. C. *Environ. Sci. Technol.* **1999**, *333*, 469.

(14) Urbansky, E. T. *Bioremediation J.* **1998**, *2*, 81.

(15) Moody, C. A.; & Field, J. A. *Environ. Sci. Technol.* **1999**, *33*, 2800–2806.

(16) Moody, C. A.; Hebert, G. N.; Strauss, S. H.; Field, J. A. *Eviron. Sci. Technol.*, accepted for publication.

(17) Olsen, G. W.; Burris, J. M.; Mandel, J. H.; & Zobel, L. R. *J. Occup. Environ. Med.* **1999**, *41*, 9, 799.

(18) Renner, R. *Environ. Sci. Technol.* **2000**, *34*, 371A.

(19) Tullo, A. *Chem. Eng. News*, **2000**, *May 22*, 9.

(20) Tullo, A. *Chem. Eng. News*, **2000**, *May 29*, 12.

(21) US EPA, **2000**. <www.epa.gov/safewater/mcl.html>.

(22) Pontius, F. W. *AWWA Jour.* **2000**, *92*, 3, 40.

(23) Gullick, R. W.; Lechevallier, M. W.; Barhorst, T. S. *J. AWWA* **2001**, *January*, 66.

(24) Caliamanis, A.; McCormick, M. J.; Carpenter, P. D.; *J. Chromatog. A* **2000**, *884*, 75.

(25) Frenzel, W.; Liu, C. Y.; Oleksy-Frenzel, J. *Anal. Chim. Acta* **1990**, *233*, 77.

(26) Linares, P. Luque de Castro, M. D.; Valcarcel, M. *Anal. Chim Acta* **1984**, *161*, 257.

(27) Seto, Y.;Tsunoda, N.; Ohta, H.; Shinohara, T. *Anal. Chim. Acta* **1993**, *276*, 247.

(28) Chinaka, S.; Takayama, N.; Michigami, Y.; Ueda, K. *J. Chromatog. B* **1998**, *713*, 353.

(29) Sohlenius, A.-K.; Eriksson, A. M.; Hogstrom, C.; Kimland, M.; DePierre, J. W. *Pharmacol. Toxicol.* **1993**, *72*, 90-93.

(30) Schnellmann, R. G. *Toxic. in Vitro* **1990**, *4*, 71–74.

(31) Meussdoerffer, J. N.; Niderprüm, H. *Chem. Z.* **1980**, *104*, 45–52.

(32) Chan, D. B.; Chian, E. S. K. *Environ. Prog.* **1986**, *5*, 104–109.

(33) Perfluorooctyl Sulfonates; Proposed Significant New Use Rule: *Fed. Regist.* **2000**, *65 (202)*, 62319–62333.

(34) Giesy, John P.; Kannan, K. *Environ. Sci. Technol.*, **2001**, *35*, 1339–1342.

(35) Kannan, K.; Koistinen, J.; Beckmen, K.; Evans, T.; Gorzelany, J. F.; Hansen, K. J.; Jones, P. D.; Helle, E.; Nyman, M.; Giesy, J. P. *Environ. Sci. Technol.*, **2001**, *35*, 1593–1598.

(36) Kannan, K.; Franson, J. C.; Bowerman, W. W.; Hansen, K. J.; Jones, P. D.; Giesy, J. P. *Environ. Sci. Technol.*, **2001**, *35*, 3065–3070.

(37) Olsen, G. W.; Burris, J. M.; Mandel, J. H.; Zobel, L. R. *J. Occup. Environ. Med.* **1999**, *41*, 799–806.

(38) Moody, C. A.; Field, J. A. *Environ. Sci. Technol.* **2000**, *34*, 3864–3870.

(39) Moody, C. A.; Hebert, G. N.; Strauss, S. H.; Field, J. A. *Environ. Sci. Technol.*, submitted for publication.

(40) Clark, D. L.; Clark, J. F.; Clapsaddle, B. J.; Chambliss, C. K.; Miller, S. M.; Anderson, O. P.; Strauss, S. H. Manuscript in preparation.

(41) Hebert, G. N. Ph.D. Dissertation, Colorado State University, Fort Collins, CO. Manuscript in preparation.

(42) Griffiths, P. R.; & de Haseth, J. A. *Fourier Transform Infrared Spectrometry*. Wiley, New York 1986.

(43) Regan, F.; Meaney, M.; Vos, J. G.; MacCraith, B. D.; & Walsh, J. E. *Analyt. Chim. Acta* **1996**, *334*, 85.

(44) Ahn, D. J.; & Franses, E. I. *AIChE J.* **1994**, *40*, 1046.

(45) Barja, B. C.; Tejedor-Tejedor, M. I.; & Anderson, M. *Langmuir* **1999**, *15*, 2316.

(46) Degenhardt, J.; & McQuillan, A. J. *Langmuir* **1999**, *15*, 4595.

(47) Dobson, K. D.; & McQuillan, A. J. *Spectrochim. Acta* **1999**, *55A*, 1395.

(48) Dobson, K. D.; & McQuillan, A. J. *Langmuir* **1997**, *13*, 3392.

(49) Hug, S. J. *J. Coll. Interface Sci.* **1997**, *188*, 415

(50) Persson, P.; Nilsson, N.; & Sjöberg, S. *J. Coll. Interface Sci.* **1996**, *177*, 263.

(51) Yang, Lin; & Saavedra, S. S. *Anal. Chem.* **1995**, *67*, 1307.

(52) Chambliss, C. K.; Odom, M. A.; Morales, C. M. L.; Martin, C. R.; & Strauss, S. H. *Anal. Chem.* **1998**, *70*, 757.

(53) [a]Chambliss, C. K.; Strauss, S. H.; & Moyer, B. A. *Solvent Extr. Ion Exch.* **1999**, *17*, 553. [b]Chambliss, C. K.; Odom, M. A.; Martin, C. R.; Moyer, B. A.; & Strauss, S. H. *Inorg. Chem. Communications* **1999**, *1*, 435.

(54) Clark, J. F.; Clark, D. L.; Whitener, G. D.; Schroeder, N. C.; & Strauss, S. H. *Environ. Sci. Technol.* **1996**, *30*, 3124.

(55) Clark, J. F.; Chamberlin, R. M.; Abney, K. D.; & Strauss, S. H. *Environ. Sci. Technol.* **1999**, *33*, 2489.

(56) Strauss, S. H. *Metal Ion Separation and Preconcentration: Progress and Opportunities*. Bond, A. H.; Dietz, M. L.; & Rogers, R. D., Eds. ACS Symposium Series 716, 1999. American Chemical Society, Washington, DC 156.

(57) Hebert, G. N.; Odom, M. A.; Craig, P. S.; Strauss, S. H. Manuscript in preparation.

Appendix A

A.1 List of Analytes used to Make Up a Seawater Simulant

Table A.1. Concentration of analytes used to make up the seawater simulant[a]

analyte	mM
NaCl	458.00
Mg SO_4	26.00
H_3BO_3	0.32
$MgCl_2$	26.00
$CaCl_2$	10.00
KCl	5.00
KBr	0.75
K2CO3	2.30

[a]Concentrations of analytes were similar to those reported by Fergusson, J. E. Inorganic Chemistry and the Earth Chemical Resources, Their Extraction, Use and Environmental Impact, Pergamon Press, New York, 1982.